Optical Sensor Design and Development for Identification of Fluids Using Nanotags

by

Başarbatu Can

A Thesis Submitted to the
Graduate School of Sciences and Engineering
in Partial Fulfillment of the Requirements for
the Degree of

Master of Science

in

Electrical and Electronics Engineering

Koç University

August, 2014

ABSTRACT

Barcode technology is an important concept for product identification and tracking. However, conventional barcodes cannot be used for identification of liquids. In this thesis, design and characterization of an optical sensor for identification of liquids using nano-tags are presented. The proposed system uses Quantum dots (QDs) for tagging due to their wide absorption and narrow emission spectrum, high quantum efficiency and high resistance to photo-bleaching.

Several light collection architectures are explored in the course of this thesis including imaging based system, high numerical aperture lens coupled to a single detector and fiber optic based system. This research is focused primarily on the fiber optic based system due to its distinct advantages in terms of cost, mobility and sensitivity.

The proposed fiber optic sensor consists of a fiber optic probe, a detection unit and illumination unit and a signal processing unit. Through detailed optimization of each block in the system, quantum dots can be detected in sub-pM concentrations in transparent liquids such as water. On the other hand, detection of nano-tags in non-transparent liquids is rather challenging due to complex interactions between the medium and the quantum dots. In this thesis research, a novel background subtraction algorithm is implemented to overcome this problem. This algorithm achieved to extract pure quantum dot signal from the readings with a detection limit in the 100 pM range. The optical performance of the system is simulated by using Monte Carlo method for quantum dots dispersed liquids. The simulations results show close correlation with the measurement data. The results obtained are far beyond the state-of-the art and has potential to open new research directions to use quantum dots for in-line monitoring of various kinds of precious liquids.

ÖZETÇE

Barkod teknolojisi ürün tanımlama ve takibi için önemli bir kavramdır. Bununla birlikte, geleneksel barkod teknolojisi, sıvıların tanımlanması için kullanılamaz. Bu tezde, nano-etiketler kullanarak sıvıları tanımlayan optik sensörün tasarımı ve karakterizasyonu anlatılmıştır. önerilen sistemde, geniş absorpsiyon ve emisyon spektrumu, yüksek kuantum verimi ve florışıldama bozulmasına karşı yüksek direnci nedeniyle, etiketleme için Kuantum noktacıkları (QDs) kullanılmaktadır.

Bu tezde, görüntüleme tabanlı sistem, tek dedektöre bağlanmış yüksek sayısal açıklığa sahip olan lens ve fiber optik tabanlı sistem olmak üzere farklı ışık toplama mimarileri incelenmiştir. Bu araştırma, maliyet, taşınırlık ve hassasiyet açısından belirgin avantakları olan fiber optik tabanlı sistem üzerine odaklanmıştır.

Önerilen fiber optik sensör, bir fiber optik kablo, bir algılama ünitesi ve bir aydınlatma birimi ile bir sinyal işleme biriminden oluşmaktadır. Sistemdeki her bir bloğun detaylı optimizasyonu ile, su gibi saydam sıvılar içinde pM altı konsantrasyonlarında kuantum noktacıkları saptanabilmektedir. Öte yandan, saydam olmayan sıvılar içinde nano etiketlerinin tespiti, ortam ve kuantum noktacıkları arasındaki karmaşık etkileşimler nedeniyle oldukça zordur. Bu tez araştırmasında, bu sorunu aşmak için, yeni bir arka plan çıkarma algoritması uygulanmaktadır. Bu algoritma, 100 pM seviyesinde bir algılama sınırı ile saf kuantum noktacığı sinmyalini yapılan okumalardan ayrıştırabilmiştir. Sistemin optik performansı sıvılar içinde dağılmış kuantum noktaları için Monte Carlo yöntemi kullanılarak simüle edilmektedir. Simülasyon sonuçları ölçüm verileri ile yakın korelasyon göstermektedir. Elde edilen sonuçlar, günümüz teknolojisiyle yapılan sistemlerin sonuçlarından çok daha iyi ve çeşitli değerli sıvıların, hat üzerinde izlenmesi için kuantum noktacıkları kullanımı yolunda, yeni araştırmalara yön vermek için potansiyele sahiptir.

ACKNOWLEDGMENTS

I would like to thank Prof. Hakan Urey for helping me with his creative ideas through out my research. His ability to think differently helped me a lot and make my research more interesting. I would also like to thank Dr. Emre Heves and Dr. Fehmi Civitçi for their tremendous helps. They have been not only research colleagues but also friends to me. I would like to thank Dr. Vedat Akgün and Quantag for letting me see and learn the industrial part of research.

It would have been impossible to complete my studies without the help of my colleagues and good friends at OML. Beside his helps, I want to thank Dr. Kaan Akşit for appreciating my bad jokes. I am also thankful to Assoc. Prof. Göksenin Yaralıoğlu and Assoc. Prof. Funda Yağcı Acar for taking part in my thesis committee.

I would like to thank all my home-mates Şansal Başaran, Sinan Hamulu, Ahmet Mungan and Muhammed Ali Mungan for their support. I would also like to thank Galatasaray and especially Didier Drogba for their efforts.

Last but not least, I want to thank Simin Görgülü for supporting me without questioning my attitude and believing in me since the beginning of my studies.

TABLE OF CONTENTS

LIST OF TABLES

LIST OF FIGURES

NOMENCLATURE

a	:	Particle Diameter
b	:	Threshold for photon weight
c_c	:	Cladding Thickness of the Collection Fiber
c_i	:	Cladding Thickness of the Illumination Fiber
cm	:	Centimetre
d_c	:	Core Diameter of the Collection Fiber
d_i	:	Core Diameter of the Illumination Fiber
d_s	:	Distance Between Illumination and Collection Fiber
EM	:	Electromagnetic
FFT	:	Fast Fourier Transform
K	:	Calibration Constant
m	:	Relative Refractive Index
mm	:	Millimetre
M_h	:	Height of the Light Scattering Medium
M_l	:	Length of the Light Scattering Medium
M_w	:	Width of the Light Scattering Medium
MC	:	Monte Carlo
MFP	:	Mean Free Path
n	:	Number of Particles in Unit Volume

NA	:	Numerical Aperture
ND	:	Optical Density Filter
nm	:	Nanometer
PDF	:	Probability Density Function
PD_*	:	Power Measured by Photodetecor at "*" nanometers
ppm	:	Parts Per Million
ppb	:	Parts Per Billion
r	:	Coordinate in cylindrical coordinates
RGB	:	Red Green Blue
RMS	:	Root Means Square
ROC	:	Radius of Curvature
s	:	Photon Travel Distance
SNR	:	Signal to Noise Ratio
TIA	:	Transimpedance amplifier
QD	:	Quantum Dot
QE	:	Quantum Efficiency
QSH	:	Water Soluble Quantum Dot
QPP	:	Organic Soluble Quantum Dot
W	:	Weight of photon
x	:	Coordinate in Cartesian coordinates

x'	:	Updated x coordinate
x^*	:	Relative size parameter
y	:	Coordinate in Cartesian coordinates
y'	:	Updated y coordinate
z	:	Coordinate in Cartesian coordinates
z'	:	Updated z coordinate
ε	:	Uniformly distributed Random Variable in the interval [0,1]
θ	:	Coordinate in cylindrical coordinates
μm	:	Micrometre
μ_t	:	Interaction Coefficient
μ_x	:	Directional Cosine in x direction
μ_y	:	Directional Cosine in y direction
μ_z	:	Directional Cosine in z direction
μ'_x	:	Updated Directional Cosine
μ'_y	:	Updated Directional Cosine
μ'_z	:	Updated Directional Cosine
σ_{eff}	:	Effective Cross Section
σ_{abs}	:	Absorption Cross Section
σ_{sc}	:	Scattering Cross Section
ψ	:	Coordinate in spherical coordinates

Chapter 1

INTRODUCTION

1.1 Barcoding and Applications

Barcoding is widely used among manufacturers to identify and track their products in order to prevent counterfeiting, product adulteration, unauthorized distribution etc. Product tracking is first proposed in 1948 by Bernard Silver [8]. The aim of the project was to read the product information during the check out and to monitor the stocks in real time. Using this information, manufacturer would be able to optimize the supply chain to maximize the profit. First approach to the problem was to use an ultraviolet ink to determine the code. However, this approach was not feasible because of the instability and the cost of the material. In addition to these disadvantages, ink could be removed easily [9].

A better solution is introduced by Bernard Silver and Norman J. Woodland in their patent called "Classifying Apparatus and Method" [10]. They invented an optical reader containing scanner, light source and a photo detector. Sensor measures the reflectance of scattered light from the barcode. Since the barcode has black rectangles with different widths, output signal can be processed as a pulse modulated signal, where the pulse widths contain product information. First generated barcode is shown in figure 1.1. [10]

1.2 Barcoding in Liquids

Barcoding liquids cannot be accomplished by using the same technology used for solid products, unless labelling the solid box, in which the liquid is kept, is

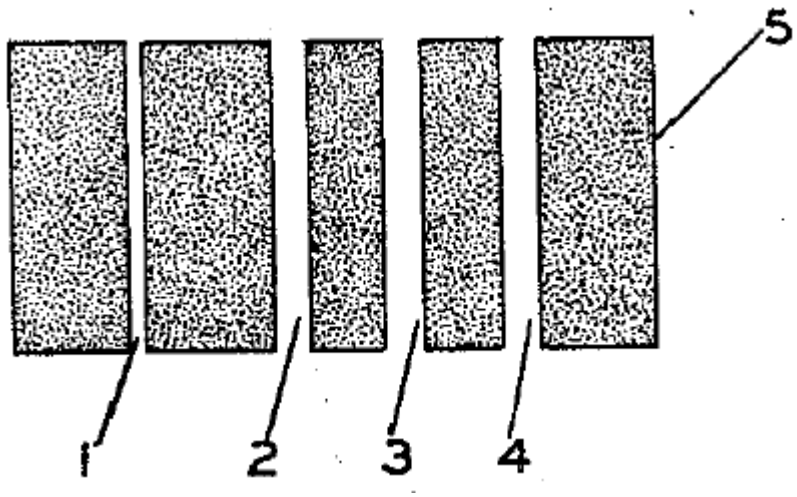

Figure 1.1: First Barcode

sufficient. A solution for liquid products can be to label the product itself. There are several technologies for tagging liquids including optical encoding, chemical encoding, graphical encoding, electronic encoding and physical encoding [11]. These technologies are briefly explained in the following chapters.

1.2.1 Optical Encoding

Liquids are encoded using the optical information of the added particles. There are several optical measurement methods for extracting spectrum information including absorbance, reflectance, fluorescence, infrared and Raman spectroscopy [12]. One application is functionalizing viruses with fluorescence dyes in order to detect them. Lukacs Z. showed simultaneous determination of ion of HIV antibodies, hepatitis C antibodies and hepatitis B antigens [13]. Same fluorescence sensing method is also used in the sensors described in this thesis. Tagging agents are excited and their fluorescence signal is detected. Mechanism of fluorescence and other optical transduction methods are shown in figure1.2 [14]. Energy of the photon is absorbed by the electron. Electron changes its energy state with the absorbed energy and then, it comes back to its initial energy level by emitting a photon.

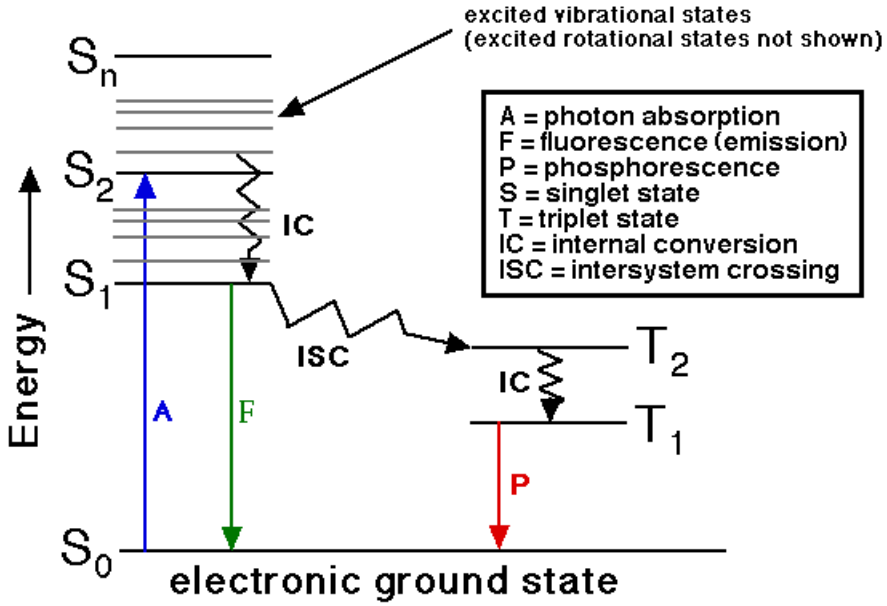

Figure 1.2: Mechanism for Fluorescence Emission

Emissions from different fluorescent particles have two properties for code generation; wavelength and intensity. Number of emission peaks is equal to the number of particles types used in the system. Intensity of the specific wavelength is determined by the concentration of the corresponding particle type. Total number of codes, can be calculated by,

$$C = N^M - 1 \tag{1.1}$$

where C is the total number of codes, M is the total number of fluorescent particles and N is the total intensity level [11]. Using a sensitive sensor and sufficient amount of fluorescent particles, it is possible to generate thousands of codes. Labelling using quantum dots is a good example to this application [15]. Depending on the spectral and intensity resolution of the sensor, total number of particle types and intensity levels can be increased. However, as the components increases, more complex deconvolution techniques should be used to extract the desired fluorescence information [16]. Han et.

al described a tagging system containing 3 different quantum dots and 10 different intensity levels. Codes were generated by inserting specific amount and type of quantum dots into the beads. Code readout of the system is shown in the figure 1.3 [15].

In this thesis liquids are tagged using the same technique. In addition, effect of the media's emission is corrected by post-processing which will be discussed in the following sections.

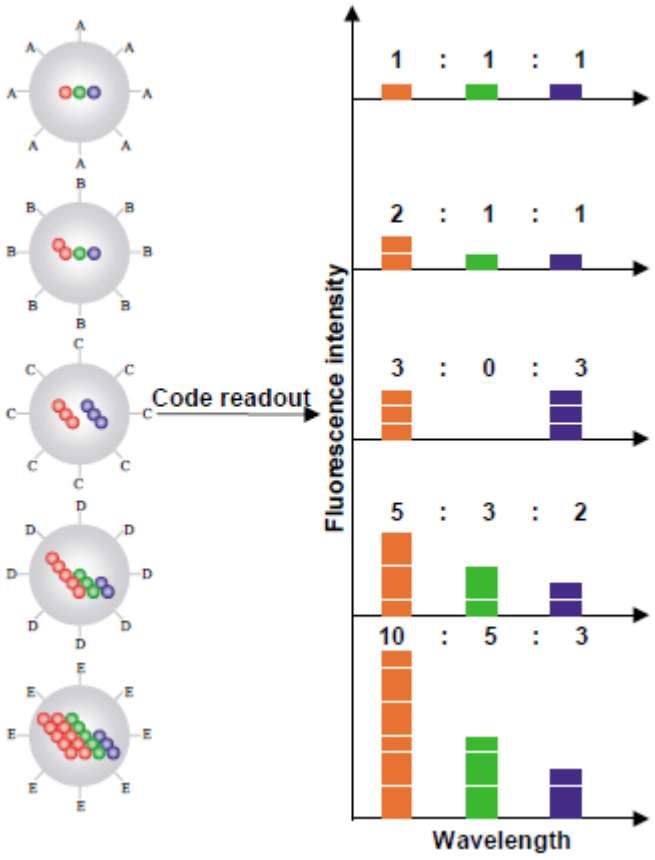

Figure 1.3: Spectral Barcoding

1.2.2 Chemical Encoding

Magnetic nanoparticles can be used to label liquids. If the particles are engineered in a way that they only attach to a certain type of molecule, they can be seperated using their difference in magnetic susceptibility. [17] In this thesis, magnetic manipulation of particles is also studied and will be mentioned in chapter 2.1.

1.2.3 Graphical Encoding

Graphical encoding of liquids is similar to fluorescence encoding. The main difference between these methods is the number of parameters that can be used to generate codes. In fluorescence encoding, the variables are emission peaks and intensity. However in the graphical encoding, in addition to aforementioned variables, spectral placement of the emission peaks of the fluorescent particles can also be used. This approach increases the total number of codes drastically while making the sensing mechanism more expensive and sophisticated. An exemplary graphically encoded particle is shown in figure 1.4 [18].

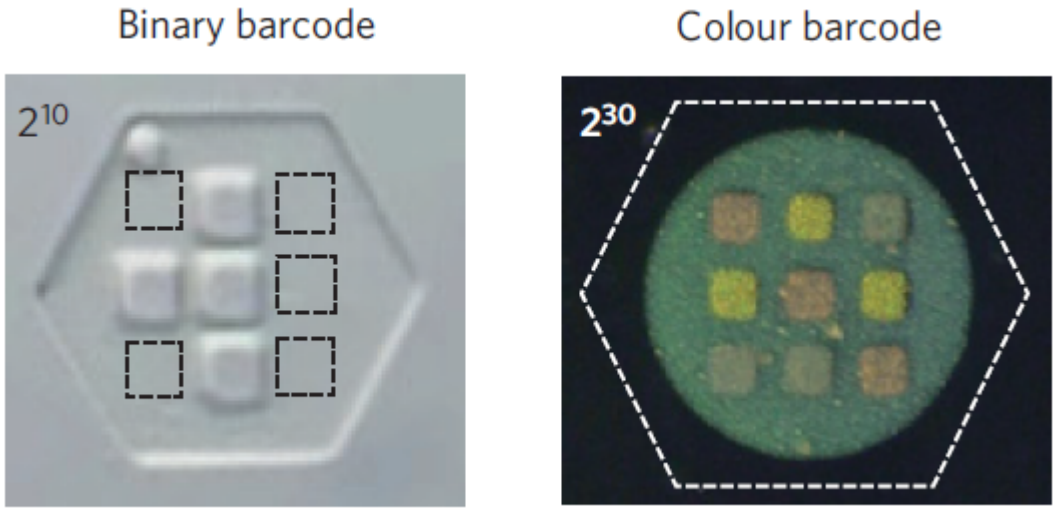

Figure 1.4: Two graphically encoded beads, size of the beads are 10μm

.

Size of the particles shown in the figure 1.4 are in the order of 10μm. They are created in a flow line. Graphical patterning is done by illuminating the structure with UV light and modulating the field using spatial light modulator. Total number of barcode for two different cases are shown in figure 1.4.

1.2.4 Electronic Encoding

Tagging of liquids using radio frequency is first studied by two groups [19, 20]. The micro devices used for labeling have RF transponders. Size of each device is $250x250x100\mu m$ and it responds uniquely to a RF pulse [11]. Number of codes that can be generated is very high. For further improvement, memory can also be added so that history of the particle can also be tracked or updated. However, although the devices are chemically inert, it is impossible to use them in multiplexed assays because of the size of the devices.

1.2.5 Physical Encoding

Separation of particles which are used for labelling the liquids can also be done using the size and the magnetic permeability of the particle. Size separation is widely done by adding magnetic nano particles to the solution because, magnetic force is proportional to size. [21] This method will be explained in detail in section 2.1.

1.3 Difference Between Quantum Dots and Fluorescent Dyes

Tagging of the liquids can be done using the methods described in section 1.2. In this thesis, main focus is on the detecting the tagging information by measuring the fluorescence signal of fluorescent particle tagged liquids. There are two main particles that can be used as fluorescence markers; quantum dots and organic dyes. Quantum dots are nanometer sized semiconductors with unique optical properties. Details are explained in chapter 1.4.

Table 1.1 shows comparison of some properties of quantum dots and organic dyes. In the application of tagging liquids, several of these properties are very important

and affects the readout design. First parameter is the emission bandwidth of the particle. Several fluorescent particles will be used to dig the barcode information into liquid and the spectral overlap of the emissions of the particle should be as low as possible. As seen from table 1.1, quantum dot is a better candidate for tagging. Another important property is the absorption of the particle. Quantum dots have wide absorption spectra while organic dyes have discrete absorption spectra. In order to excite a liquid tagged by multiple organic dyes, multiple excitation sources are necessary. If the total number of quantum dots in the system is updated, every sensor should also be updated at the same time. In addition, having an excitation source in the system increases its cost and complexity. Third important property to be discussed is the resistance to photobleaching. Photobleaching occurs when the particle is excited for a long time. Fluorescence of organic dyes vanish fastly after a few fluorescence measurement experiments. Particles can also be excited by ambient light and if they are not resistant to photobleaching, their fluorescence signal will degrade over time and it will be impossible to extract the code information.

Considering the aforementioned advantages, in this thesis, quantum dots are used for fluorescence measurements and tagging.

Property	**Organic Dye**	**QD**[a]
Absorption spectra	Discrete bands, FWHM[b] 35 nm[c] to $80-100nm$[d]	Steady increase toward UV wavelengths starting from absorption onset; enables free selection of excitation wavelength
Molar absorption coefficient	$2.5*10^4-2.5*10^5 M^{-1}cm^{-1}$(at long-wavelength absorption maximum)	$10^5-10^6 M^{-1}cm^{-1}$at first exitonic absorption peak, increasing toward UV wavelengths; larger (longer wavelength) QDs generally have higher absorption
Emission spectra	Asymmetric, often tailing to long-wavelength side; FWHM, $35nm$[c] to $70-100nm$[d]	Symmetric, Gaussian profile; FWHM, $30-90nm$
Stokes shift	Normally$<50nm$[c], up to $>150nm$[d]	Typically $<50nm$ for visible wavelengthemitting QDs
Quantum yield	$0.5-1.0$ (visible[e]), $0.05-0.25$ (NIR[e])	$0.1-0.8$ (visible), $0.2-0.7$ (NIR)
Fluorescence lifetimes	110 ns, mono-exponential decay	$10-100$ ns, typically multi-exponential decay
Two-photon action cross-section	$1*10^{-52}-5*10^{-48}cm^4 s\ photon^{-1}$ (typically about $1*10^{-49}$ $cm^4 s\ photon^{-1}$	$1*10^{-52}-5*10^{-48}$
Solubility or dispersibility	Control by substitution pattern	Control via surface chemistry (ligands)
Binding to biomolecules	Via functional groups following established protocols Often several dyes bind to a single biomolecule Labeling-induced effects on spectroscopic properties of reporter studied for many common dyes	Via ligand chemistry; few protocols available Several biomolecules bind to a single QD Very little information available on labeling-induced effects
Size	0.5 nm; molecule	660 nm (hydrodynamic diameter); colloid
Thermal stability	Dependent on dye class; can be critical for NIR-wavelength dyes	High; depends on shell or ligands
Photochemical stability	Sufficient for many applications (visible wavelength), but can be insufficient for high-light flux applications; often problematic for NIR-wavelength dyes	High (visible and NIR wavelengths); orders of magnitude higher than that of organic dyes; can reveal photobrightening
Toxicity	From very low to high; dependent on dye	Little known yet (heavy metal leakage must be prevented, potential nanotoxicity)
Reproducibility of labels (optical, chemical properties)	Good, owing to defined molecular structure and established methods of characterization; available from commercial sources	Limited by complex structure and surface chemistry; limited data available; few commercial systems available
Applicability to single-molecule analysis	Moderate; limited by photobleaching	Good; limited by blinking
FRET	Well-described FRET pairs; mostly single-donor single-acceptor configurations; enables optimization of reporter properties	Few examples; single-donormultiple-acceptor configurations possible; limitation of FRET efficiency due to nanometer size of QD coating
Spectral multiplexing	Possible, 3 colors (MegaStokes dyes), 4 colors (energy-transfer cassettes)	Ideal for multi-color experiments; up to 5 colors demonstrated
Lifetime multiplexing	Possible	Lifetime discrimination between QDs not yet shown; possible between QDs and organic dyes
Signal amplification	Established techniques	Unsuitable for many enzyme-based techniques, other techniques remain to be adapted and/or established

Table 1.1: Comparison of properties of organic dyes and QDs [1]. Properties of organic dyes are dependent on dye class and are tunable via substitution pattern. Properties of QDs are dependent on material, size, size distribution and surface chemistry. [a]Emission wavelength regions for QD materials (approximate): CdSe, $470-660nm$; CdTe, $520-750nm$; InP, $620-720nm$; PbS, $>900nm$; and PbSe, $>1000nm$. [b]FWHM, full width at half height of the maximum. [c]Dyes with resonant emission such as fluoresceins, rhodamines and cyanines. [d]CT dyes. [e]Definition of spectral regions used here: visible, $400-700nm$; and NIR, $>700nm$.

1.4 Properties of the Quantum Dots

Quantum dots are semiconductor particles with dimensions less than 10 nm. Particles preserve the propoerties of the bulk material and because of the dimensions of the particles, electrons and holes are confined in all dimensions. Semiconductor colloidal QDs composed of very small crystals of semiconductor material surrounded by a layer of organic ligands that are chemically bonded to the surface of the crystal, providing electronic and chemical passivation of dangling bonds and solubility in polar or non-polar solvents, determined by the ligand species.

The most crucial property of these quantum dots are the quantum confinement phenomena. If the size of the semiconducting crystal is reduced to the point where the electron and/or hole wave functions begin to be squeezed into a region smaller than their characteristic Bohr radius, their allowed Eigen energies increase compared to that of bulk. Bohr radius, r_b is calculated by

$$r_b = \varepsilon \frac{m}{m^*} r_{hydrogen} \tag{1.2}$$

where ε is the dielectric constant of the material, $r_{hydrogen}$ is the Bohr radius of the hydrogen atom, m is the mass and m^* is the effective mass of the excited particle [22]. A first order approximation to the size-quantized electronic properties of a semiconductor quantum dot is provided by the particle-in-a-sphere model in which QD is modeled as a small sphere of semiconducting material and the perfect insulator surrounding it. The particle-in-a-sphere model predicts an inverse-squared dependence of quantum dot bandgap, $E_{g,QD}$ on the radius of the nanocrystal, [22]

$$E_{g,QD} = E_g + \frac{\hbar^2 \Pi^2}{2R^2} [\frac{1}{m_e^*} + \frac{1}{m_h^*}] \tag{1.3}$$

where E_g is the bulk semiconductor bandgap, $\hbar$ is reduced Planck constant and m_e^* and m_h^* are the effective masses of electrons and holes in lattice, respectively. Thus, decreasing quantum dot size leads to an increase in bandgap and a shift of photon absorption and emission maxima towards shorter wavelengths, compared to the bulk

semiconductor material.

The bandgap of a nanocrystal begins with that of bulk material and subsequently shifts up in energy as the size gets smaller. For instance, CdSe and CdS can be tuned across the entire visible spectrum by varying the bandgap energy from 1.8 eV to 3.1 eV (corresponding to a shift from 400 nm to 700 nm), a dramatic change considering the bulk bandgap energy of CdSe is 1.73 eV. Figure 1.5 shows absorbance spectrum shift of CdSe as the particle size changes. [23].

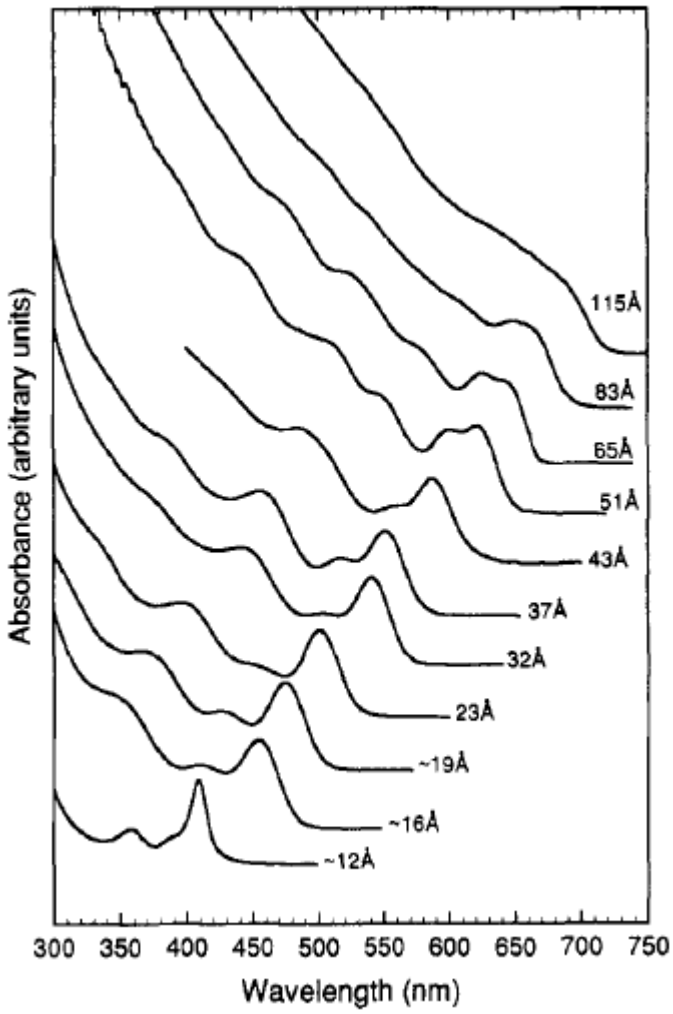

Figure 1.5: Room temperature optical absorption spectra of CdSe nanocrystallites dispersed in hexane and ranging in size from 12 to 115 Å.

Figure 1.6 shows the change of emission wavelength and size of the quantum dot [24]. According to equation 1.3, as the size of the quantum dot increases, energy of the emitted photon decreases.

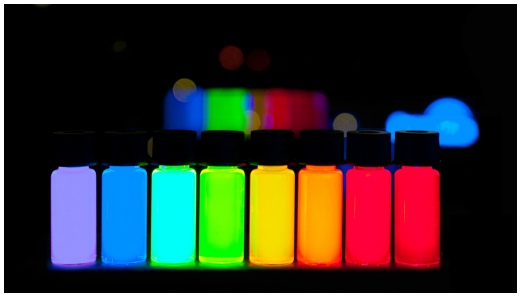

Figure 1.6: Photo of ZnCdSeS alloyed Quantum Dots produced by Plasmachem. Size of the quantum dots increases from left to right [2].

1.5 Fluorescence Spectrometry

Every material has different electromagnetic radiation including fluorescent and non-fluorescent radiations therefore, by looking at this property it is possible to uniquely address every material. We will focus on fluorescent radiation. Human eye is sensitive to only small portion of this spectrum corresponding to 390 to 750 nm as shown in the figure 1.7. Spectrometers are devices, which are used to measure the intensity of light over the electromagnetic spectrum. For sensing quantum dot emissions, fluorescence spectroscopy is used. In fluorescence spectroscopy, light to be analysed passes through grating and gets detected by sensor array [25].

Han *et al.* proposed a system for reading the fluorescence information of quantum dot barcoded systems and measured their spectrums using fluorescence spectrometer. The propesed system is sensitive but bulky. In order to simplify the system, less sensitive but mobile systems can be used. For example if the interested wavelengths are already defined in the system, user can use specific color filters to match the wavelengths. This technology was used with CCD (charge couple device) to detect red, green and blue colors respectively in order to create an image [26]. Filters with

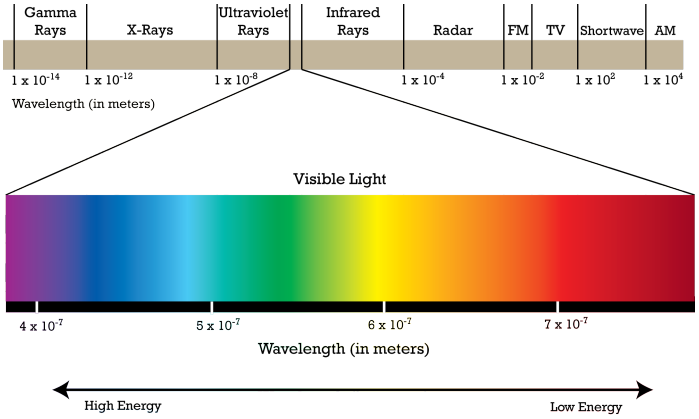

Figure 1.7: Electromagnetic Spectrum

different pass bands can be used in the system to detect different portions of the spectrum. L. G. Glasser and D. J. Troy implemented a system containing a turning mechanical disk with band pass filters [27].

Although the ordinary fluorescence spectrometers have good resolution and sensitivity, they are bulky and expensive. Using color filters can decrease complexity of the sensor array by only examining a portion of the spectrum. Guiding light to the detectors and using color filters can greatly decrease the complexity of the system creating cheap, mobile and alignment free sensor. If fibers are used for sample illumination and back scattered light collection, the distance between source and sample decreases, increasing the light collection efficiency of the system. This configuration is implemented by several groups. Measured signals can change depending on the application. Raman signal [28], fluorescence from tissue [29] or emission of dye [30] can be measured and quantified.

1.6 Contribution of the thesis

Main contributions of this thesis are in the design of very sensitive, mobile, low cost fiber optic fluorescence sensor and in modelling of this system with Monte Carlo method. From the contributions of this thesis, Quantag Nanotechnology Research and

Manufacturing Inc. is established.

We showed several preliminary fluorescence sensor designs and showed that fiber optic sensor is the best one for our application. Minimum detectable quantum dot concentration in water is measured as 1 pM. A patent describing the system is folded [31].

Thesis work starts with background information about the sensors, quantum dots and tagging of liquids. In chapter 2 preliminary sensor designs and results are given. At the last section of chapter 2, detailed explanation of fiber optic sensor is given. Each part is explained separately. In chapter 3, Monte Carlo simulations are given. Detailed explanation of each step of the algorithm and corresponding results are explained. Simulation results are matched to the experimental results, which are measured in non-emissive liquid, with a scale factor of 0.104.

In the last chapter, we measured quantum dot emission in highly absorbent and emissive liquids. Lowest quantum dot concentration of 100 pM is reached. In order to measure low concentration levels, an algorithm called "background subtraction algorithm" is introduced in to the system which distinguishes the fluorescence of the liquid from the emission of the quantum dot.

To conclude, throughout the investigation of several light collection architectures, fiber based system is found out to be the best option for our application. Using fiber based system, minimum detection limit of 1 pM in water is reached. The relation between the concentration and collected quantum dot emission is linear. So it is possible to generate fluorescence codes. Measurement is also done in absorbent mediums. By applying background subtraction algorithm, detection limit of 100 pM reached.

Chapter 2

OPTICAL SENSOR DESIGN

Quantum dots are nanocrystals made of semiconductor materials. They emit photon at specific wavelengths according to their radius, under illumination of a shorter wavelength photon as described in chapter 1.4. Emission peak and intensity of quantum dots are two main parameters for tagging liquids. Different quantum dot types correspond to different emission peaks and their intensity is proportional to their concentration. For example, in a system with 5 quantum dots and 10 intensity levels, there are 10^5 different tags. Figure 2.1 shows sample emission spectrum of a tagged liquid according to aforementioned system.

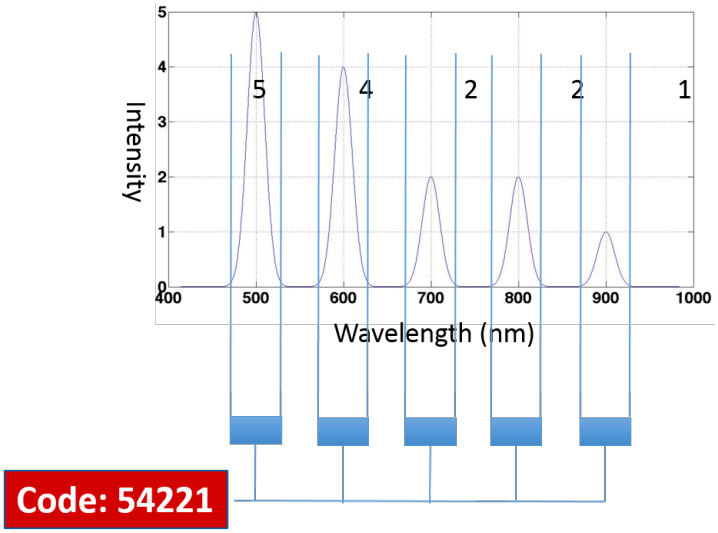

Figure 2.1: Sample emission spectrum of quantum dot tagged liquid in a coding system containing 5 quantum dots and 10 intensity levels

All sensors have similar operating mechanism as shown in figure 2.2.

Sample is illuminated by a source. Since the system's input is the fluorescence of the

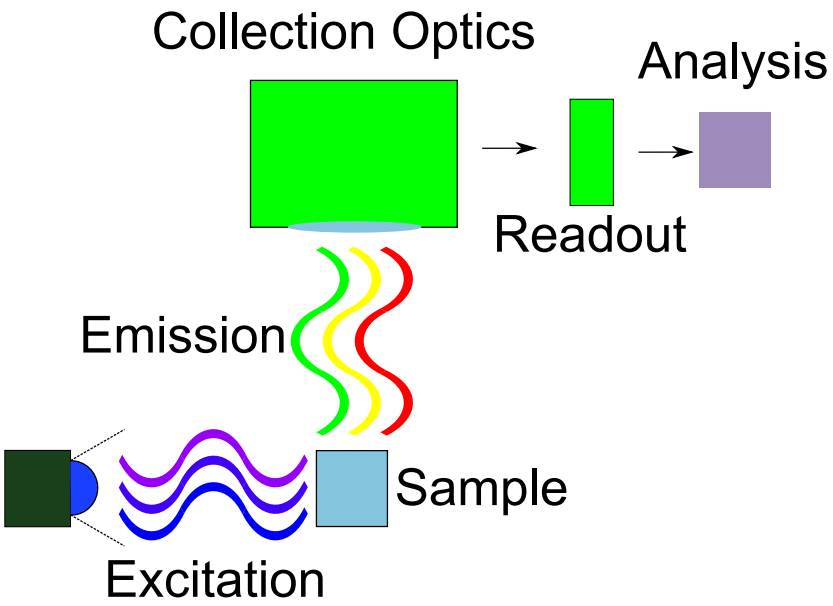

Figure 2.2: Sensing System Mechanism

sample, excitation wavelength is shorter than the emission wavelength of the quantum dots. Emitted light from sample is collected by collection optics and fluorescence information is digitized. Using post-processing techniques, information is transformed into tag information.

For this thesis we have considered several sensor designs for emission detection of the quantum dots. These designs differ from each other depending on their collection optics and readout systems. These designs are;

- Magnetic Concentrator
- CCD Based Barcode Reader
- Microscope Lens Based Barcode Reader
- Fiber Based Barcode Reader

Performance of each design is discussed at the end of subsections based on their optical collection efficiency, setup complexity and fluorescence sensitivity.

Different quantum dots are used for system characterization. These are KUdots (quantum dots synthesised in Koc University in Polymer and Nanomaterial Research Group) and commercial quantum dots from Ocean Nanotech Inc.

2.1 Magnetic Concentrator

Cost of the system is proportional to the amount of quantum dots used in the system. One option for decreasing the cost is to collect particles at one location to increase the local concentration of the quantum dots to measure the emission signal with a higher SNR. In order to collect the quantum dots in the fluid, an external force should be applied. In this chapter, magnetic capturing of the quantum dots is discussed. However, quantum dots are not magnetic and cannot be moved by applying magnetic field. To overcome this, quantum dots attached to iron oxides particles should be synthesised. In the experiments explained in this chapter, iron oxide particles were used.

Similar system is explained by Gao et. al [32]. In this work, quantum dots are connected to magnetic particles and movement of magnetic particles are controlled using external magnets. However, particles are not collected on the same location to increase the local concentration so as the emission intensity. Main idea of the setup is to separate particles by applying magnetic field.

In our system, flow speed and displacement of the magnetic particles should be 0 so that particles will emit light at the desired location where the system has its highest light collection efficiency. Calculation of the forces acting on the magnetic particles is described in [33]. Net magnetic force acting on a particle is;

$$F_{mag} = \frac{\Delta\chi V_p}{\mu_0}(\nabla B)B \tag{2.1}$$

where $\Delta\chi$ is the relative magnetic susceptibility between the material and the medium, V_p is the volume of the particle, μ_o is the permeability of free space, B is the magnetic field applied on the particle and ∇ is the gradient operator. From the

equation 2.1, it can be deducted that in order to have high magnetic force, susceptibility, volume or the magnetic field or its gradient should be large. For susceptibility, we are limited by the material properties. If iron oxide is used, it has a susceptibility of 720. The volume of the particle grows with the third power of its radius meaning bigger particles are easier to attract. Limitation in this property is the bead size of the nano particles. Avarage size of the quantum dots is between 2 nm and 10 nm. Attaching a 100 um iron oxide to quantum dots is not feasible since we will not be able to measure quantum dots emission intensity. Magnetic field and its gradient are the key properties in this equation that we can engineer. In order to generate high magnetic field, big coil with high current flow rate or a big magnet is needed. Only the amplitude of the field is not enough to generate the force, if the field is spatially uniform, no force is generated. To differantiate the field over the area of interest, magnetic concentrators are needed. Magnetic concentrator can be a simple triangular iron. Magnetic flux line tend to go inside the iron thus generating high magnetic gradient at the tip of the triangle. Finite element modelling based simulations are done using COMSOL. Distribution of the field is shown in figure 2.3. It can be seen that magnetic flux lines are concentrated on the tip of the object.

Second force acting on the particle is the drag force [21]. It can be calculated by;

$$F_{drag} = 6\pi r \eta u_{flow} C_w \tag{2.2}$$

where r is the particle radius, η is the viscosity of the medium, u_{flow} is the flow speed of the fluid and C_w is the geometrical constant which is related with the shape of the object in which fluid flows. By summing up two force, net force can be calculated as,

$$F_{net} = F_{mag} + F_{drag} \tag{2.3}$$

System schematic shown in the figure 2.4 is simulated using finite element modelling in COMSOL. Permanent magnet and iron concentrator is used. Magnetic particles

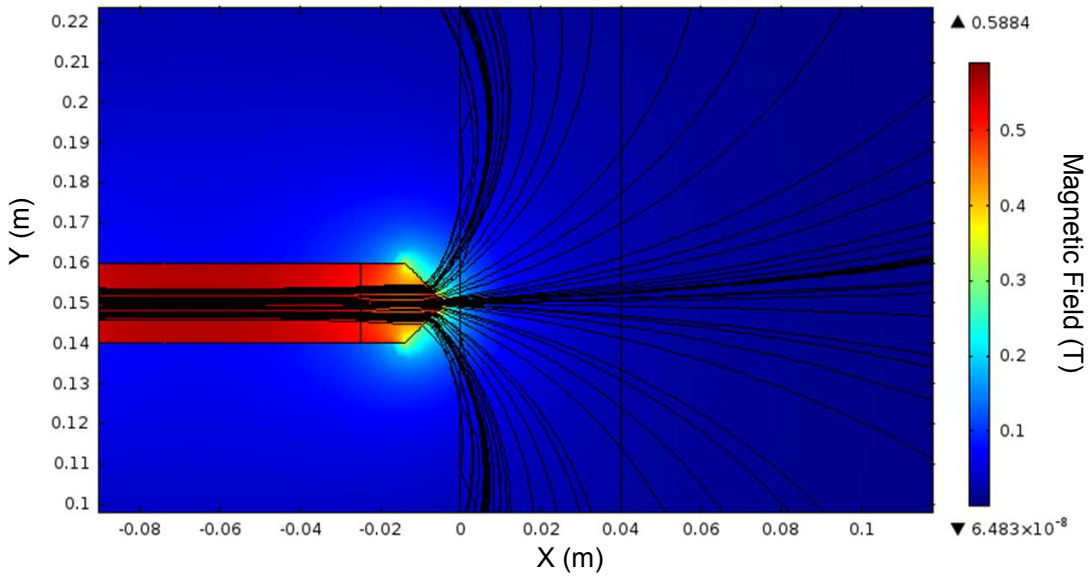

Figure 2.3: Magnetic Field Distribution

to be captured are also defined as iron particles and the fluid is defined as water. However, depending on the applications other liquids different from water such as oil also investigated. Coordinate system used in figure 2.4 is also used for the figures 2.5, 2.6, 2.7 and 2.9.

Meshing of the system is done several time to verify convergence of the solutions. In figure 2.5, different meshings can be seen. As the mesh size decreases, solutions should converge. In order to optimize the total time needed for computation and the exactness of the solution, such a comparison is necessary.

Magnetic field amplitudes of a random points from three solutions with different meshing geometries were compared. As seen in fig 2.6, as the mesh size decreases, solutions converge to a value showing that there is no need for pushing high accuracy.

Problem is solved for two different physics; fluid flow and magnetic field. Then two different solutions are combined together to calculate particle trajectories under drag force and magnetic force. Trajectories of particles flowing in fluid is shown in figure 2.7.

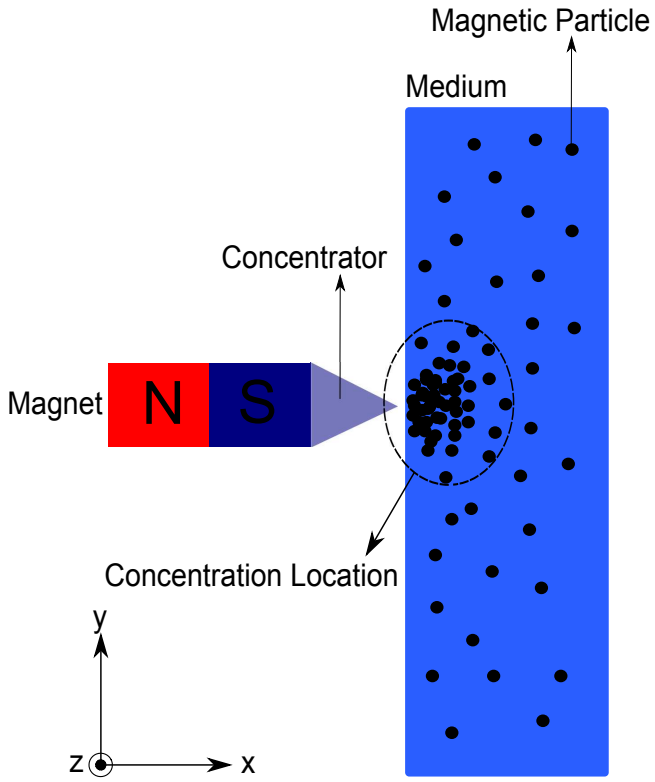

Figure 2.4: Magnetic Concentrator System

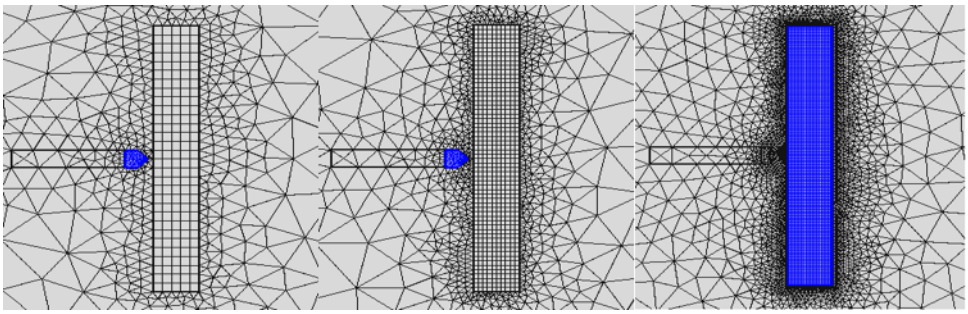

Figure 2.5: Coarse, Normal and Fine Meshing of the System

In order to verify the simulation, an experiment whose setup is shown in the figure 2.9, is conducted for particle tracking. Setup contains one camera, fluid traveling conduit, magnet and 200 μm size iron particles. Flow of particle inside the fluid is recorded and analyzed using video processing tool MaxTraq. Acceleration of particle

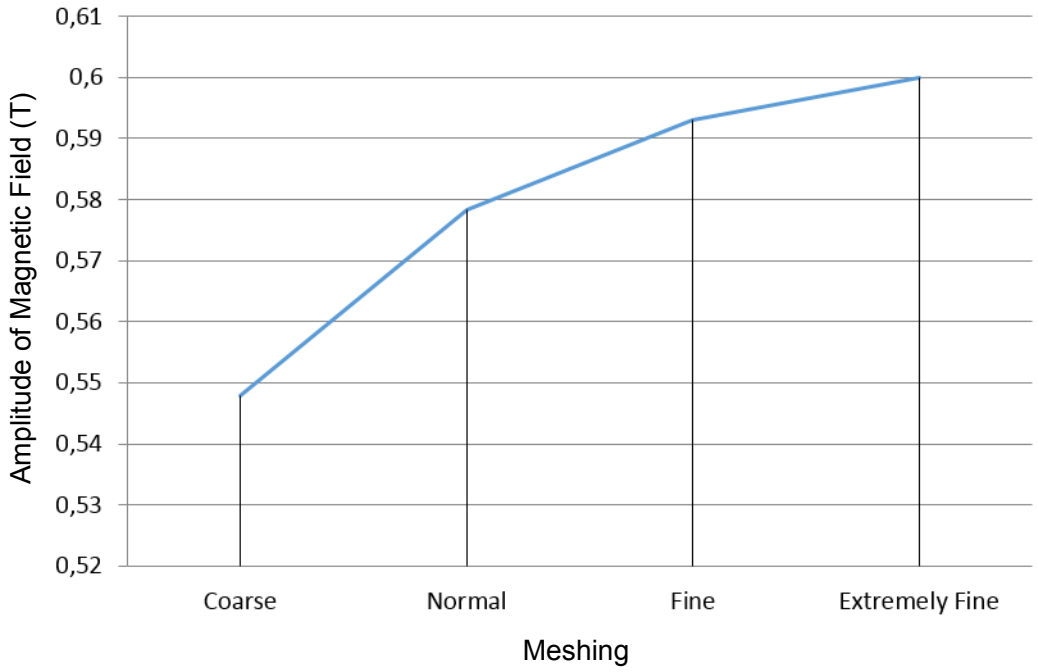

Figure 2.6: Meshing vs Amplitude of the Magnetic Field

is calculated from the video frames. Figure 2.8 shows X component of the acceleration of the particle caused by the magnetic force as 10 mm/s^2 and FEM simulation result as 11 mm/s^2. The main reason in difference between the results is caused by the size distribution of the particles used in the experiments.

In the figure 2.7, 300 nm particles are used and the flow rate is 1 mm/s. As seen from the simulation it is nearly impossible for magnetic nano particles to catch at high flow speeds. Magnetic force affecting the magnetic particle is proportional to its radius as seen from equation 2.1. Flow speed affects the drag force acting of the magnetic particle which is shown in equation 2.2. For nanometer sized particles, magnetic force cannot beat drag force and attract particles. Our hypothesis on combining quantum dots with magnetic nano particles to increase local concentration should be reconsidered.

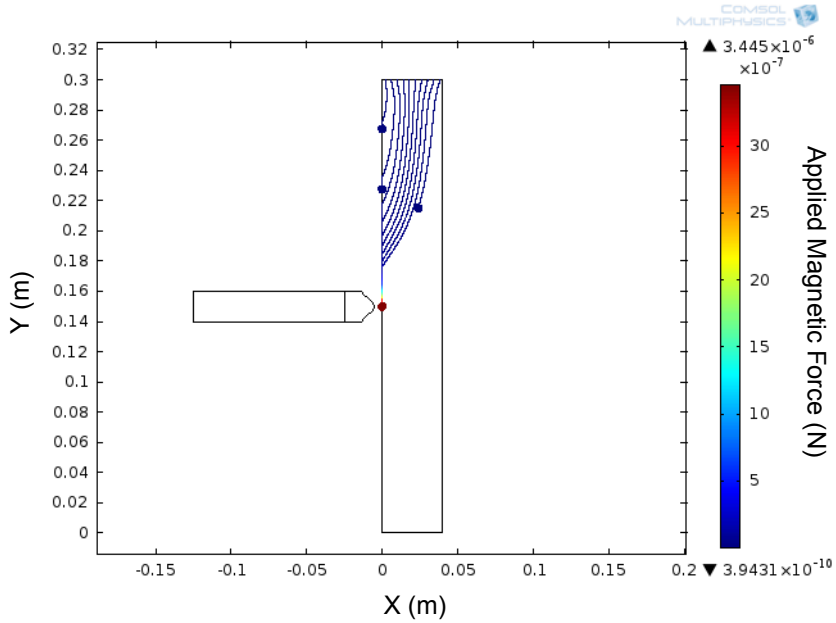

Figure 2.7: Particle Trajectories Under the Affect of Magnetic and Drag Force

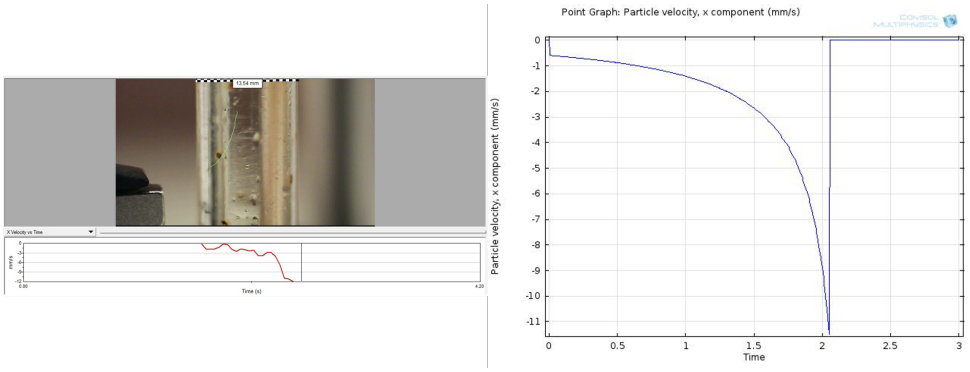

Figure 2.8: Comparison of the accelerations of the particles in x direction. (Left) The particle is traveling thorugh the channel, as the magnetic force increases, particle accelerates through the magnet. Particle trajectory is shown by green line. (Right) COMSOL simulation output, graph shows the particle acceleration in x direction.

2.2 Imaging Based Sensor

Since synthesising beads containing quantum dots and magnetic particles is hard, costly and capturing magnetic particles with diameters at nanometer range at high

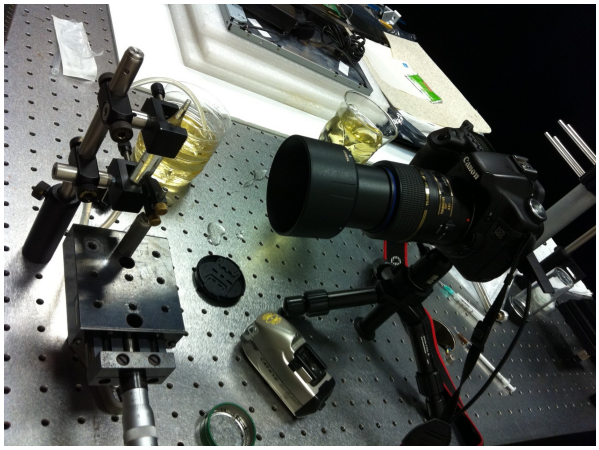

Figure 2.9: Experiment Setup for verifying particle trajectories in liquid

flow rates is nearly impossible to capture, another approach is considered in this section.

2.2.1 System Description

In this approach, aim of the sensor is to extract wavelength information of the liquid under the illumination of a excitation source. Coloured CCD cameras have pixels with red, green and blue color filters so that they can analyse red, green and blue components of the incoming light. Using the same procedure, it is possible to differentiate the quantum tagged liquids from each other by looking at the RGB components of their pictures.

System schematic is shown in figure 2.10. 5W UV source is used for illumination and coloured CCD is used for recording. At each experiment, two sets of pictures are recorded into a file. Each file contains N pictures. First set of picture is recorded with deionized (DI) water to eliminate background generated by the excitation. An algorithm is implemented using MATLAB for picture analysis. After the program is started, program shows the first picture in the file. User selects a portion of the first picture in the file for color analysis. Size of the selected portion is not important but, SNR value of the RGB components in the output figure increase with the size and

uniformity of the color distribution in the selected portion. Preferably, brightest area should be selected to have high signal to noise ratio. RGB components of first and second set for the selected portion is calculated. Their differences gives the background calibrated image. Program takes the avarage of N background calibrated figures and sums the rgb values of the individual pixels located in the selected portion. Results are normalized with respect to 255 (colors are represented with 8 bits, thus highest value is 255) and presented using bar charts. Different codes have different RGB components.

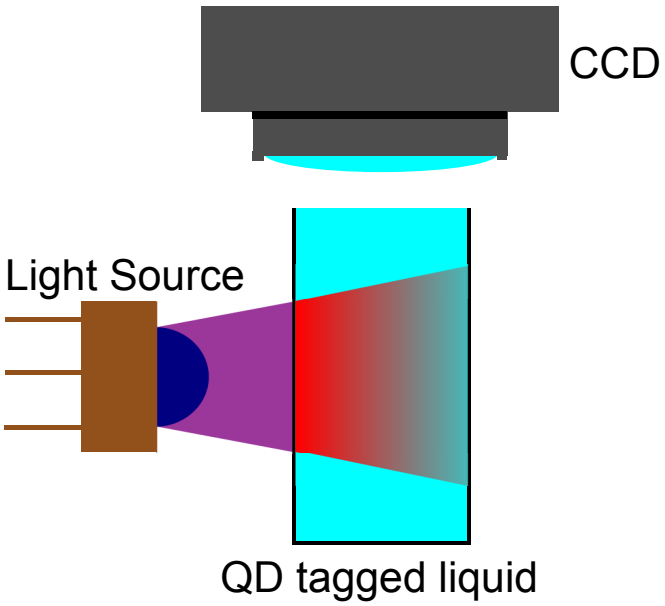

Figure 2.10: Imaging Based Sensor System

2.2.2 Results

KUdots are used for the system characterization. Aperture size of the camera is constant for all measurements. Results are discussed below.

In figure 2.11, there are 3 different results. Concentrations of the samples shown in A,B and C are 550 ppm, 55 ppm and 5.5 ppm respectively. Green is calculated as 0.8 with 30 ms exposure time while 55 ppm is measured as 0.3 with 100 ms exposure

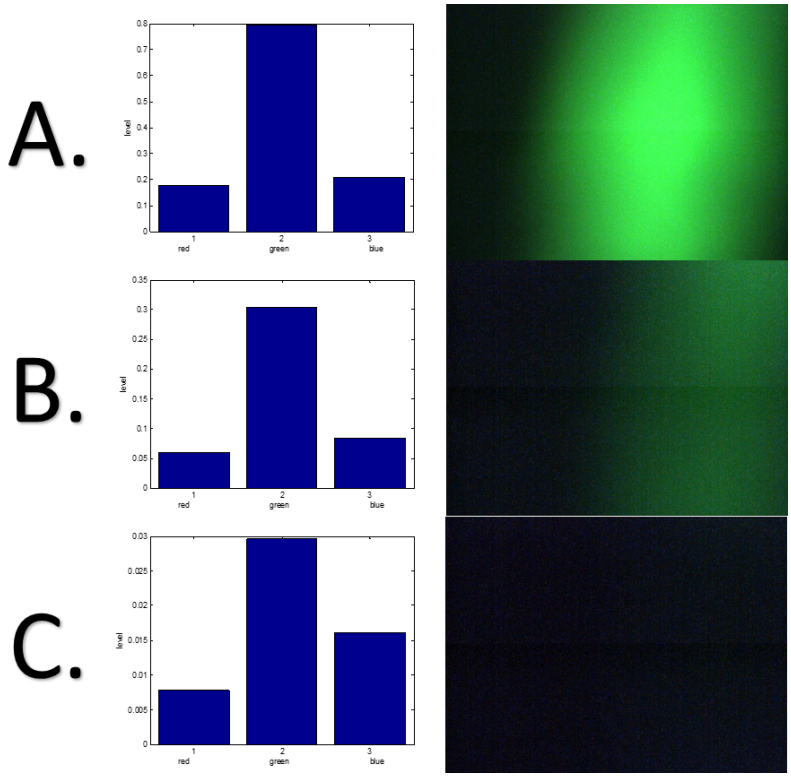

Figure 2.11: Pictures of quantum dot tagged samples under UV illumination. (A) Concentration: 550 ppm, CCD exposure: 30ms, (B) Concentration: 55 ppm, CCD exposure: 100ms, (C) Concentration: 5.5 ppm, CCD exposure: 100ms

time. Amount of light collected by the camera is linearly related with the duration of exposure time. Taking this into account normalized results are shown in table 2.1. Minimum concentration measured using this system is 5.5 ppm with KUdots. The red level in 5.5 ppm concentration is 0.06. This value is the background noise introduced by the system. Using this value, it is possible to say that SNR value of measured signal is 5 which corresponds to resolution of 1.1 ppm in concentration.

2.2.3 Conclusion

There are two main problems with this system; bulkiness of the setup and the measurement accuracy. The amount of light which can be collected by the CCD camera is limited by the imaging lens of the camera and the system is severely affected

Concentration	Exposure Time	Green Value	Normalized Green Value
550 ppm	30 ms	0.8	2.7
55 ppm	100 ms	0.3	0.3
5.5 ppm	100 ms	0.03	0.03

Table 2.1: Normalized green levels of the results shown in figure 2.11 with respect to 100 ms exposure time

by the excitation source in spite of the background calibration.

2.3 High NA Collector Based Sensor

There are several problems with the CCD based system as explained in section 2.2. It is bulky and can not be moved around easily without disturbing the alignment. More importantly, the sensitivity of the system is limited by the numerical aperture of the lens and exposure time of the camera. Another camera with better hardware can be used but since our main aim is to detect different emission peak, there is no need to make imaging. So sensitivity of the system can be pushed by measuring using single pixel of the CCD. In addition, when different sets of quantum dots, which have emissions in near infra-red region, are introduced in to the system, it is impossible to sense them using CCD since the colour filters of the CCD are not convenient.

2.3.1 System Description

To meet the requirements, which are not satisfied by the imaging based sensor, the system shown in the figure 2.12 is established. The system can be described as follows; Thorlabs DL5146 (properties of the light source will be explained in detail later in this chapter) blue-violet laser diode is used as a light source. Light coming out from the laser diode is collimated using a lens. The collimated light is sent to the microscope lens. The main reason for using the microscope lens is to have high numerical aperture so that the system will collect much more light. Emitted light from the sample is collected using the same lens and goes to the detector. There is a

color filter with center wavelength at the emission peak of the quantum dot in front of the detector.

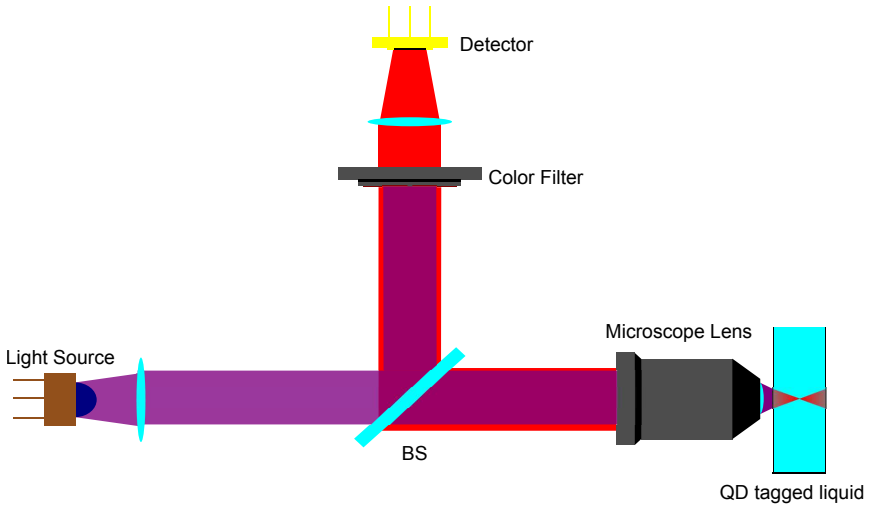

Figure 2.12: High NA Collector Based Sensor Schematic

Fluorescence signal measured by the detector is amplified using a transimpedance (TIA) amplifier. Schematic of the amplifier is shown in figure 2.13.

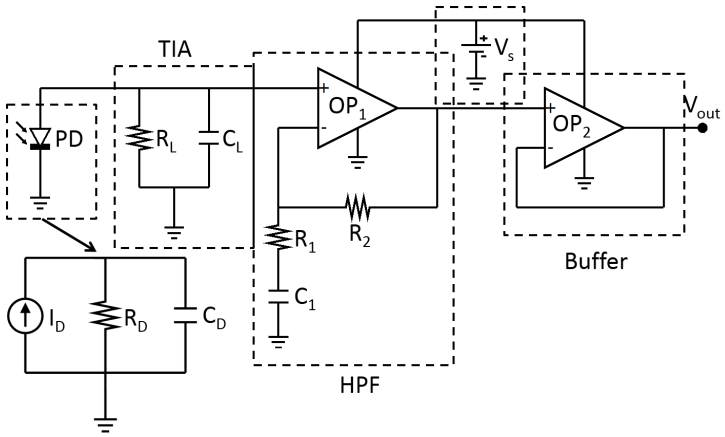

Figure 2.13: Circuit schematic of the transimpedance amplifier

Thorlabs FDS100-101S silicon photo diode is used in the circuit. It is modeled as a current source, which creates current proportional to the intensity of incident light,

resistor and a capacitor. Spectral response of the FDS100 is given in figure 2.14. as can be seen the highest response is at 950 nm.

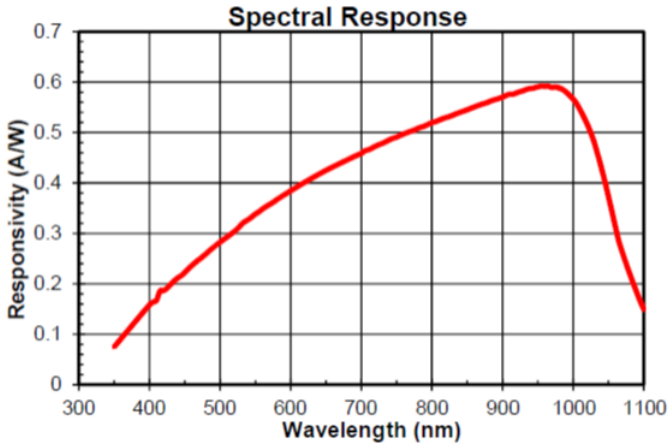

Figure 2.14: Spectral Response of FDS100 photo detector

The circuit diagram in figure 2.13 can be explained as follows; Photo detector current is converted to voltage in transimpedance amplifier part of the circuit with a load resistor. Current measured by the detector, passes through the load resistor and creates a voltage difference. This current to voltage conversion using a resistor corresponds to gain of $20x10^8$. HPF block filters the DC and low frequency components to decrease signal to bias ratio (SBR) and increase signal to noise ratio (SNR). Buffer is placed at the end of the filter to isolate system from any cascaded circuitry. Frequency analysis of the circuit is shown in the figure 2.15. There are two cut-off frequencies of the circuit located at 5 Hz and 150 Hz. Frequencies below 5 Hz and above 150 Hz are rejected by the circuit.

At the passband, circuit's gain is 166.1 dB. Any unwanted signals which have components in the pass band of the system will be amplified drastically, decreasing the signal to bias ratio. Noise performance of the circuit is also simulated. Output is shown in figure 2.16. RMS noise voltage is simulated as 25 μV. With a gain of $20x10^8$, this voltage corresponds to 12.5 fA input current which is also the system's detection limit.

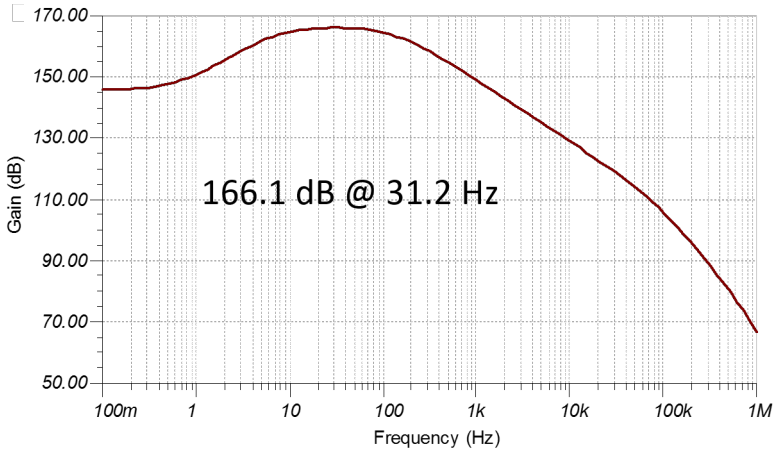

Figure 2.15: Frequency Response of the transimpedance amplifier

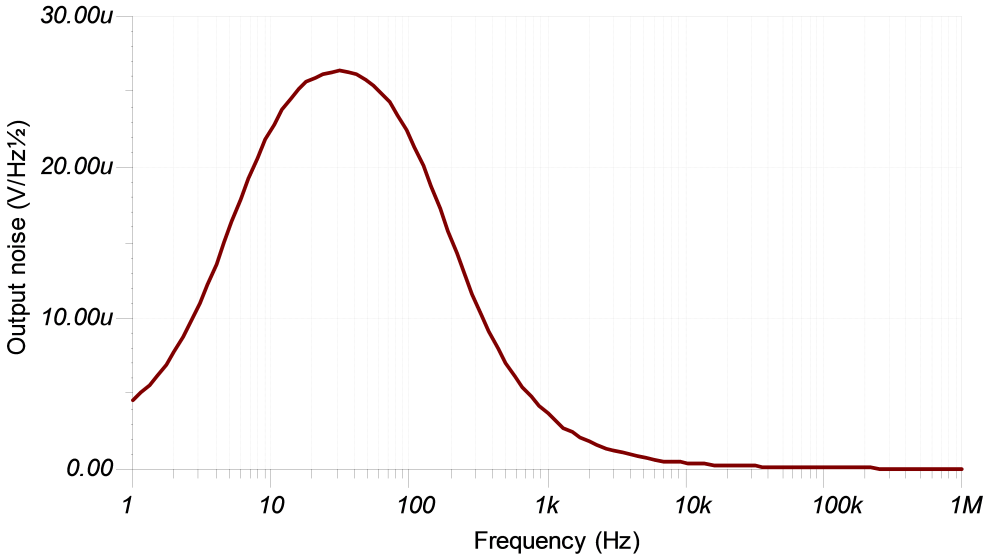

Figure 2.16: Noise Figure of the transimpedance amplifier

In order to meet the frequency response of the circuit, excitation light source is modulated at 31 Hz. In the first test results, only 50 Hz which is city line is observed at the output. Because of the high gain, it was not possible to detect the signal without shielding. Circuit placed in a aluminium box and sealed tightly. Simulation

results and measurement results are shown in figure 2.17 and figure 2.18 respectively.

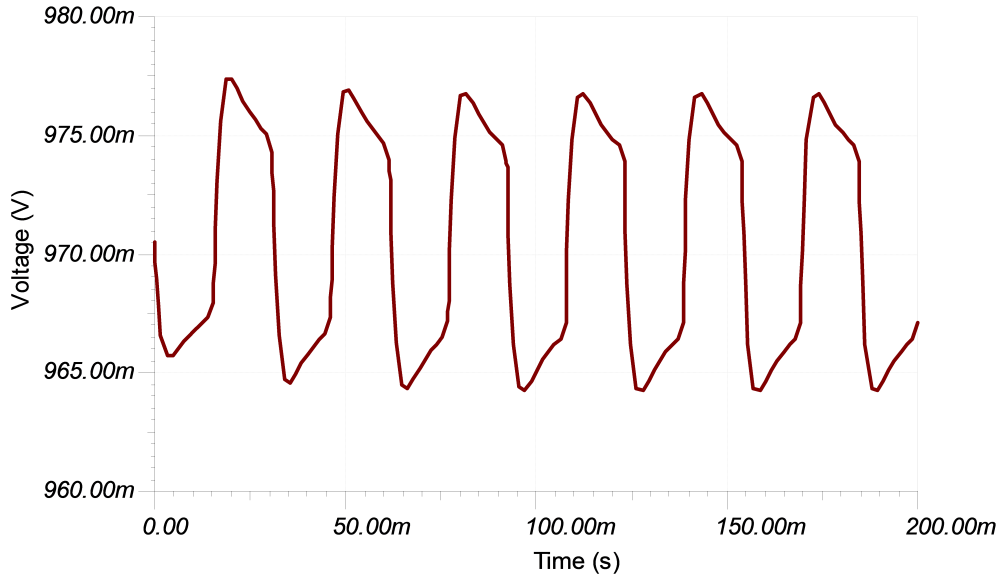

Figure 2.17: Transient Response of the Detector Circuit

2.3.2 Results

System described in the previous section is simulated in LTspice. In the simulation, 50 pA input current is applied to the system. For this input, output is 15 mV V_{p-p} and has 967 mV bias. Same system is also used for measuring emissions of quantum dots. 3 different samples were prepared using commercial quantum dots. Emission peak of the quantum dot is at 600 nm and different samples contained different concentration levels. Concentraion of final samples were 1.25 ppm, 2.5 ppm and 5 ppm. Emission measurements of these three samples are shown in figure 2.18. Output signals for 1.25 ppm, 2.5 ppm and 5 ppm are 20 mV_{p-p}, 10 mV_{p-p} and 5 mV_{p-p}. Concentration of the quantum dot is linearly proportional to the measured signal.

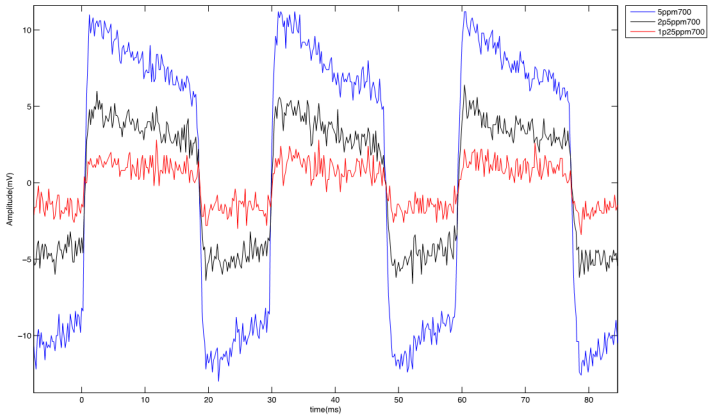

Figure 2.18: Measurement Results of Emission of Different Quantum Dot Concentrations

2.3.3 Conclusion

The sensitivity of the system is very good but the bulkiness and cost of the system is still a big problem. Apart from that, minimum detectable concentration is found 1 ppm which should be decreased to sub-ppm level. In order to solve these problems, setup shown in figure 2.12 should be reconsidered.

2.4 Fiber Based Sensor System

Main problems with the previous designs were the bulkiness, sensitivity, cost and requirement of fine alignment of the system. If the sample to be measured is in a harsh environment or it is not stationary, measurement can not be accomplished using the previous systems because sample holder is also part of the system. One possible solution is to separate the sample holder from the system by guiding the fluorescence information from the sample to the detector using fibers.

2.4.1 System Description

Schematic of the fiber based sensor is shown in figure 2.19. It contains a light source driver, a light source, a light detection circuit, a signal processing unit, a fiber probe and a fluid travelling conduit. The light source is coupled in to the fiber probe for sample excitation. Emitted light from sample is collected by the same fiber probe. Collected light transformed into digital data by the light detection circuit and the code information is extracted using signal processing unit.

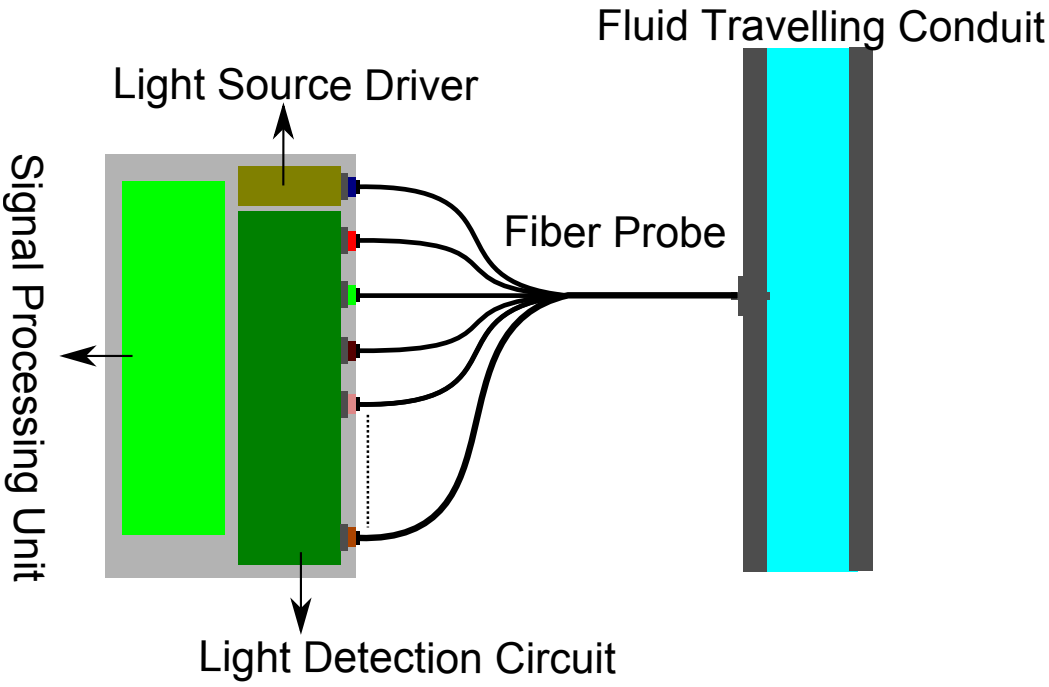

Figure 2.19: Fiber Based Sensor System

In this section, description of system components is separated into two parts as hardware and software. In hardware part, fiber probe and electronic components is explained. In addition effect of the incidience angles on color filters, geometry of the fluid travelling conduit are also discussed. In software part, algorithms used in controller electronics, data analysis and encoding are explained.

2.4.2 Hardware

2.4.2.1 Fiber Probe

Function of the fiber probe is to excite quantum dots in liquid and collect their emission. There are several parameters to be optimized in the design of the fiber probe. It should contain at least one illumination and at least one collection fiber. The number of the collection fibers should be equal or greater than the total number of quantum dots used in the system. The core diameter, cladding distance, numerical aperture of the fiber and the distance between the fibers should be optimized.

The figure of merit for a fiber optic probe with separate excitation and collection channels was introduced by Schwab and McCreery [34]. Using this approach, light collection efficiencies of fiber probes with different diameters are compared. Comparison is shown in figure 2.20.

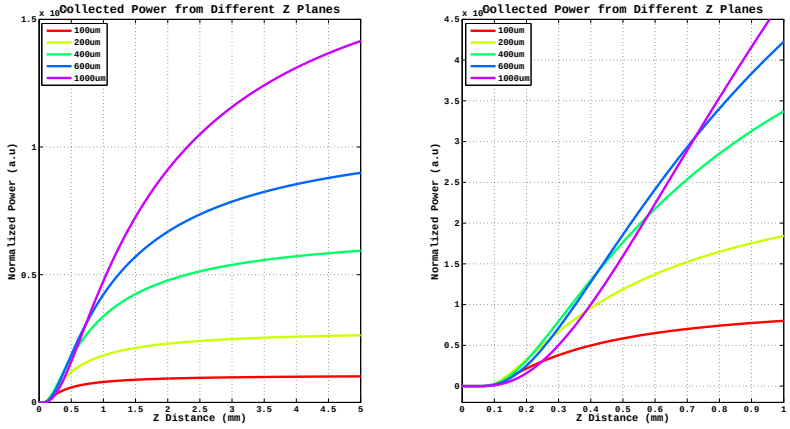

Figure 2.20: a; Power Collected by Fiber Probe from different Z Distances. b; Zoomed version of a

In the figure 2.20, collected power increases with the core diameter of the fiber. However, by looking at the zoomed graph, it can be seen that increment of 1000 μm diameter fiber is slower than the others although it catches up as the distance increases. When the working distance of the system is less than 1 mm, in the case of real time

fluorescence monitoring of micro fluidic channel, fibers with smaller diameters are more applicable. Another disadvantage of thick fibers is the bending radius. As it decreases, it is harder to bend the fiber. Fibers with high bending radius are more fragile and less resistant to non stationary, vibrating environments.

Collection efficiency of fiber bundles were analytically calculated by Schwaab and McCreery [34]. Working distance of different probes with different fiber core diameters can be seen in the figure 2.21, which shows the collected power from different distances away from the fiber tip.

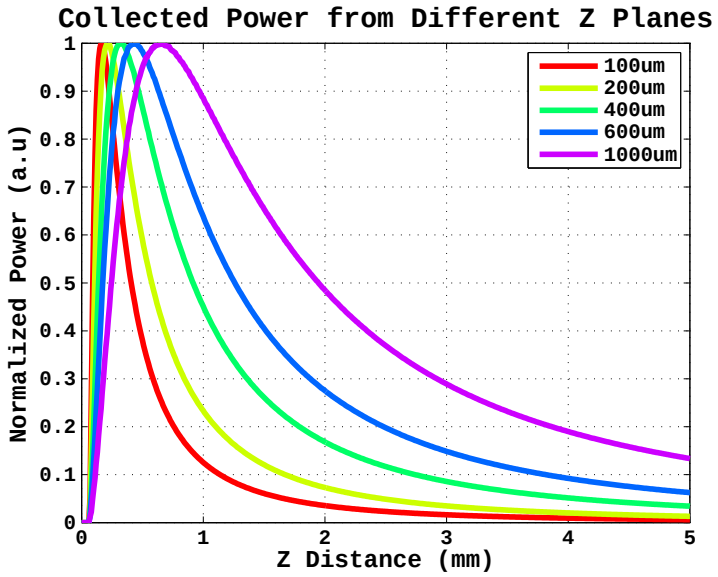

Figure 2.21: Matlab Simulation of the Power Collected by Fiber Probe from different Z Distances

Numerical aperture (NA) of an optical system is a dimensionless number that characterizes the range of angles over which the system can accept or emit light. Therefore higher NA for light collection system means more light is collected by the system. NA of a fiber depends on refractive indexes of core and cladding and can be calculated as

$$NA = \sqrt{n_{core}^2 - n_{cladding}^2} \tag{2.4}$$

The core is commonly silica with refractive index around 1.5. There are several industrial standards for NA of fiber. The most common one is 0.22. On a specific order 0.48 is also available. NA is taken as 0.48 since it is higher trough out this thesis.

2.4.2.2 Excitation Source

The light source is coupled into the fiber probe for exciting the sample. Fibers used in the system has a numerical aperture of 0.48 which is equal to 28.69° as explained in the previous section. Important point in coupling is, uniformly exciting all modes in the fiber to fully fill the illumination cone. (see chapter 3) To satisfy this, light rays going out of emission area of the light source should have high spatial frequencies.

Collected fluorescence is linearly roportional to the power of the excitation source. As the excitation power increases, SNR of the system also increases. In our system, thorlabs DL-5146-101S laser diode is used because of its high power output and narrow emission spectrum. One disadvantage is its beam divergance angles which are 19° in perpendicular and 8° in horizontal. Because of this asymmetric excitation of the fiber, output light profile is not fully gaussian making the system θ dependent.

In order to test filling efficiency of the illumination cone, experimental setup shown in figure 2.22 is established. Light source is coupled into the fiber. Output of the fiber is imaged on a scattering surface and image is observed using a coloured CCD. By observing the width of the beam at different distances, effective numerical aperture can be calculated.

Experiment is done for laser diode and LED with 0.22 fiber to investigate the effect of divergence angle in filling the illuminating cone. Relation between beam size and distance is shown for different distances in figure 2.23.

Numerical aperture calculated using LED (red line) is 0.22, while calculation with laser diode (blue line) gives effective numerical aperture of 0.14. This shows that using if LED is used as a light source it is possible to fill the numerical aperture of the fiber. However, although the output powers of LED and laser diode are in the same order, divergence angle of LED is very high. Therefore, using LED is it possible

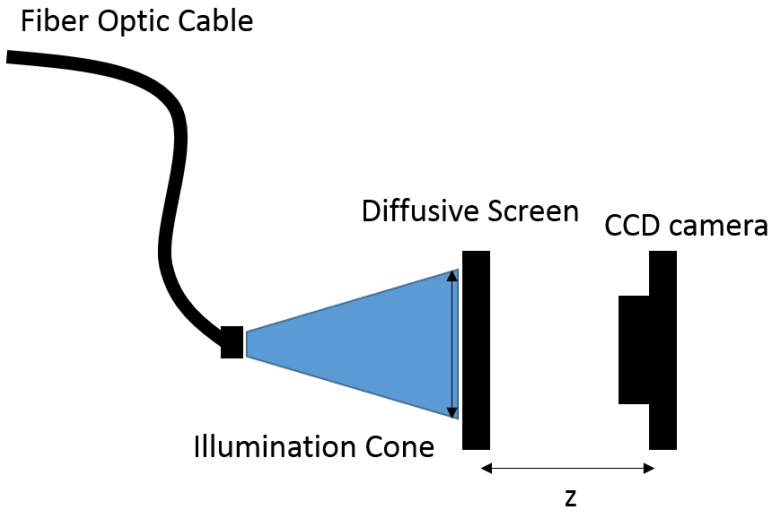

Figure 2.22: Experimental setup for characterizing the beam shape at the output of the fiber. Image of the illuminated diffusive screen is analysed via post-processing.

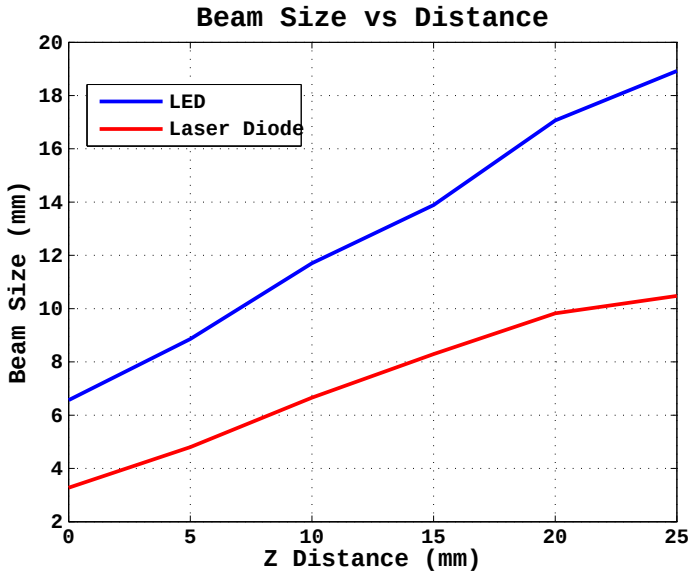

Figure 2.23: Relation between **d** and bandwidth of the beam on the diffusive screen

to fill 0.22 numerical aperture but it is not possible have high power output since the power is distributed. In order to have same result using laser diode, diffuser is

placed between laser diode and fiber probe. Light coming out of the laser diode hits the diffuser and it get scattered according to the scattering distribution of the diffuser. Although maximum angle going out of the laser diode is not enough for illuminating all the modes of the fiber, scattering caused by the diffuser will increase the effective numerical aperture of the laser diode.

In the figure 2.24, there are illumination cones of fibers with 0.48 and 0.22 numerical apertures. LED is coupled to first fiber and laser diode is coupled into the second fiber. Width of the illumination cone can be seen from the figure.

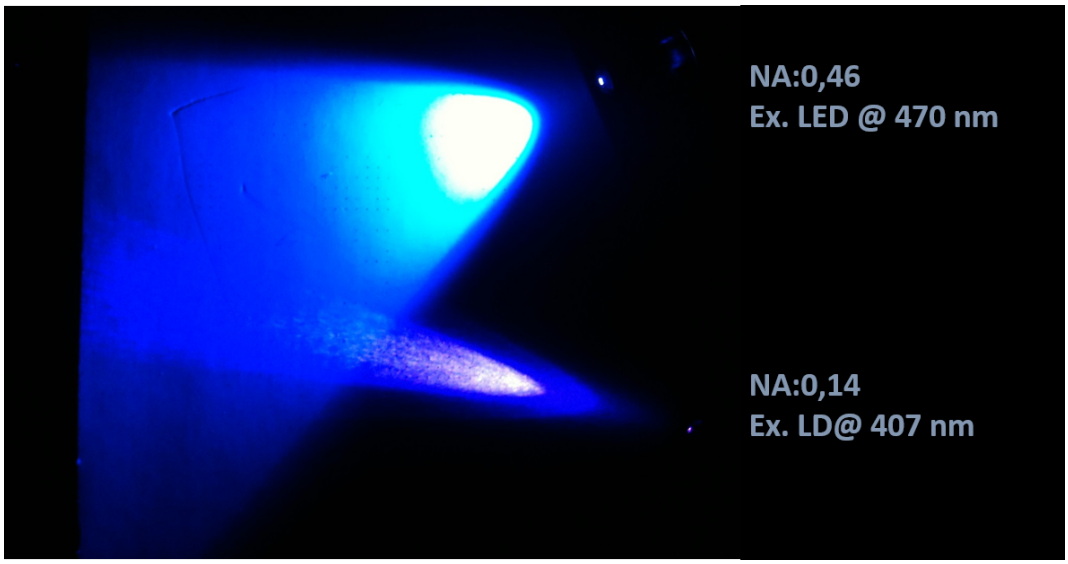

Figure 2.24: Picture of illuminating fibers with numerical apertures of 0.48 (up) and 0.22 (down)

2.4.2.3 Fluid Traveling Conduit

Fiber optical based sensor system can also be used for flowing liquids. User can make fluorescence measurements and extract the code data of the fluid during the flow. However, there are some limitations in this application because of the bubbles generated by the flow. Bubble generation depends on the viscosity, flow speed and the channel geometry. An examplary fluid conduit design is shown in the figure 2.25.

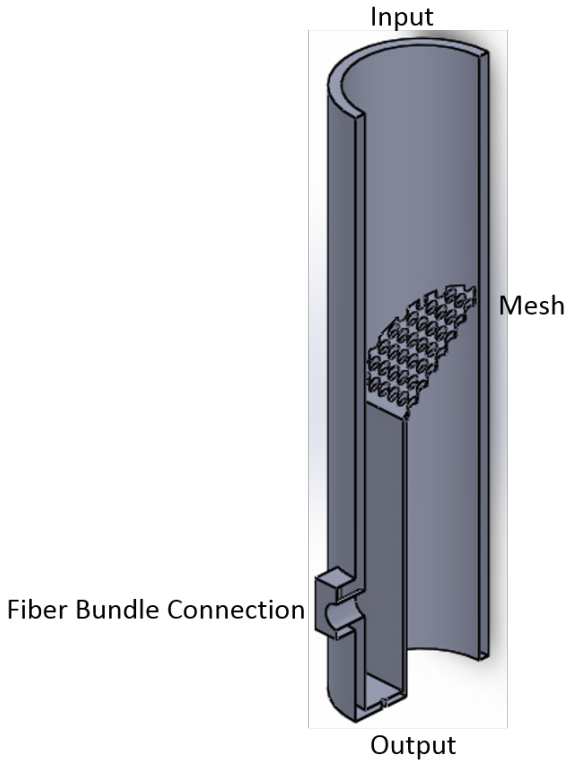

Figure 2.25: Cross section of fluid travelling conduit

As seen in the figure, fluid is separated into two ways. Tip of the fiber probe is connected to the bottom of the conduit. Meshing slows down the flow speed of the liquid. Extra liquid is collected at the narrow side of the conduit. The drain hole of the narrow side has a diameter of 4 mm. Since the pouring speed of the liquid is very low, measurement is not affected from the bubbles. In addition, remaining portion of the liquid flows through to wide side of the conduit. Therefore overall flow speed and the total filling time of the liquid remains same.

2.4.2.4 Incidence Angle Dependence on Color Filters

Emitted light from the sample is collected by the collection fibers. There are color filters placed between the collection fibers and photo detectors for filtering the necessary information for code extraction. Assemble of photo detector and color filter

is shown in figure 2.26

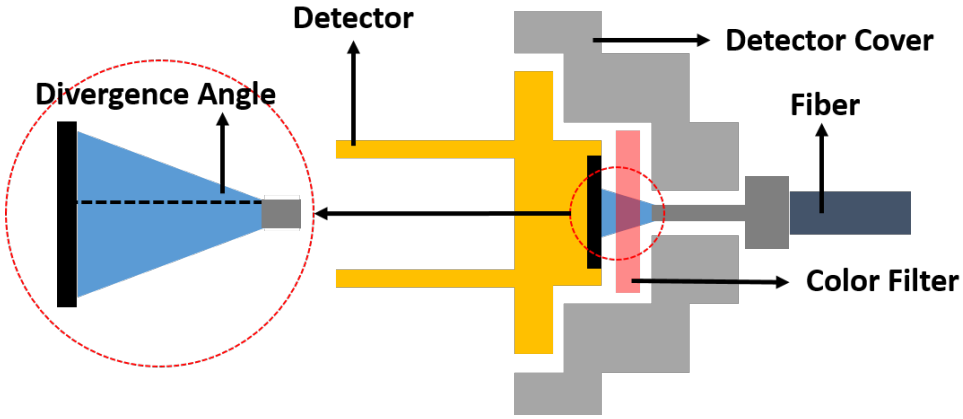

Figure 2.26: Assemble of photo detector, filter and detector cover

Maximum angles of the rays leaving the fiber is related with the numerical aperture of the fiber. When fiber with 0.48 NA is used, we expect maximum angle to be 28.69° degrees. (see table 3.1). Interferometric color filters are used in the system. They are designed for 0° degree incidence angle with transmission spectrums as shown in figure 2.27.

Different incidence angles affect the transmission spectrum of the filter decreasing the effective selective band of the system. In order to test incidence angle dependence, setup shown in figure 2.28 is established.

Light coming out of the fiber is collimated using collimator lens. Colimated beam is passed through filter. Filter is placed on a rotating stage in order to test the effect of incidence angle on filter's transmission. Results are shown in figure 2.29. Up to 10 degrees, shift in transmission maxima of the spectrum is 10 nm but as the incidence angle increases, shift increases drastically. When filter is placed at the end of a fiber with NA of 0.48, its effective bandwidth will be doubled.

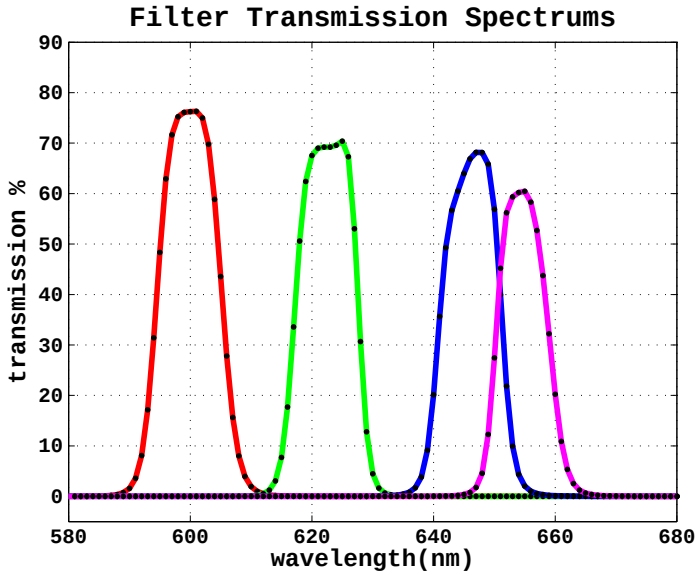

Figure 2.27: Transmission spectrum of the band pass filters

2.4.2.5 Electronics

Electronics part comprises laser diode driver and light detection circuit. LD driver circuit controls the current driving the laser diode. Stabilization of LD's output power is crucial since collected emission power is directly related to the excitation power. Thorlabs DL5146-101S is used as light source in the system. Figure 2.30 shows pin diagram of the laser diode. Feedback current generated by the photodetector inside the laser diode is used for power stabilization.

Laser is operated using IC-WKM laser driver [35]. Output power stability of the device is lower than 1%.

The other electronic part used in the system is the light detection circuit. In the preliminary optical barcode reader designs resistive transimpedance amplifiers are used. In these amplifiers, photo detector current is transformed into voltage using a resistor. Limitation of using a resistor is that it introduces thermal noise to the system. Thermal noise power can be calculated by

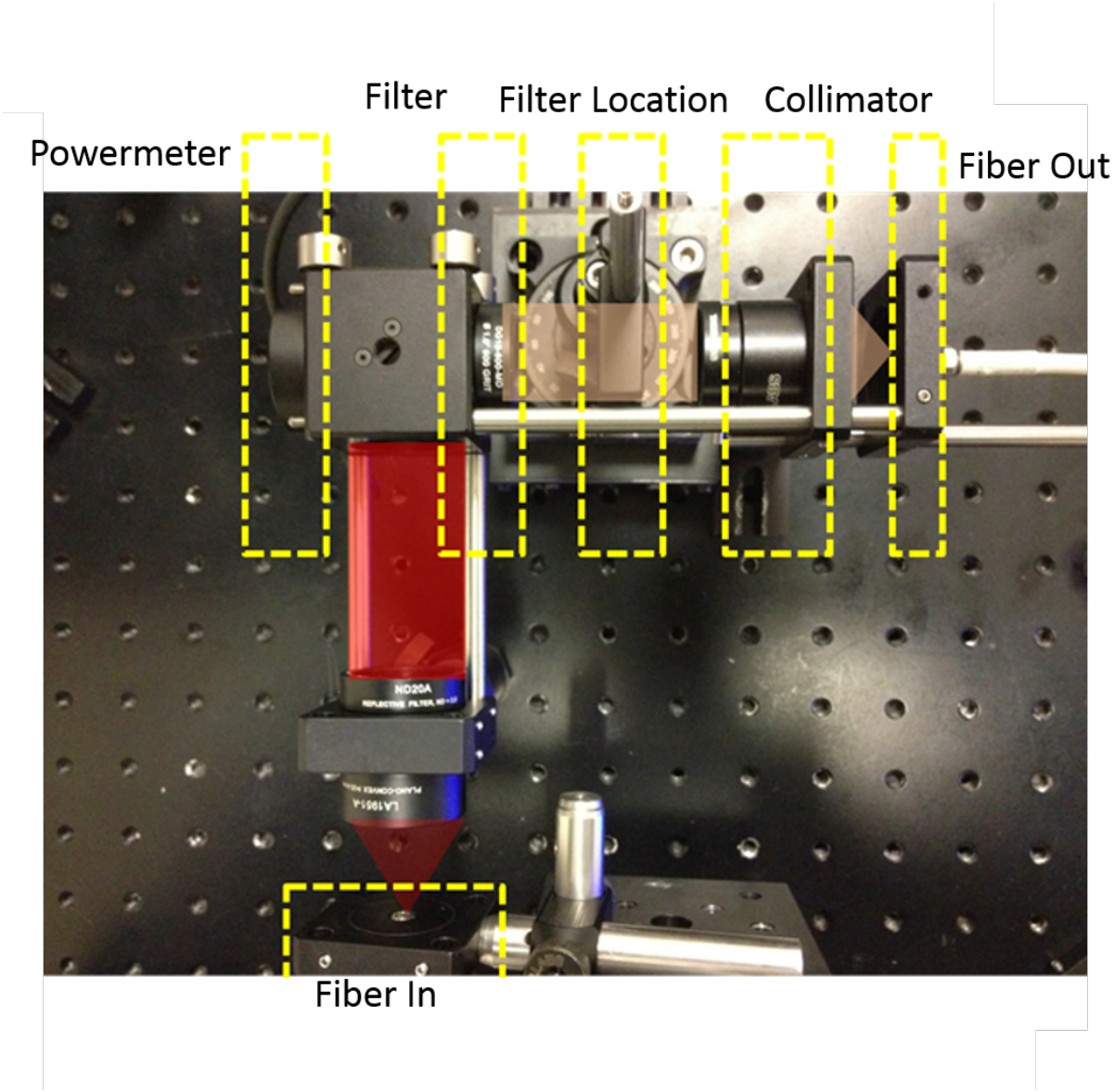

Figure 2.28: Setup for testing effect of the incidence angle on filter transmission spectrum

$$v_n^2 = \bar{4}k_bTR \tag{2.5}$$

where, k_b is the Boltzmann constant in joules per kelvin, T is the resistor's absolute temperature in kelvin, and R is the resistor value in ohms Ω [36]. Having a large

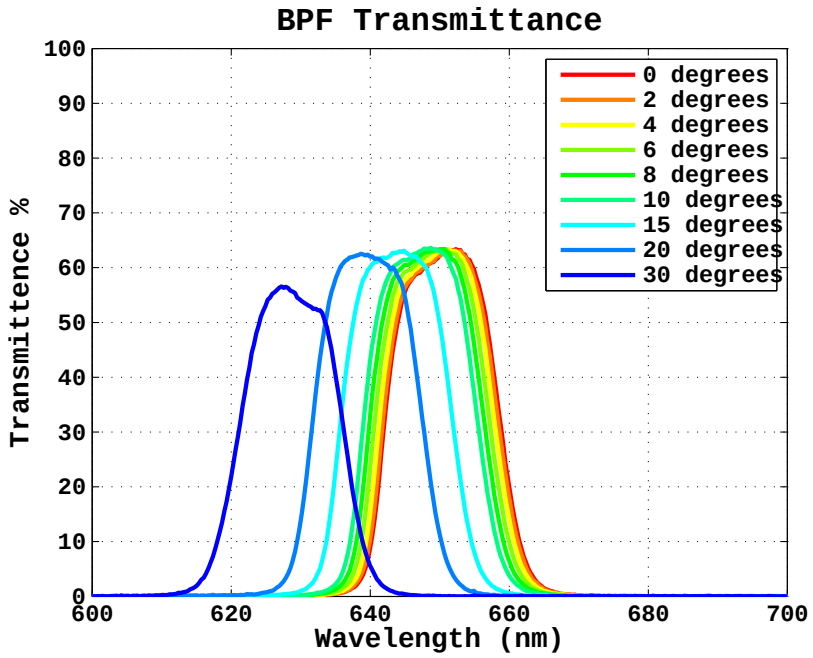

Figure 2.29: Relation between incidence angle and transmission spectrum of the color filter with a transmission peak at 600 nm

resistor, increases the noise voltage drastically.

In the fiber optic based sensor design, TI IVC102, which is a capacitive integrator, is used. Figure 2.31 shows the circuitry and operating waveform of IVC102.

Capacitive integrator circuit is immune to noise shown by equation 2.5. Noise power of the system does not increase with the gain which was the case with resistive amplifiers. Gain of the system can be controlled by changing the integration time.

2.4.3 Software

Software part of the system comprises controlling and code extraction algorithms. IVC102 is controlled using labview interface and NI-DAQ card. Code extraction is done in post processing using Matlab.

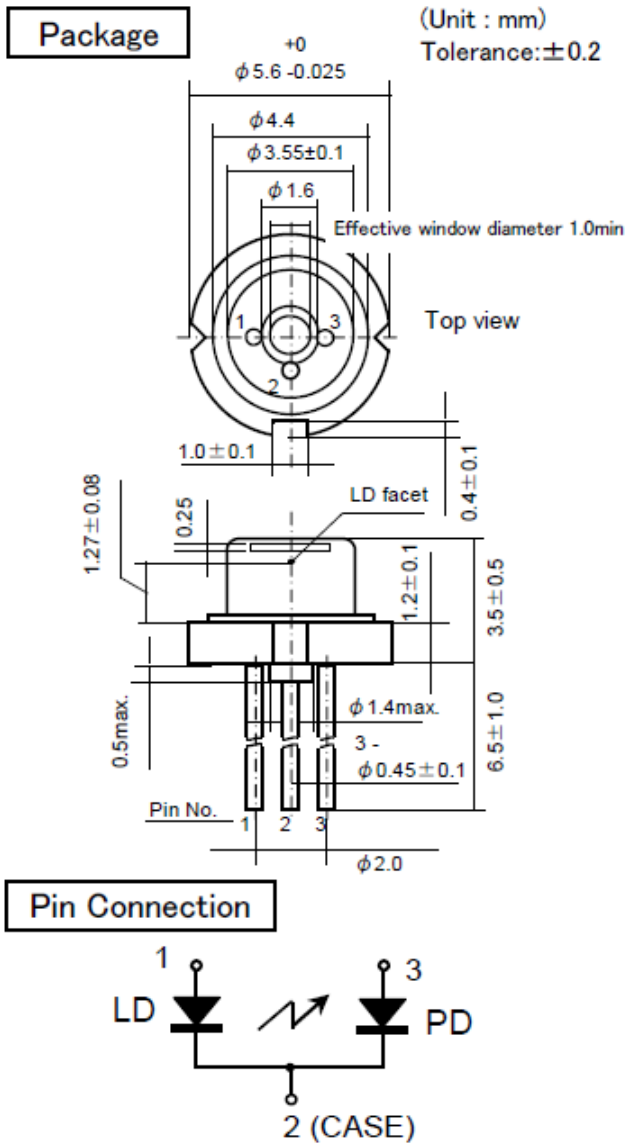

Figure 2.30: Pin Diagram and Schematic of DL-5146-101S [3]

2.4.3.1 Labview Interface

IVC102 needs two digital inputs to measure the photo detector current. As seen from figure 2.31, S1 and S2 pins are two switches controlling the integration time, reset time, hold time and pre hold time of IVC102.

Input current charges the capacitor inside the IC since the I-V relation in a capacitor

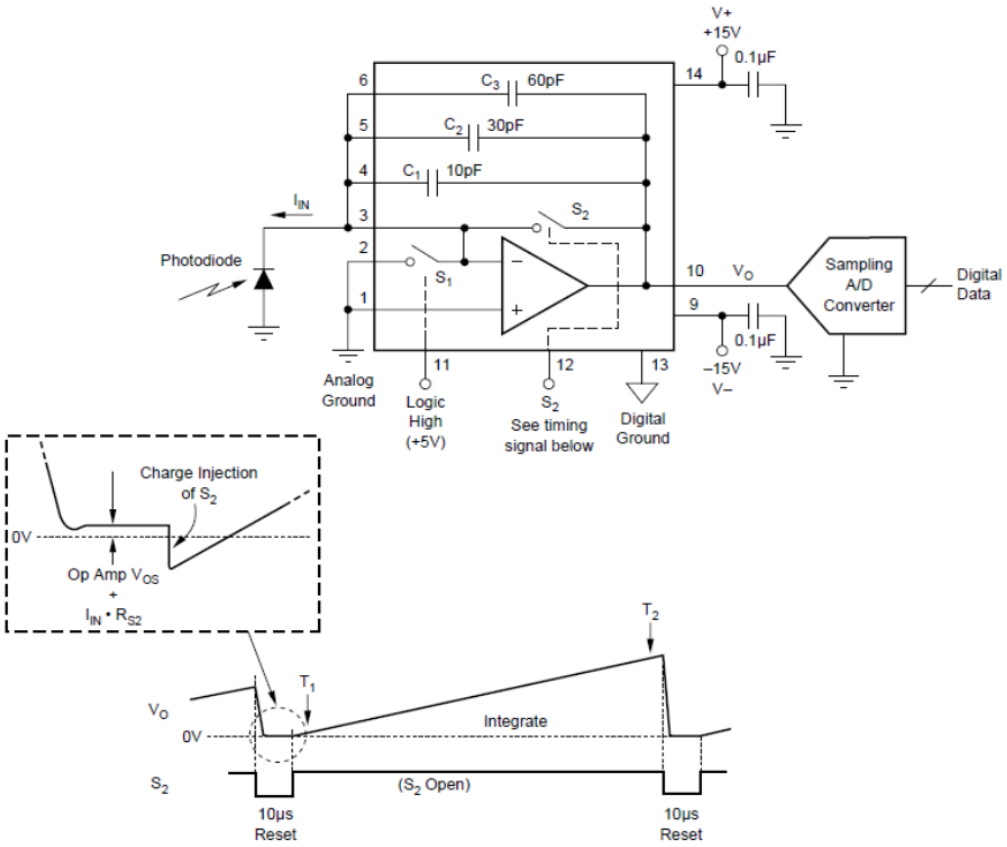

Figure 2.31: Operating Principle of IVC102 [4]

is

$$i_c = C\frac{dV_c}{dt} \tag{2.6}$$

where, C is capacitance, i_c and V_c are current and voltage of the capacitor respectively. In our configuration, capacitance value is 10 pF.

Figure 2.32 shows a labwiew interface for controlling the IVC102. Program generates two waveforms for S1 and S2. User is able to change pulse durations in S1 and S2, controlling the gain of the system. For example, when capactor value is 10 pF and integration time is 100 ms, total gain of the system can be calculated using equation 2.6 as 10^9. High gain is achieved without being affected by the thermal noise.

Voltage value across the integrating capacitor can be digitized at different time

instances. Pre-hold and hold times, which are determined by S1 and S2, can be used for reading the data. During these time durations, discharging of the integrating capacitor is prevented to read the integrated signal value. However, leakage may change the amplitude. In order to overcome this problem, another approach is introduced. Program calculates a linear fit for the linearly increasing voltage during integration (figure 2.32, right side). As seen in the right side of the figure, there are three different channels. Each of them presents measured light powers at different wavelength bands depending on the pass band of the color filter of the corresponding channel. Sampled data is shown by the green graph. Sampling frequency is 10 kHz. Linear fit, represented by the red line, is calculated using a built-in function in LabView. Slope of this linear fit is multiplied with the integration time and amplified current is displayed in picoampers. For example, just like the example given in the previous paragraph, 1 mV voltage output corresponds to 1 pA output. Calculated values are stored in an array to show real time fluorescence data of the sample. An exemplary output data is shown in figure 2.32.

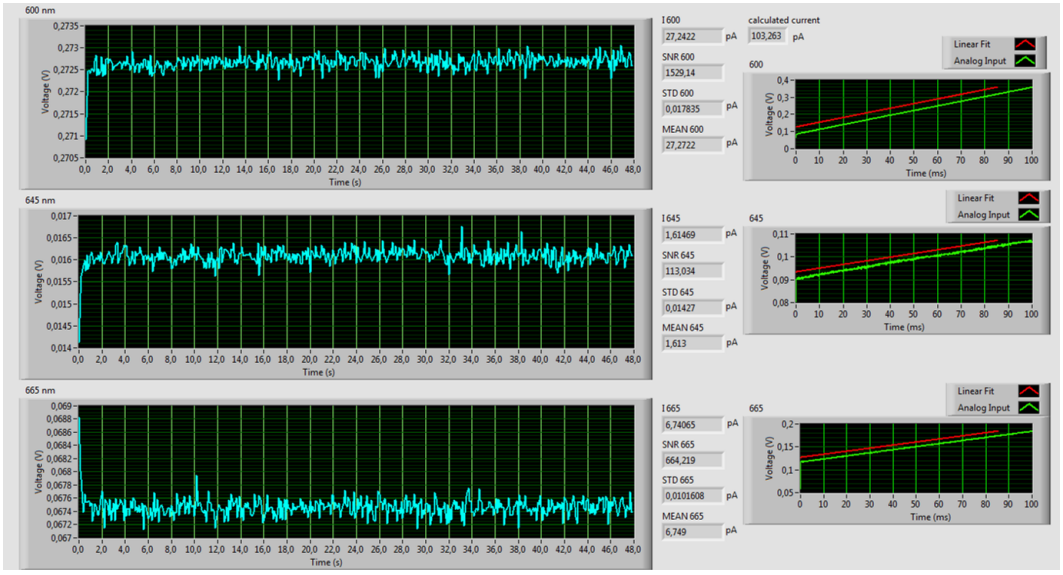

Figure 2.32: Labview Control Software

Real time fluorescence data of the system is stored in an array. Total data reading

time is determined by the user. Just after that time is completed, data is saved in a text file for post processing.

2.4.3.2 Code Extraction Algorithm

Fluorescence tagging of liquids using quantum dots has two parameters as described in section 2; emission peak and intensity. There are several algorithms introduced in the literature for code extraction [37–39]. Our algorithm is very similar to these studies but we apply slightly different post processing techniques to overcome specific problems.

Emission wavelengths of the quantum dots are separated using the color filters in the system. If there are N quantum dots and M intensity levels in the system, code of the liquid can be expressed as;

$$\bar{x} = \begin{pmatrix} \alpha_1 \\ \alpha_2 \\ \vdots \\ \alpha_N \end{pmatrix}, \tag{2.7}$$

where α is a number between 0 and M. If there are no spectral overlap between the quantum dot emissions, it would be possible to calculate M by single measurement. However, spectral overlap diversify the problem. In order to overcome this, basis functions of the system are generated. Basis functions are the fundamental components of liquid barcodes. For example, for a system with 3 quantum dots, basis codes are (100), (010) and (001). Every other code created for the system will be linear combination of the basis codes. In the case of spectral overlap, the 1 in (100) will affect the second 0, making the code components linearly dependent.

Matrix containing all the basis functions can be expressed as;

$$\bar{\bar{F}} = \begin{pmatrix} \gamma_{11} & \gamma_{12} & \cdots & \gamma_{1N} \\ \gamma_{12} & \gamma_{22} & \cdots & \gamma_{2N} \\ \vdots & \vdots & \ddots & \vdots \\ \gamma_{1N} & \gamma_{2N} & \cdots & \gamma_{NN} \end{pmatrix}, \tag{2.8}$$

where γ values are the power values measured at different wavelengths. If the quantum dots had no spectral overlap equation 2.8 should equal to NxN unit matrix.

The power values measured for the specific fluid is given by

$$\bar{A} = \begin{pmatrix} \gamma_1 \\ \gamma_2 \\ \vdots \\ \gamma_N \end{pmatrix}, \tag{2.9}$$

.

$\bar{x}$, can be calculated by inserting $\bar{A}$ and $\bar{\bar{F}}$ into

$$\bar{A} = \bar{\bar{F}}\bar{x} \tag{2.10}$$

.

Chapter 3

MODELING AND VERIFICATION OF QD IN TRANSPARENT LIQUIDS

In this chapter, Monte Carlo (MC) method based modelling of the fiber optic system is explained. MC method is a category of computational methods that involves random sampling of a physical quantity [40]. For the case of light particle interaction, method uses simple geometrical photon propagation techniques and probability density functions in order to compute deflection and scatter trajectories of the photons. Aim of the simulation is to determine the collected fluorescence intensity of the excited quantum dots inside a medium. Lots of photons are tracked to simulate the system within an acceptable accuracy. More photons give more accurate solution but consumes more computational power.

This chapter is organized as follows, first the problem definition including the problem geometry is given. Next, generation of random events and probability density functions used in the algorithm is explained. After that, detailed description of the algorithm is given. Algorithm is composed of several parts. These parts are; creating the geometry, photon launch, photon propagation, photon scattering, photon termination and photon collection. Detailed description of these parts are given in the subsections of this chapter. In addition, method is implemented using JDK 1.4 in Net Beans 7.4 IDE and source codes of the parts can be found in appendix A.

A cross sectional view of the problem geometry is shown in figure 3.1. For simplicity, system with only two fibers is simulated to decrease the computational power but multiple collection fibers case is also discussed in chapter 3.2. If there are more than one type of quantum dot in the system, simulation also considers their interaction.

System contains one illumination fiber and one collection fiber. Illumination fiber

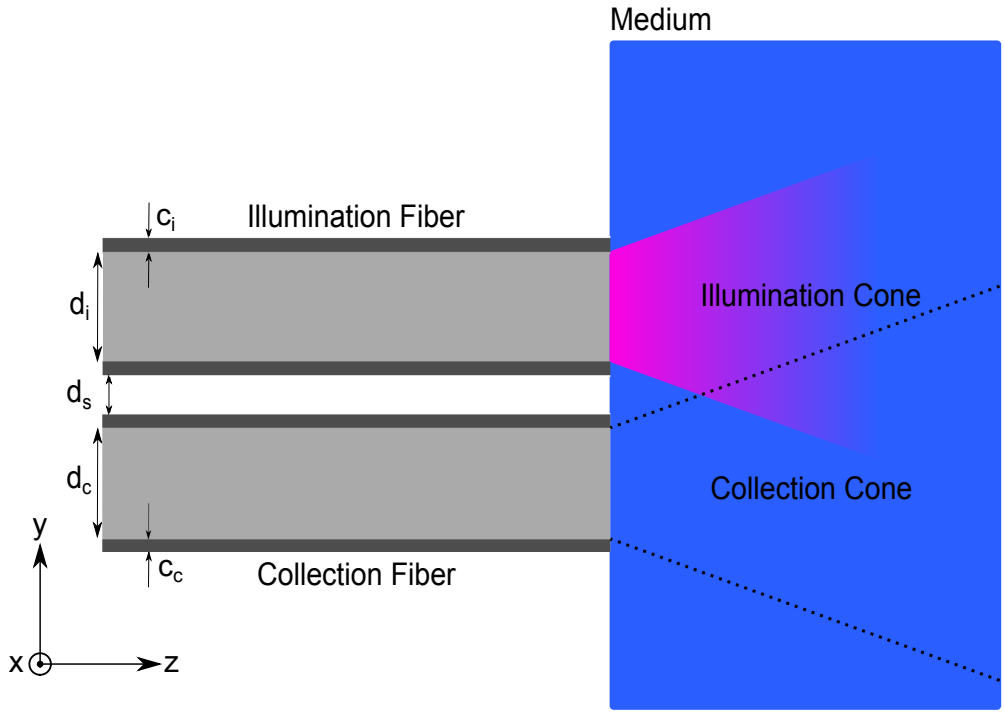

Figure 3.1: problemSchematic

and collection fiber are facing to the same side of the medium to collect backscattered light. Fibers can be described by the following parameters: the core diameter (d_i and d_c), cladding thickness (c_i and c_c), numerical aperture (NA), core refractive index n_{core} and cladding refractive index n_{clad}. The spacing between the fibers (d_s) is a design parameter which can be modified accordingly for specific applications but in this thesis, unless stated otherwise, it is taken as zero.

Photons leaving the illumination fiber propagate in z direction. Scattering and absorption propertieos of the photon depends on the physical properties of the medium. These properties can be described as: medium width M_w, length M_l, height M_h, interaction coefficient (μ_t), absorption cross-section (σ_{abs}) and scattering cross-section (σ_{sc}). Relation of medium parameters with each other is explained in chapter 3.4

Cartesian coordinate system is used to define the problem and trace the photons. The origin of the system is located at the center of the illumination fiber. The z axis

is always normal to the medium surface and photons travel in -z direction. xy plane is the medium surface. Cylindrical coordinate system is used for photon generation because of the cylindrical symmetry of the fibers. Initial coordinates of photons are calculated by uniform sampling of r and θ. Cartesian and cylindirical coordinate system shares the same z axis. A moving spherical coordinate system, whose z axis is aligned with the photon propagation direction, is used for calculating the deflection angle θ and azimuthal angle ψ.

3.1 Inserting Probability Density Functions into Simulation

In the emission simulation of quantum dots, there are several predefined probability density functions to calculate photon propogation. For example, deflection angle distribution of a photon after scattering from a reflective sphere can be simulated by Rayleigh Scattering theory [41]. Algorithm needs to generate random variables to sample these kinds of distributions. Inverse transform sampling method is used to generate random variables [42]. Inverse transform sampling can be explained as follows; a random variable with probability density distribution of $p(x)$ wanted to be generated. Consider a uniformly distributed random variable ξ in the interval $[0, 1]$. Using ξ and $p(x)$,

$$\xi = \int_0^{x_1} p(x)\,\mathrm{d}x, \tag{3.1}$$

x_1, which is the random number which has a distribution of $p(x)$.

3.2 Explanation of the Algorithm

In this chapter MC algorithm is explained in detail using state schematic as shown in the figure 3.2.

Algorithm can be divided into four main parts, geometry initiation, photon launch, photon propagation and data collection.

Geometrical boundaries of the problem are set and the physical properties of the

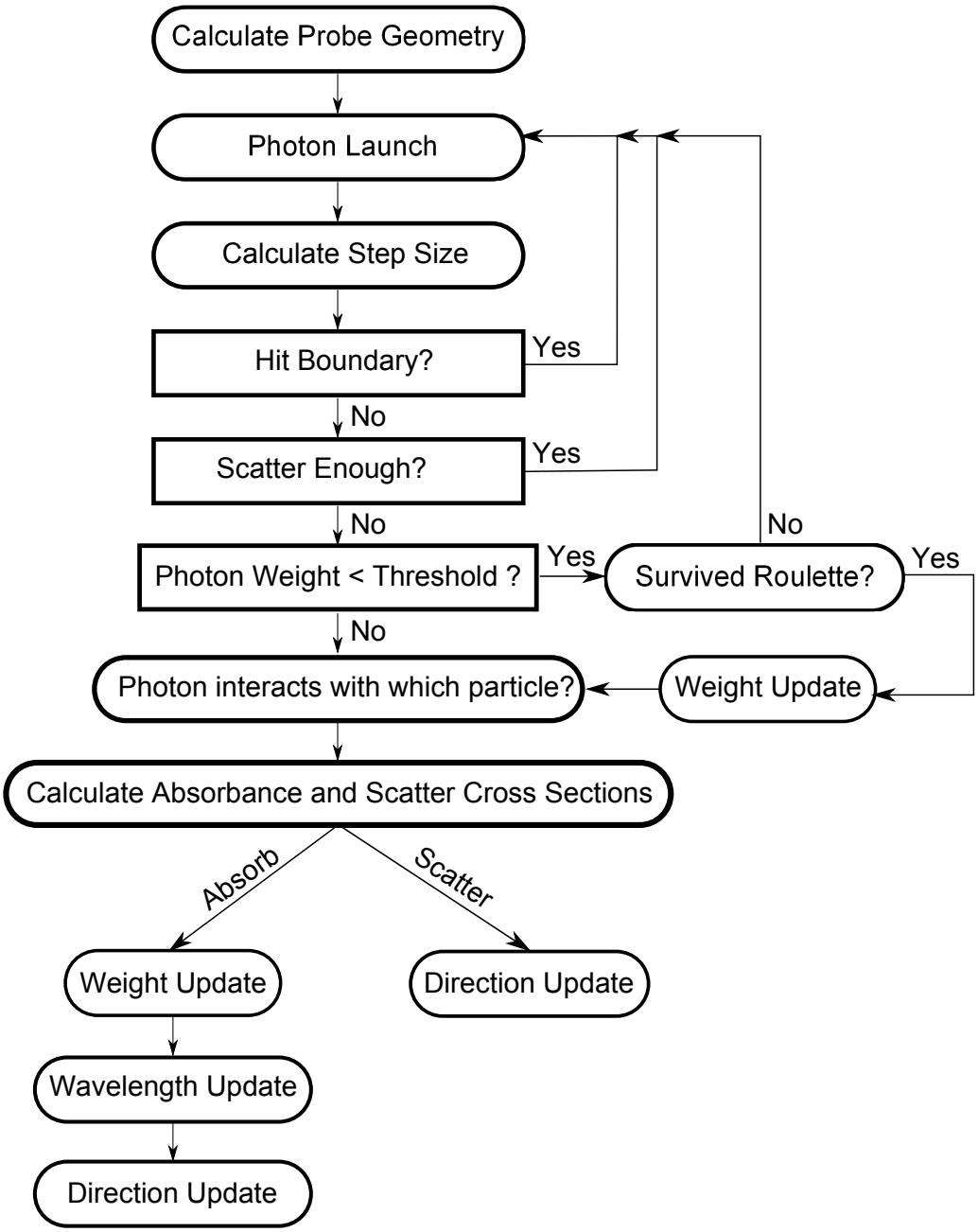

Figure 3.2: Monte Carlo Algorithm Diagram

medium is calculated. Total number of quantum dots and their individual concentrations are introduced to the simulation.

For the probe geometry, there are several options. For time consuming computa-

tions, probe with two fiber is considered but for easier simulations, multiple collection fibers are used. An exemplary probe with multiple collection fibers is shown in figure 3.3.

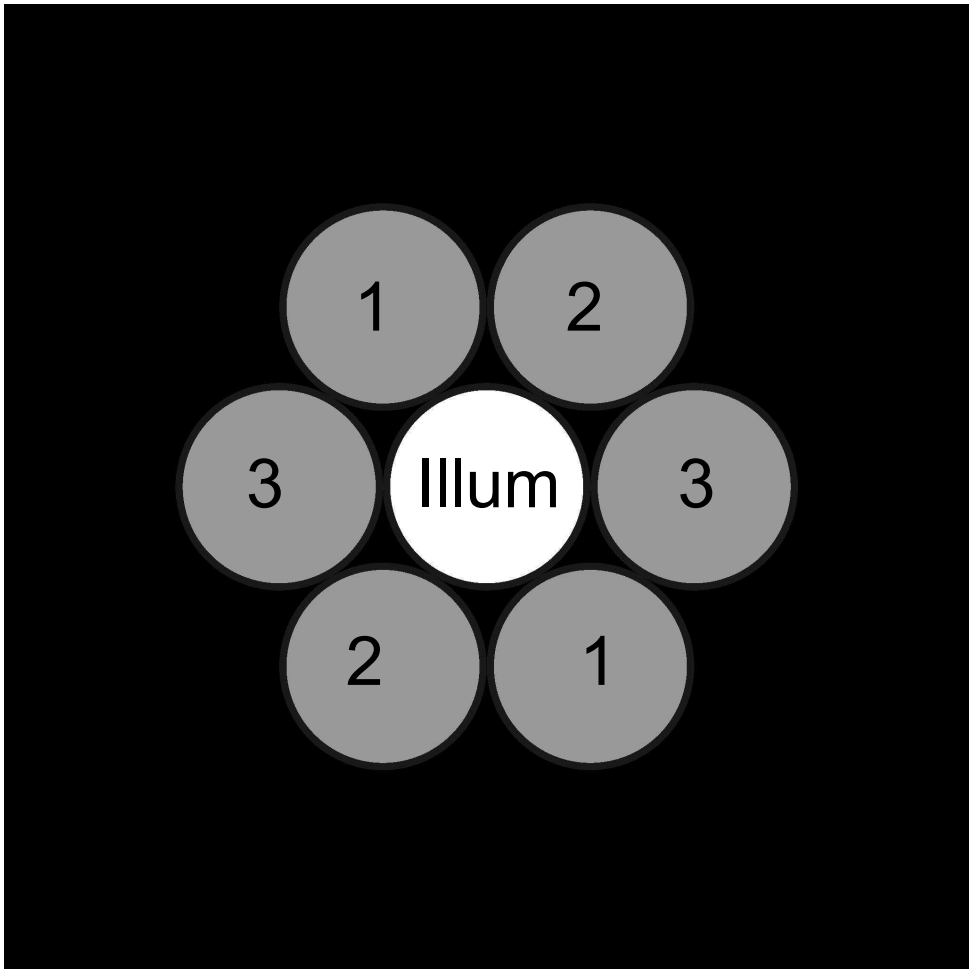

Figure 3.3: Fiber Probe Tip Example

As seen in the figure there are 7 circles each one representing the tip of a fiber facing to the medium. The brightest circle is the tip of the illumination fiber. It center is also the origin of the problem. The 6 surrounding fibers are the collection fibers.

In the second part photon are initialized and launched from the illumination fiber. Location assignment and directional cosine calculation of each photon propogating from the illumination fiber are calculated as shown in section 3.4. Total number of

the photons to be tracked is determined by the user. In the simulation explained in this thesis, 10^9 photons are tracked.

In the third part photon propagation is calculated. Total propagation distance depends on the mean free path of the medium. Calculation of the distance and moving the photon are explained in 3.4.

Program tracks photon in a while loop. While loop terminates if the photon is assigned as dead. There are several checks for photon termination which are explained in section 3.6. When the propogation distance is lower than a threshold value, in the code this threshold is defined as the "glue value", distance is recalculated. This can be defined as the minimum step size of the algorithm. After a valid computation of the propogation distance, photon is propagated.

If photon survives after propagation, it is assumed that it has hit a quantum dot. If there are more than one quantum dot in the system, program selects the intersected quantum dot according to interaction coefficients of the particles. Interaction coefficient is the reciprocal of the mean free path and it can be calculated using equation 3.8. Assume there are 3 quantum dots in the system and their interaction coefficients are μ_{t1}, μ_{t2} and μ_{t3} respectively. Algorithm is shown below;

$$QDSelection = \begin{cases} QD1 & : if \xi < \frac{\mu_{t1}}{\mu_{t1}+\mu_{t2}+\mu_{t3}} \\ QD2 & : if \frac{\mu_{t1}}{\mu_{t1}+\mu_{t2}+c_3} \leq \xi < \frac{\mu_{t1}+\mu_{t2}}{\mu_{t1}+\mu_{t2}+\mu_{t3}} \\ QD3 & : if \frac{\mu_{t1}+\mu_{t2}}{\mu_{t1}+\mu_{t2}+\mu_{t3}} \leq \xi < 1 \end{cases} \tag{3.2}$$

After the quantum dot is selected, program compares the scattering and absorption cross sections of the quantum dot - photon intersection in order to select the event. Decision algorithm is described as the following;

$$Event = \begin{cases} absorption & : if \xi \leq \frac{\sigma_{abs}}{\sigma_{eff}} \\ scatter & : if \xi > \frac{\sigma_{abs}}{\sigma_{eff}} \end{cases} \tag{3.3}$$

Note that ξ is a random generated number. (see section 3.1). Photon properties are updated accordingly as described in the section 3.5. Probability density functions

used in these computations are described in section 3.1.

In the photon collection part, program checks the locations of each photon. Acceptance specifications are described in section 3.7. After the photon is checked for the acceptance of a collection fiber, new photon is launched and same calculations are redone.

Total successful hits and total power is plotted with respect quantum dot concentration levels.

3.3 Photon Statistics used in the Algorithm

Algorithm uses several probability density functions to determine trajectories upon scattering and emission. Scattering of photon from particle is explained in [41]. In Rayleigh scattering, intensity of the scattered photon is depended on the incidence angle. The relation is shown in equation 3.4. This equation is valid for unpolarized light.

$$I = I_0 \frac{1 + cos^2(\theta)}{2R^2} \left(\frac{2\pi}{\lambda}\right)^4 \left(\frac{n^2 - 1}{n^2 + 2}\right)^2 \left(\frac{d}{2}\right)^6 \tag{3.4}$$

θ is the scattering angle, R is the distance to the particle, n is the refractive index of the particle, d is diameter of the particle and λ is the wavelength of the incoming photon. As the wavelength of the incidence photon decreases, intensity increases. This also explains why sky looks blue because blue photons are more likely to scatter. In the simulation, intensity distribution given by the Rayleigh scattering is taken as the probability density function of the photon deflection angle after scattering. [5] Angle distribution of the scattered light from the particle is shown in figure 3.4.

Another distribution used in the algorithm is exponential distribution. It is given by equation 3.5

$$f(x;\lambda) = \begin{cases} \lambda e^{-\lambda x} & : x \geq 0 \\ 0 & : x < 0 \end{cases} \tag{3.5}$$

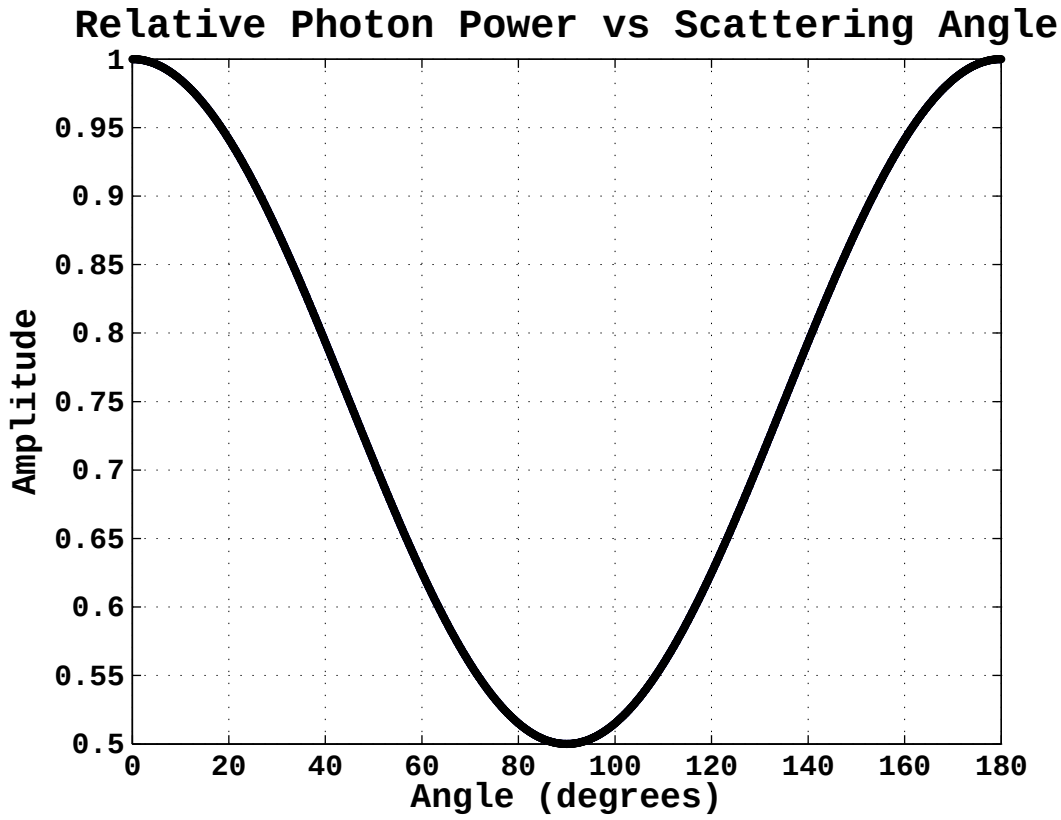

Figure 3.4: Intensity distribution of the scattered light with respect to scatter angle, Rayleigh Distribution [5]

Parameter λ determines the decaying of the function. This distribution is used in determining the event probability of photon as it travels through the medium. As the travelled distance increases it is more likely for a photon to scatter or get absorbed.

3.4 Photon Propogation

Each photon is described by a class with the following properties; spatial locations, directional cosines, weight, wavelength, total scatter number and one boolean for determining the life time of the photon.

Directional cosines and spatial locations are in the cartesian coordinates and are hold in an array. They are used to calculate the propagation direction of the

photon. Weight of the photon changes upon absorption by quantum dot. Additional weight decreasing events can be introduced. Weight of the photon affects its life time. Wavelength is used in calculating scattering and absorption probabilities. Total scatter number of each photon is also saved for termination.

After the probe geometry is created, photons are launched from the illumination fiber. In order to initialize a photon, initial location and directional cosines should be determined. Location is selected uniformly by sampling the illumination fiber tip area. Unifrom sampling is done using cylindirical coordinates. r is sampled between 0 and d_i and θ is sampled between 0 and 2π. Since the problem is defined in cartesian coordinates cylindirical to cartesian trasnformation is needed. However, when this transformation is done by multiplying r with cosine and sine of θ, point distribution in the fiber tip area is not uniform. To prevent this, equation 3.6 should be used for transformation. Point distributions for two different samplings are shown in figure 3.5

$$x = \sqrt{r}cos\theta, \tag{3.6a}$$

$$y = \sqrt{r}sin\theta, \tag{3.6b}$$

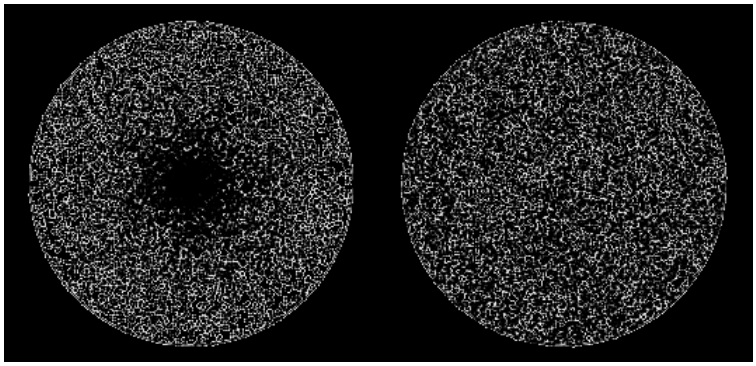

Figure 3.5: Point Distribution Over Unit Dist. On the right, equation 3.6 is used so that the point distribution is unifrom over the area. On the left, point ditribution is not uniform and has a higher density close to the center of the disk. [6]

	0.22	0.48
air	12.71	28.69°
water	9.52	21.15°
oil	8.61	19.06°

Table 3.1: Acceptance Angles for different Mediums and Numerical Apertures

Initial directional cosines of the photons are determined according to the numerical aperture of the illumination fiber and refractive index of the medium. Maximum launching angle of an outgoing photon is calculated by equation 3.7. Acceptance angles for different refractive indexes and numerical apertures are shown in table 3.1. In the simulation which is described in this section, medium is water and the numerical aperture of the fiber is 0.48.

$$NA = n_{medium} sin\theta \tag{3.7}$$

Photons travel between the quantum dots according to the mean free path of the medium. Mean free path is a quantity which defines the average distance that a photon can travel before a successive interaction which is the collision with a quantum dot. It can be calculated using equation 3.8 where l is mean free path, n is the number of target particles per unit volume and σ_{eff} is the effective cross sectional area, which can be calculated using equation 3.9 [43].

$$l = (n\sigma_{eff})^{-1} \tag{3.8}$$

The concentration and type of the quantum dot determines the mean free path of the solution. As the concentration decreases, n from equation 3.8 decreases. Other element of the equation is the effective cross sectional area. As the physical properties of the nano particles change, photon intersecion rates also change and this affect the optical properties of the medium [44, 45]. Effective cross section area can be calculated as;

$$\sigma_{eff} = \sigma_{abs} + \sigma_{sc}. \tag{3.9}$$

Effective cross section is the sum of two cross sections. Absorption cross section (σ_{abs}) determines the probability of photon to be absorbed by a quantum dot. It can be calculated using the equation 3.10,

$$\sigma_{abs} = 3.82 \times 10^{-21}\varepsilon \tag{3.10}$$

where ε is the molar absorptivity of the quantum dot [46]. It is deducted from the absorption graph of the material. In the monte carlo simulation, QDs from Ocean Nanotech is used. Properties of the quantum dot used in the simulation were taken from the Ocean Nanotech.

Scattering cross section (σ_{sc}) determines the probability of photon to be scattered by a quantum dot. Scattering probability depends on the refractive index and diameter of the particle and wavelength of the photon. [41] First relative size parameter should be calculated;

$$x^* = \left(\frac{2\pi a}{\lambda}\right) \tag{3.11}$$

When $x^* << 1$, Rayleigh theory is applicable. Since the particle size range of quantum dots are in the range of 10 nm, the assumption is valid. Relative refractive index of the to particle with respect to medium is also needen for computation. It can be calculated as;

$$m = \frac{n_{sph}}{n_{med}}, \tag{3.12}$$

Using x^* from equation 3.11 and m from equation 3.12;

$$\sigma_{sc} = 8/3\pi a^2 x^{*4} \left(\frac{m^2 - 1}{m^2 + 2}\right) \tag{3.13}$$

can be calculated. Mean free path calculated from the formula that described

in equation 3.8 is used in the exponential probability density function to determine the average travel distance of photon. When the concentration is very low, it is less likely for a photon to interact with a quantum dot. So as the travel distance increases, probability of event should decrease. Using this information, pdf of travel distance, s, can be calculated as,

$$p(s) = exp(-\mu_t s). \tag{3.14}$$

Equation 3.14 calculates the probability for a photon for traveling s. μ_t, the intersection coefficient, is the reciprocal of mean free path. Figure 3.6 shows the relation between the concentration of the quantum dot versus mean free path. The effective cross section is same for each concentration value.

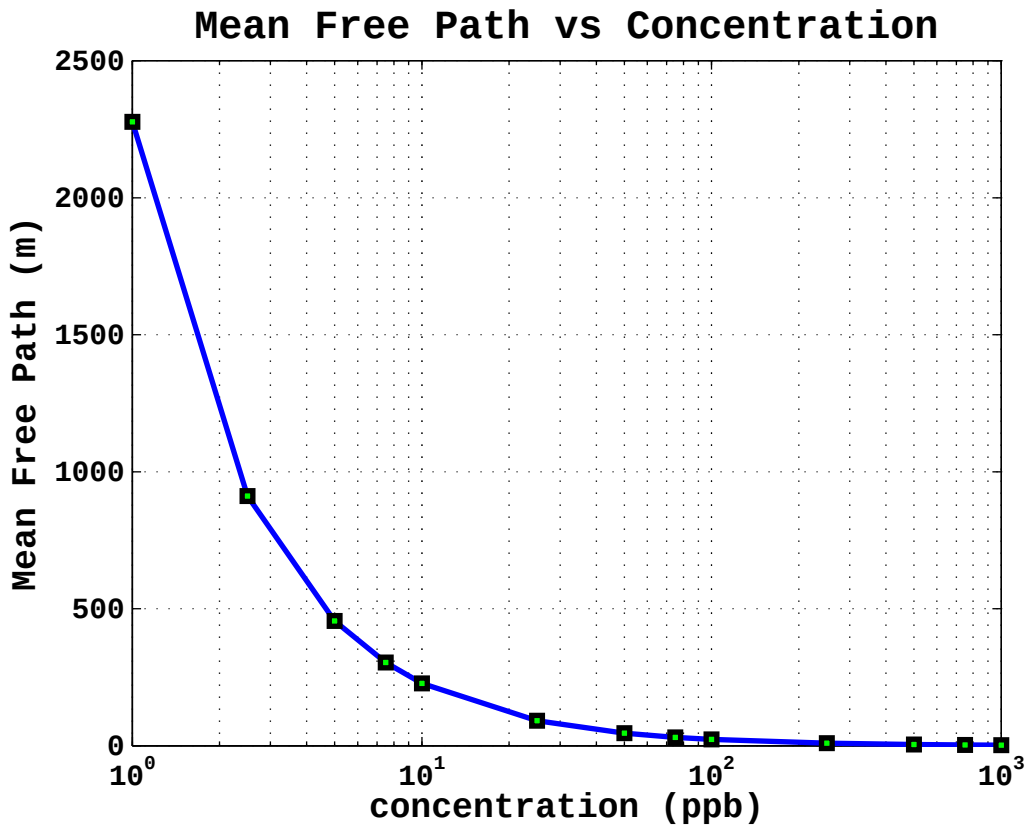

Figure 3.6: Relation between Mean Free Path and Concentration of quantum dot

Program updates the x,y and z locations of the photon to move it as explained in [45]. Update is described in equation 3.15. s is the propagation distance of the photon.

$$x' = x + \mu_x s, \tag{3.15a}$$

$$y' = y + \mu_y s, \tag{3.15b}$$

$$z' = z + \mu_z s, \tag{3.15c}$$

3.5 Photon Scattering and Absorption

Scattering or absorption events occurs as the photon hits to a quantum dot. Probability of scattering or absorption depends on the relative cross sections of events, which are represented with σ_{abs} and σ_{sc}. These values are recalculated at every intersection according to the wavelength of the incoming photon and the physical properties of the intersected quantum dot. Recalculation is done using the formulas explained in section 3.4. Comparison of the cross sections is simply done by generating a random number and comparing it with a threshold value which is proportional to the scattering or absorption cross sections. After selection, photon properties should be updated. Each event is described below.

3.5.1 Absorption

When absorption cross section is selected, photon is absorbed by the quantum dot. After absorption, photon's power is updated and its wavelength is also updated into a longer wavelength depending on the emission peak of the selected quantum dot. In the simulation excitation source is at 408 nm and emission peaks of quantum dots are at 600 nm and 645 nm. Algorithm also calculates the probability of 600 nm photon absorption by quantum dot with emission at 645 nm. But its absorption cross section

is relatively small compared to 408 nm.

Weight of the emitted photon at higher wavelength is updated according to the quantum efficiency of the quantum dot. Quantum efficiency is the ratio of number of emitted photons to number of absorbed photons. For example if 100 photon are absorbed by the quantum dot and 80 photons are emitted in the longer wavelength, the quantum efficiency or the quantum yield of the corresponding dot is 0.8. In our experiments water soluble QSH600 and QSH 645 are used with quantum efficiencies of 0.8 and 0.75.

After updating the weight of the photon, program also updates the wavelength. Locations of photon is same after the intersection. New direction of the emitted photon is sampled uniformly in the spherical coordinates and transformed into cartesian coordinates.

3.5.2 Scattering

Rayleigh scattering of the photons from the quantum dots can be described by the scattering cross section of the QDs. From the Rayleigh scattering function, in section 3.4, scattering θ is calculated and it is assigned as the deflection angle α of the photon. Directional cosines of the photon is updated as the following;

$$\mu'_x = \frac{sin(\theta)}{\sqrt{1-\mu_z^2}}(\mu_x\mu_z cos(\psi) - \mu_y sin(\psi)) + \mu_x cos(\theta) \tag{3.16a}$$

$$\mu'_y = \frac{sin(\theta)}{\sqrt{1-\mu_z^2}}(\mu_y\mu_z cos(\psi) + \mu_x sin(\psi)) + \mu_y cos(\theta) \tag{3.16b}$$

$$\mu'_z = -sin(\theta)cos(\psi)\sqrt{1-\mu_z^2} + \mu_z cos(\theta), \tag{3.16c}$$

where θ is the deflection angle and ψ is the azimuthal angle. ψ is sample uniformly between 0 and 2π.

3.6 Photon Termination

Program checks the situation of the photons before determining for scattering or absorption. There are 3 different checks. First one is the geometry check. If photon leaves the problem boundary, it is terminated. Second check is the scattering condition. Total number of scatters done by a photon is limited by the user in order to decrease the need for computational power (absorption is also count for scattering). If photon scatters more than the threshold value, program no longer tracks the photon and terminates it. Third check is the weight check. Each photon has equal weight and the weight changes as they are absorbed. If the weight of the photon is lower than a threshold value which is b, program plays a roulette for photon's termination. A random number ξ between 0 and 1 is generated and using ξ number weight of the photon (W) is updated as shown;

$$W = \begin{cases} bW & if \xi \leq 1/b \\ 0 & if \xi > 1/b \end{cases} \tag{3.17}$$

This method conserves energy yet terminates photons in an unbiased manner. The combination of photon roulette and splitting that is contrary to roulette, may be properly used to reduce variance. [47]

3.7 Photon Collection

At every propagation, program checks the z coordinate of the photon. When it is 0, it means that a photon is travelled through the medium and arrived to the z=0 plane. For the analysis, user can select the wavelength to be observed. Since we want to simulate the emission of the quantum dot, photons which have wavelengths different from the wavelength that we are interested in, are filtered out. If the photon is on the collection fiber tip, dot product of the directional cosines of the photon and the normal of the surface is calculated to find out the incidence angle. Photon with incidence angles smaller than the maximum acceptance angle of the fiber. If the incidence angle

is smaller than the acceptance of the fiber, photon will be guided through the fiber.

3.8 Comparison of Simulation and Experiment Results

3.8.1 Fiber Probe Collection Efficiency vs Distance

Program is used for simulating the experiment shown in figure 3.7. LD5146, 408 nm laser diode is coupled to illumination fiber. Fiber probe is positioned in front of a reflective diffuser [7]. Illuminated surface scatters the source and light is collected via collection fibers.

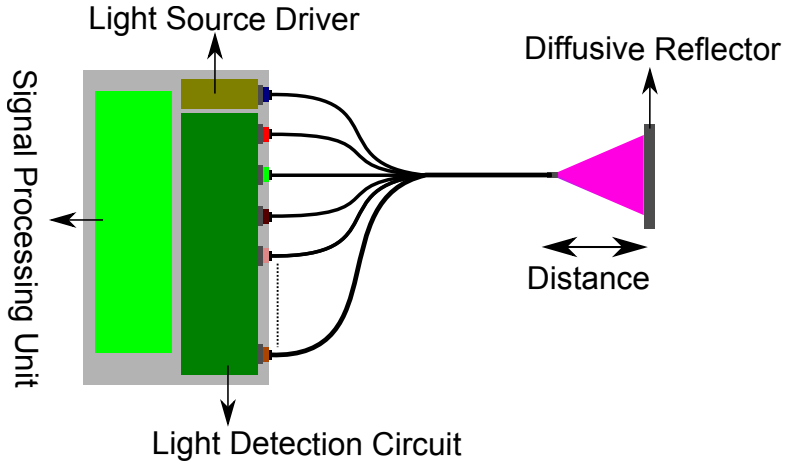

Figure 3.7: Experiment setup for simulating the fiber probe system's light collection efficiency where rays are scattered from a reflective diffuser at different lateral distances from the fiber probe.

Relation between the collected power and distance of diffuser from fiber probe tip be very similar to figure 2.20 with slight difference in the peak value. Main reason in this difference is the angular dependence on reflected rays from the diffuser as shown in the figure 3.8.

Center fiber illuminates the medium and 6 fiber collect fluorescence as shown in figure 3.3. 6 fibers make 3 groups and fluorescence collected by each group connected to a photo detector.

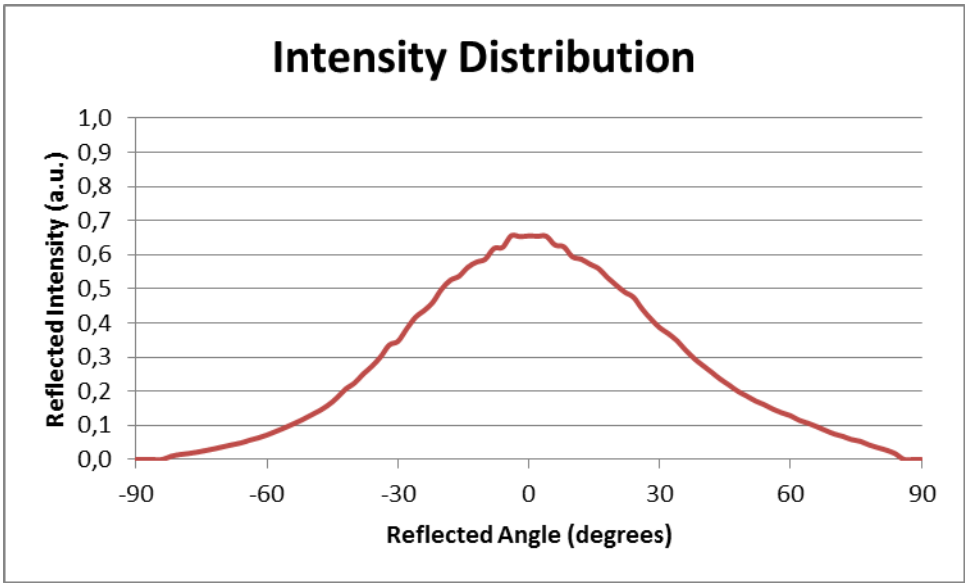

Figure 3.8: Angle Dependence of the Intensity of the Reflected Ray upon scattering from DG05-220 Thorlabs, reflective and diffusive screen [7]

As seen from the matching of simulation onto experiment from the figure 3.9, MC algorithm simulates photon launch and photon propagation very good. Power collected by 3 different groups are same because of the cylindrical symmetry of the problem.

3.8.2 Fluorescence measurement of QD600

Fluorescence of quantum dot (ocean nanotech, water soluable quantum dot) is simulated using the monte carlo algorithm. For calculating the scattering cross section of the particles, diameter of the quantum dot is taken as 6.5 nm (size of the ligan). Medium geometry is limited by the boundaries of the sample holder. Width and height of the sample holder is 1 cm and 10 cm respectively.

As the concentration of the quantum dots increases, it is more probable for a photon to get absorbed. Hence, for high concentration levels excitation photons cannot propagate for long distance, saturating the collected power level. This is called quenching of the quantum dots [48]. The simulation of the problem is shown in figure 3.10.

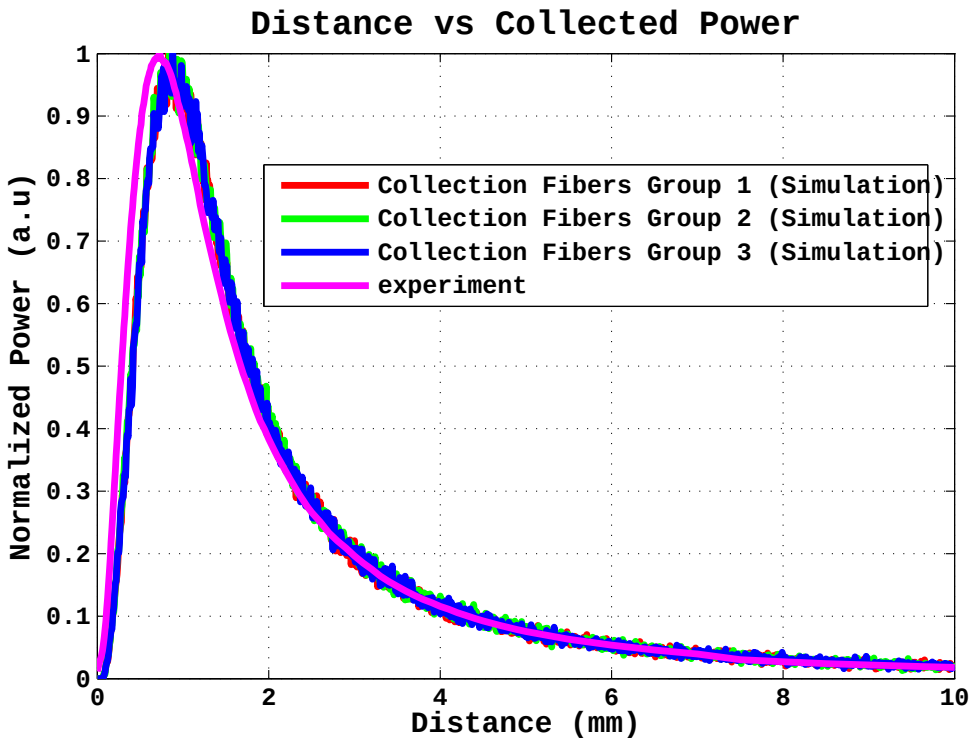

Figure 3.9: Comparison of simulation results with experimental data of the setup described in figure 3.7. 3 numbers indicate 3 different groups of collection fibers.

Using the fiber probe based system, fluorescence of quantum dot is measured. There are several corrections in the simulation data for calibration. Energy of the excitation photon is 408 nm while emitted photon is 600 nm. Energy of photon is calculated by

$$E = \frac{h}{c\lambda} \tag{3.18}$$

where, E is the energy of photon, h is the Planck constant, c is the speed of light in vacuum and λ is the wavelength of the photon [49]. Therefore, if the wavelength of the photon increases from 408 nm to 600 nm, its energy will be multiplied by 0.68. In addition, filter transmittance is 0.8 at the opertaing frequency. From figure 2.14, spectral response of silicon at 600 nm is 0.4. Lastly, because of the 0.48 numerical

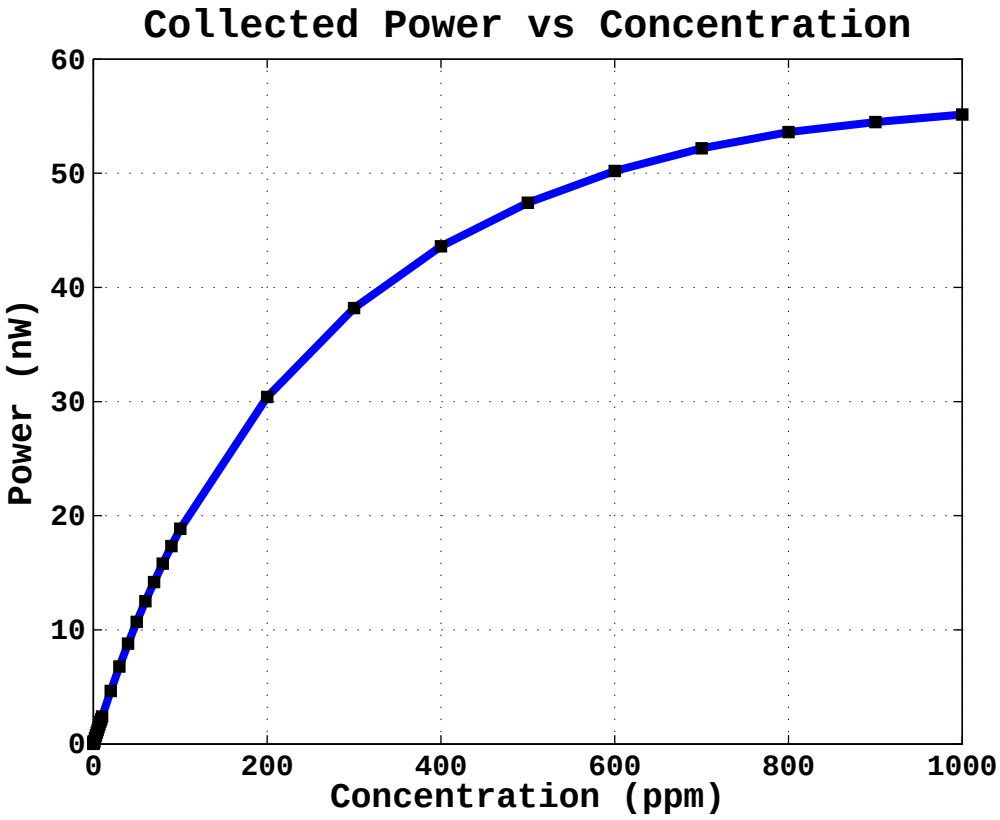

Figure 3.10: Collected Power vs Distance

aperture pf the fiber, effective area of the photodetector is not large enough to collect al the light coming through. This percentage can be calculated as the following; sensing area of the photodetector is 3 mm and maximum angle of ray coming out of the fiber is 28.69°. The distance between fiber tip and photo detector is around 3mm. Diameter of the spotsize at the photo detector is 6.28 mm which introducers an extra multiplier of 0.48. BVy multiplying every constant, it is possible to find $0.68 * 0.8 * 0.4 * 0.48 = 0.104$ which is the main multiplier for calibration. Emission wavelength of the quantum dot is 600 nm. Note that in the simulation, excitation and emission wavelength in the system are taken as single wavelength for ease in computation. Comparison of MC method and experiment result is shown in figure 3.11.

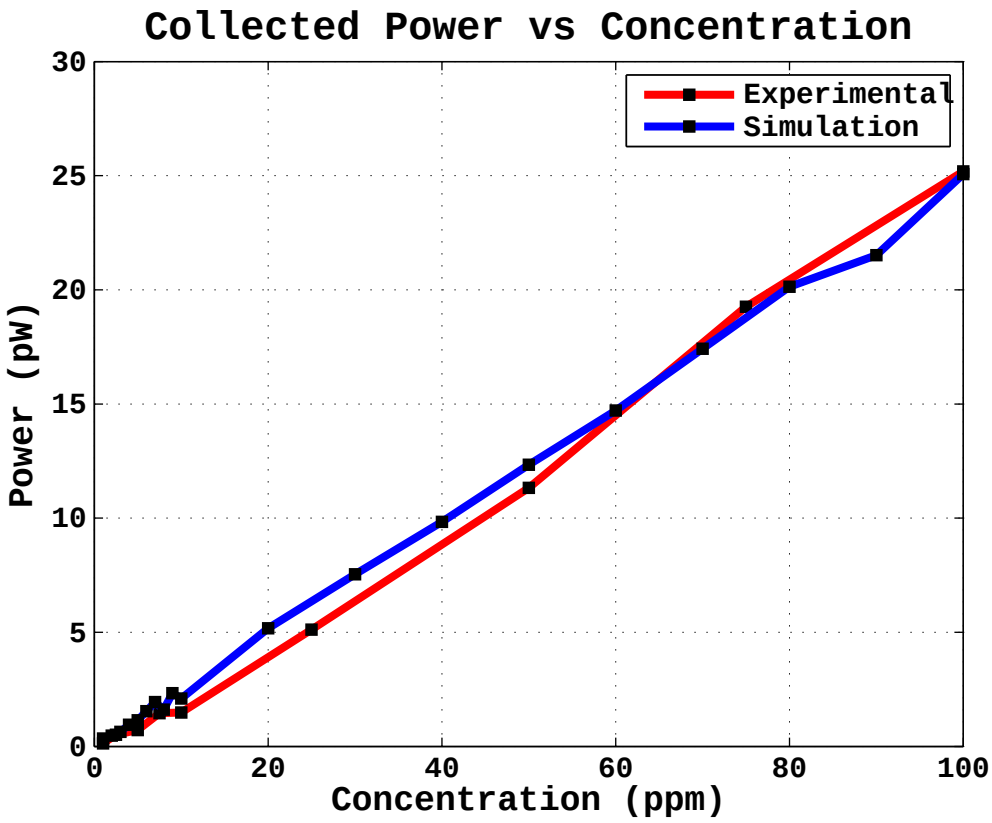

Figure 3.11: Comparison of experimental data and simulation of emission of QSH600, Simulation data is multipled by correction factor of 0.104 for fitting.

Chapter 4

MEASURING OF QD EMISSION IN NON-TRANSPARENT LIQUIDS

In the previous chapters, emission measurement of quantum dots in transparent liquids is discussed. When transparent liquids are excited, they do not emit light and they do not absorb the excitation photons. So when the solution is excited, only quantum dot emission is measured. However, when the liquid is non-transparent, light coming from the excitation source is absorbed by the medium. Total excitation photons absorbed by the quantum dots change. In addition, fluorescence of the medium affects the measured emission signal of the quantum dot. In order to make an accurate measurement, modification in sensor probe design and new algorithm is needed. In this section, modification of the system described in chapter 2.4 is explained and measurement are done using the same system.

4.1 Highly Absorbent Mediums

Water has no emission or absorption in the visible band of the spectrum. In addition, since the water particles are small, scattering cross section of the water particles are very small and photon are less likely to scatter from a water particle (see chapter 3). These properties made water a very suitable medium for fluorescence measurement. However, when we want to tag oil, gasoline and diesel, emission of the medium affects the results. When the liquid has its own fluorescence it should be added as a new fluorescence source which creates a background on our results.

QPP 645 (quantum dot with emission peak at 645 and it is soluable in oil) is used to tag oil at concentration levels of 0, 0.1 and 1 ppm respectively. Fiber based system with a band pass filter which has a center wavelength at 645 nm is used. Figure 4.1

shows the spectrum of oil. In the same figure, yellow bar indicates the band at which the power is measured. Signal on the photodetector can be calculated by

$$PD_{645} = \int_a^b f(x)\,\mathrm{d}x \tag{4.1}$$

where $f(x)$ is the spectrum of the liquid.

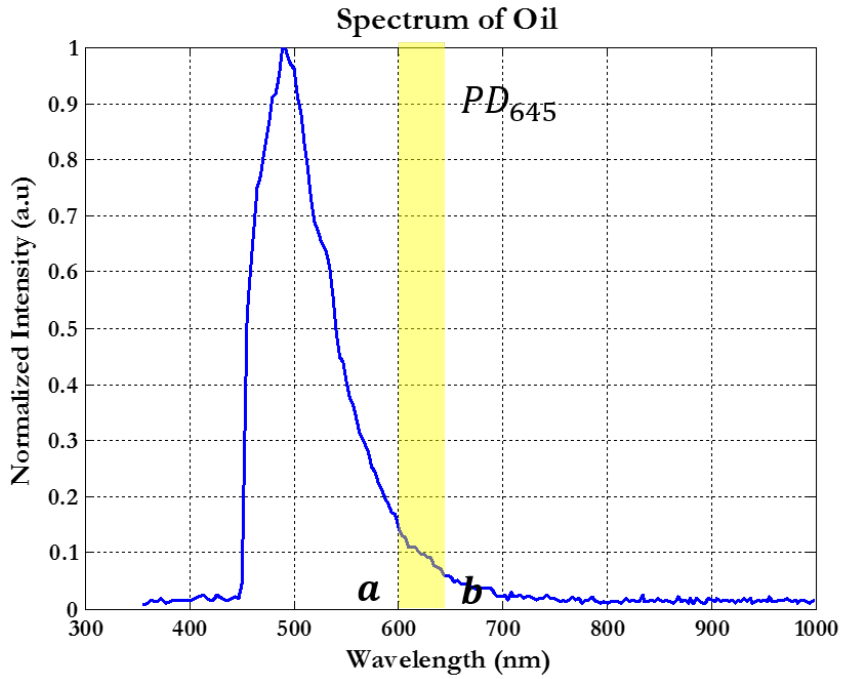

Figure 4.1: Spectrum of oil. Yellow bar indicates the measured band of the spectrum

Using the band pass filter indicated by the yellow bar, fluorescence levels can be measured. Results are shown in figure 4.2.

As seen in the figure 4.2, output of the each channel is fluctuating. If the fluorescence values weren't measured by time and instantaneous measurements were used, it was impossible to distinguish the different concentration levels. The difference between concentration levels cannot be extracted using simple background subtraction. There should be some relation between the fluorescence of the medium and the emission of the quantum dot. In order to test this affect, fluorescence of tagged oils were measured.

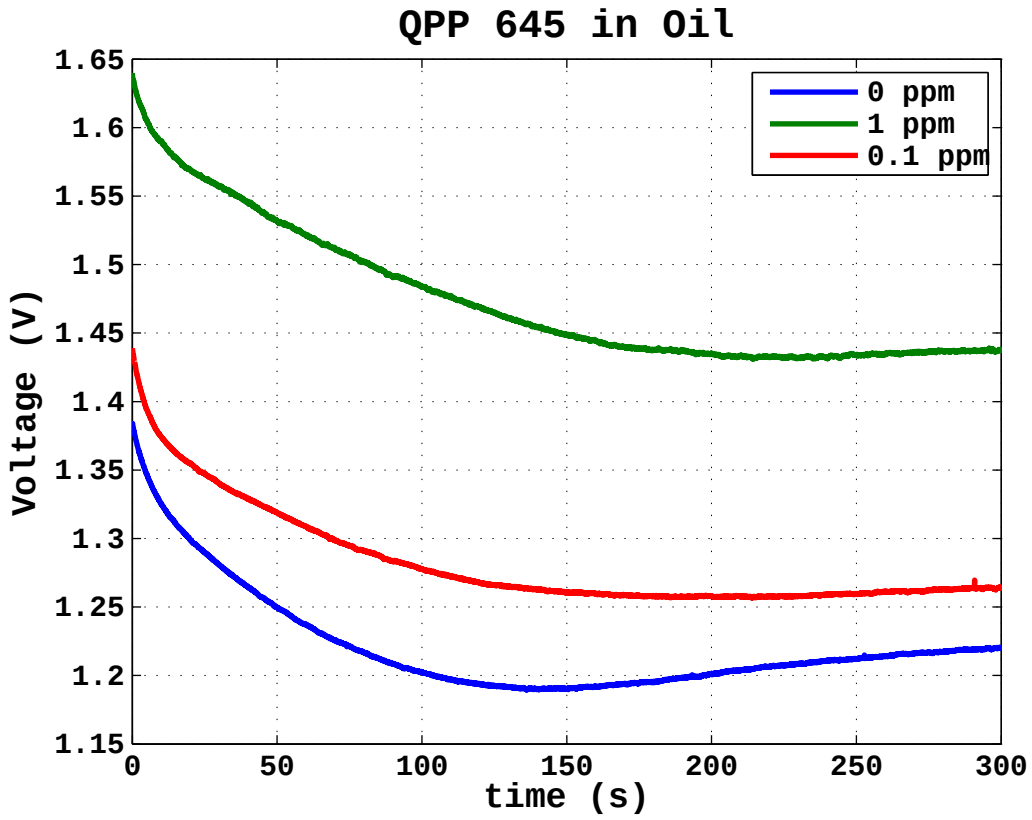

Figure 4.2: Fluorescence measurement of QPP645 in oil.Concentration levels are 0,0.1 and 1 respectively

Measurements are shown in the figure 4.3.

By looking at the figure 4.3, it can be seen that as the concentration level of the quantum dot increases, fluorescence from the medium decreases. This relation can be explained as the following; the total number of photons exciting the sample is same for tagged and untagged oil. However, in the case of the tagged oil, quantum dots also absorb photons. Therefore, total number of photons absorbed by the medium, also the fluorescence intensity, which is proportional to the absorbed photons, decreases.

In order to distinguish the fluorescence levels shown in the figure 4.2, signals should be calibrated according to the intensity. There are several methods for identifying these highly absorbent materials such as fluorescence spectroscopy, NIR spectroscopy,

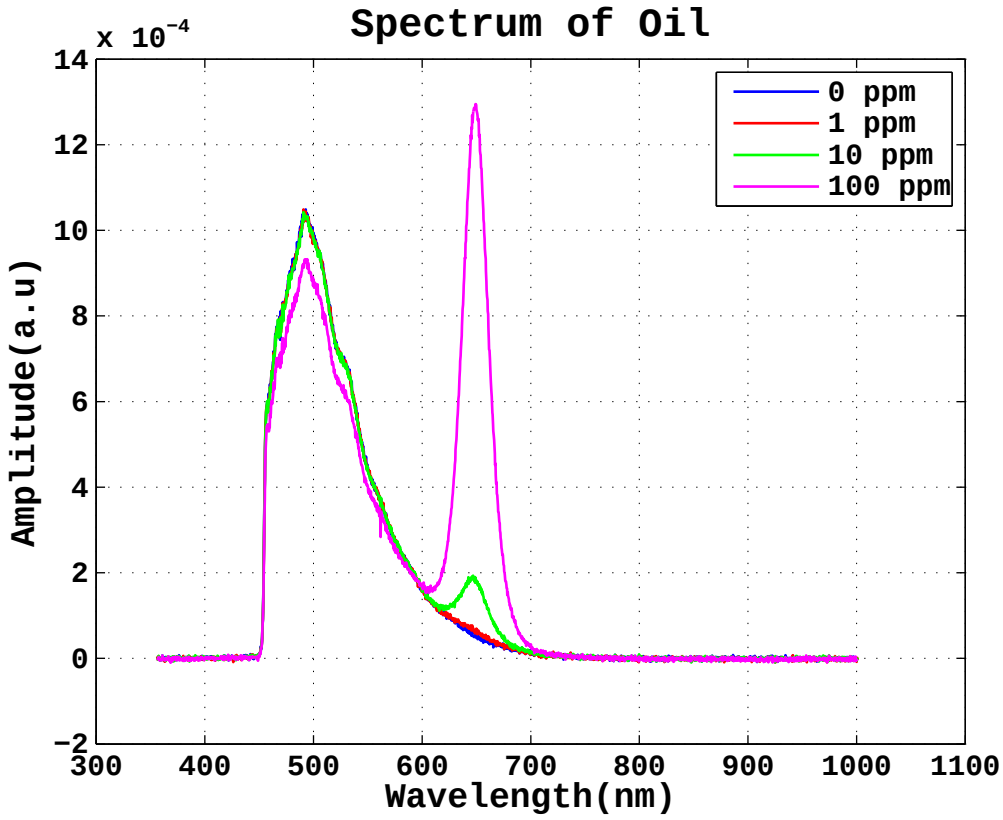

Figure 4.3: Spectrum of oil tagged with different concentrations of QPP. Concentration levels are 0 ppm, 1 ppm, 10 ppm and 100 ppm.

Raman spectroscopy or by using markers as described in chapter 1 [50] [51] [51].

4.2 Dynamic Background Subtraction

Change in photon absorption of the medium effects the measurement accuracy of the system. However, if the fluorescence of the medium is also monitored real time, quantum dot emission can be calibrated accordingly. Maximum fluorescence signal of the medium is observed at 500 nm. So if the measurement system is modified to measure yellow bands indicated by the yellow bars shown in the figure 4.4 calibration can be done accordingly.

Similar to tellow bar explanation,which is used to calculate equation 4.1, shown in

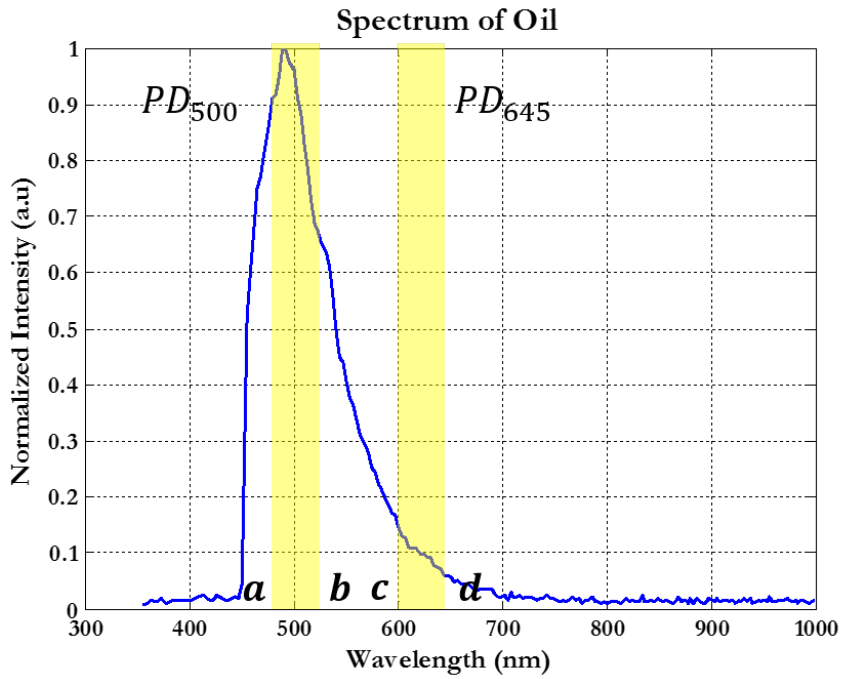

Figure 4.4: Spectrum of oil. Yellow bars indicates the measured band of the spectrum

figure 4.1, photodetector current can be calculated in a similar fashion by,

$$PD_{500} = \int_a^b f(x)\,\mathrm{d}x, \tag{4.2}$$

and

$$PD_{645} = \int_c^d f(x)\,\mathrm{d}x. \tag{4.3}$$

The system cannot be calibrated using a simple calibration which means that we need to define a new algorithm to correct the signals. The linearity property of the fluorescence of the medium can be used to extract the necessary information. The temporal fluctuations in the fluorescence spectrum of the medium are same for all limited bands in the spectrum. These bands can be the signals filtered by 645 nm and 500 nm band pass filters respectively. But looking at the fluorescence signal of pure oil shown in the figure 4.2, we can say that the ratio is not constant. So there should be some offsets in each channel disturbing the linearity of the system. The algorithm

should calculate these offsets and extract the emission information of the quantum dots. Algorithm can be described by the following steps; First, C_1, C_2 pair should be calculated such that minimizing the variance of

$$\frac{PD_{645} - C_1}{PD_{500} - C_2}. \tag{4.4}$$

Using C_1, C_2, calibrating constant k is calculated by

$$k = \langle \frac{PD_{645} - C_1}{PD_{500} - C_2} \rangle_t. \tag{4.5}$$

Using equations 4.4 and 4.5, quantum dot emission can be calculated using

$$PD^*_{645} = \frac{(PD_{645} - C_1) - k(PD_{500} - C_2)}{k(PD_{500} - C_2)}. \tag{4.6}$$

4.3 Results

Equation 4.6 is applied on the fluorescence data of the quantum dot shown in the figure 4.2. Output fluorescence signals after the processing is shown in the figure 4.5.

As seen from the figure 4.5, fluorescence signals from different concentration levels of quantum dots are distinguished. Moreover intensity levels of the emission signal are linearly proportional to the concentration of the quantum dots. Therefore using this system, it is possible to generate various fluorescence codes.

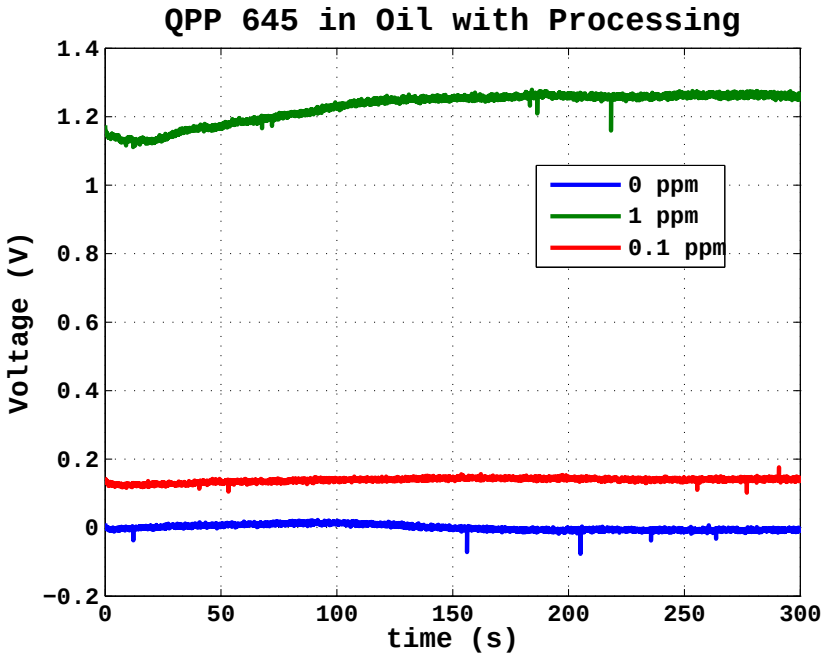

Figure 4.5: Fluorescence measurement of quantum dot tagged oil, fluorescence signal levels are calibrated using dynamic background subtraction algorithm

Chapter 5

CONCLUSION AND DISCUSSION

In this thesis we propoesed a simple, robust, easy to implement, cheap, alignment free and precise sensor and methodology for measuring fluorescence of quantum dots in liquids. Several sensor designs are described. Capturing magnetic particles combined with quantum dots are analysed. Fluorescence sensors including CCD based sensor, microscope lens based sensor and fiber optic based sensor implemented and analysed. Collection efficiency of the fiber based system is calculated and has been found as the best candidate for the application. Barcode information extraction out of sample's spectrum is explained. Minimum concentration level of 1 pM achieved with SNR of 5 using QSH 600 (ocean nanotech, water soluable quantum dot) under the illumination of 1 mW, 408 nm laser diode.

System is simulated using Monte Carlo methods. Different physical properties scored to calculate emission of the quantum dot. Method is tested by measuring the distance depended collection efficiency of the system. Physical properties including absorption cross sections and scattering cross sections were calculated for the simulation. Simulation results were compared with the experiment results and goof agreement is found.

Methodology for measuring quantum dot emission in highly emissive and absorbent materials is described. Sensor is modified for measuring the medium fluorescence. Different concentration of QPP 600(ocean nanotech, organic soluable quantum dot) inside oil is measured. Using the method it was possible to detect 100 ppb QPP 600.

Appendix A

APPENDIX

A.1 APPENDIX A: Java Code for Monte Carlo Computation

Photon class:

```
//author Basarbatu CAN

package qdemissionfiber3d;

public class photon {

    double x,y,z;
    double ux,uy,uz;
    double lambda;
    double weight;
    double scatters;
    boolean dead;

    public photon(double x,double y,double z,double ux,double uy,double uz,double
        lambda,double weight){
        x=this.x;
        y=this.y;
        z=this.z;
        ux=this.ux;
        uy=this.uy;
        uz=this.uz;
        lambda=this.lambda;
        weight=this.weight;
        this.scatters=0;
        this.dead=false;
    }

    public double[] getCoordinates(){
        double[] xyz = new double[3];
        xyz[0]=this.x;
        xyz[1]=this.y;
        xyz[2]=this.z;
```

```
        return xyz;
    }

    public void setCoordinates(double[] newCoordinates){
        this.x=newCoordinates[0];
        this.y=newCoordinates[1];
        this.z=newCoordinates[2];
    }

    public double[] getDirectionalCosines(){
        double[] uxuyuz = new double[3];
        uxuyuz[0]=this.ux;
        uxuyuz[1]=this.uy;
        uxuyuz[2]=this.uz;
        return uxuyuz;
    }

    public void setDirectionalCosines(double[] newDirectionalCosines){
        this.ux=newDirectionalCosines[0];
        this.uy=newDirectionalCosines[1];
        this.uz=newDirectionalCosines[2];
    }

    public double getLambda(){
        return this.lambda;
    }

    public void setLambda(double newLambda){
        this.lambda=newLambda;
    }

    public double getWeight(){
        return this.weight;
    }

    public void setWeight(double newW){
        this.weight=newW;
    }

    //coordinate updates
    public void move(double s,double controlledZ){
        //if the photon is traveled beyond the desired z direction, its coordinates
            are modifyed accordinly.
        if(this.z+this.uz*s<controlledZ){
```

```
            s=(controlledZ-this.z)/this.uz;
            this.x+=this.ux*s;
            this.y+=this.uy*s;
            this.z+=this.uz*s;
        }else{
            this.x+=this.ux*s;
            this.y+=this.uy*s;
            this.z+=this.uz*s;
        }
    }

    //directional cosine updates, take this function to screen function
    public void reflect(double[] surface){
        double div=Math.pow(surface[0],2)+Math.pow(surface[1],2)+Math.pow(surface
            [2],2);
        double a = (this.ux*surface[0]+this.uy*surface[1]+this.uz*surface[2])/div;
        this.ux-=2*a*surface[0];
        this.uy-=2*a*surface[1];
        this.uz-=2*a*surface[2];
    }

    public void scatter(){
        this.scatters+=1;
    }

    public boolean isDead(){
        return this.dead;
    }

    public void kill(){
        this.dead=true;
    }
}
```

Fiber class:

```
//author Basarbatu CAN

package qdemissionfiber3d;
import java.util.Random;

public class fiber {

    photon photon;
    double x,y,z;
```

```
double coreDiameter, cladThickness;
double ncore, nmedium, na;
boolean isillum;
boolean isEnabled;
double outPower;
double numberOfPhotons;
double totalPower, totalHit;
double filterWavelength;

//defining the surface of the fiber
double[] surface = new double[3];

//defining the acceptence angle
double AcceptenceAngle;

public fiber(photon photon, double x, double y, double z, double coreDiameter, double
    claddingThickness, double ncore, double nmedium, double na, double outPower,
    double numberOfPhotons, double filterWavelength, boolean isillum, boolean
    isEnabled){

//photonIn
    this.photon=photon;

    //cartesian coordinates of the fiber
    this.x=x;
    this.y=y;
    this.z=z;

    //physical quantities of fiber
    this.coreDiameter=coreDiameter;
    this.cladThickness=claddingThickness;
    this.ncore=ncore;
    this.nmedium=nmedium;
    this.na=na;
    this.outPower=outPower;

    //number of photons to be simulated
    this.numberOfPhotons=numberOfPhotons;

    //charaterization of the fiber
    this.filterWavelength=filterWavelength; //wavelength of the filter which is
        at the end of the fiber
    this.isillum=isillum; //true if the fiber is illumination fiber
```

```
        this.isEnabled=isEnabled; //true is the fiber is illumination OR collection
            fiber

        //contruction calculation
        //define the surface of the fiber
        surface[0]=0;
        surface[1]=0;
        surface[2]=-1;
        AcceptenceAngle=Math.asin(this.na/this.nmedium); //calculating the acceptence
             angle of the fiber in the specified medium.
        totalPower=0;
        totalHit=0;
    }

    public void setLocation(double[] xy){ //set the x y location of the fiber
        this.x=xy[0];
        this.y=xy[1];
    }

    public void setCoordinates(double[] xyz){ //set x y z location of the fiber
        this.x=xyz[0];
        this.y=xyz[1];
        this.z=xyz[2];
    }

    public double[] getCoordinates(){ //return x y z coorditanes of the fiber
        double[] xyz = new double[3];
        xyz[0]=this.x;
        xyz[1]=this.y;
        xyz[2]=this.z;
        return xyz;
    }

    public void setWavelength(double newWavelength){ //set the filter wavelength
        this.filterWavelength=newWavelength;
    }

    public double getWavelength(){ // get the filter wavelength
        return this.filterWavelength;
    }

    public void sendPhoton(){ //initialize photon and send it from the tip of the
        fiber into the medium.
        //location calculation
```

```
        double tetaFib=new Random().nextDouble()*Math.PI*2;
        double rFib=new Random().nextDouble();
        double px=Math.sqrt(rFib)*Math.cos(tetaFib)*this.corediameter/2+this.x;
        double py=Math.sqrt(rFib)*Math.sin(tetaFib)*this.corediameter/2+this.y;
        double pz=this.z;

        //angle calculation
        double iltetaR=(new Random().nextDouble()*2-1)*AcceptenceAngle;
        double ilaziR=new Random().nextDouble()*Math.PI*2;
        double pux=Math.sin(iltetaR)*Math.cos(ilaziR);
        double puy=Math.sin(iltetaR)*Math.sin(ilaziR);
        double puz=Math.cos(iltetaR);

        //photon creation
        double lambda=408e-9;
        double[] xyz = new double[3];
        xyz[0]=px;
        xyz[1]=py;
        xyz[2]=pz;
        this.photon.setCoordinates(xyz);
        double[] uxuyuz = new double[3];
        uxuyuz[0]=pux;
        uxuyuz[1]=puy;
        uxuyuz[2]=puz;
        this.photon.setDirectionalCosines(uxuyuz);
        this.photon.setLambda(lambda);
        this.photon.setWeight(this.outPower/this.numberOfPhotons);
        this.photon.dead=false;
        this.photon.scatters=0;
    }

    //check if the incoming photon is accepted to the fiber
    public void isPhotonIn(photon photonIn){
        if(photonIn.getLambda()==this.filterWavelength){ //if the filter wavelength
            is equal to the photonOut
            double R = Math.sqrt(Math.pow(photonIn.x-this.x, 2)+Math.pow(photonIn.y-
                this.y, 2));
            if((R<=this.corediameter/2)){ //if the photon is inside the core
                double tetaInMedium = Math.acos(dotProduct(photonIn.
                    getDirectionalCosines(),surface));
                if((tetaInMedium<=this.AcceptenceAngle)){ //if the incidince angle of
                    photon is accepted by the fiber
                    //calculate fresnel coefficients to update the input intensity
                        upan refraction.
```

```
                    double tetaInFiber=Math.asin((this.nmedium*Math.sin(tetaInMedium)
                        )/this.ncore);
                    double Rs=Math.pow(Math.abs((this.nmedium*Math.cos(tetaInMedium)-
                        this.ncore*Math.cos(tetaInFiber))/(nmedium*Math.cos(
                        tetaInMedium)+this.ncore*Math.cos(tetaInFiber))), 2);
                    double Rp=Math.pow(Math.abs((this.nmedium*Math.cos(tetaInFiber)-
                        this.ncore*Math.cos(tetaInMedium))/(nmedium*Math.cos(
                        tetaInFiber)+this.ncore*Math.cos(tetaInMedium))), 2);
                    photonIn.setWeight(photonIn.getWeight()*(1-(Rs+Rp)/2));
                    this.totalPower+=photonIn.getWeight();
                    this.totalHit+=1;
                    photonIn.kill(); //after the weights at the detectors are updated
                         photon is killed and not traced any more.
                }else{
                    photonIn.kill();
                }
            }else{
                photonIn.kill(); //photon is not in the core diameter of this fiber
                    or it is not accepted by the NA. Photon is killed and not traced
                    anymore.
            }
        }else{
            photonIn.kill(); //Photon is @ different wavelength, it is filtered out.
        }
    }

    public void refresh(){ //clear the detector at the end of the fiber
        this.totalPower=0;
        this.totalHit=0;
    }

    //dot product
    public double dotProduct(double[] a,double[] b){
        double sum=0;
        for (int i=0;i<a.length;i++){
            sum+=a[i]*b[i];
        }
        return sum;
    }
}
```

Quantum Dot class:

```
//author Basarbatu CAN
```

```
package qdemissionfiber3d;

public class QD {

    double concentration;
    double MolarExt585;
    double emissionWavelength;
    double quantumEfficiency;
    double initialDensity; // mg/ml
    double initialMol; //mol
    double initialVolume; //mL
    double rparticle;
    double nQD;
    double scatteringCrossSection;
    double absorptionCrossSection;
    double interactionCrossSection;
    double scatteringCoefficient;
    double absorptionCoefficient;
    double interactionCoefficient;
    double meanFreePath;

    //constants
    double avagadro = 6.02e23;

    public QD(double concentration,double initialDensity, double initialMol,double
        initialVolume,double rparticle,double MolarExt585,double nQD,double
        emissionWavelength,double quantumEfficiency){
        this.concentration=concentration; //in ppm
        this.initialDensity=initialDensity; //in mg/mL
        this.initialMol=initialMol; //in mol
        this.initialVolume=initialVolume; //in mL
        this.rparticle=rparticle; // in m
        this.MolarExt585=MolarExt585; // in L/(mol*cm)
        this.nQD=nQD;

        //optical prop
        this.emissionWavelength=emissionWavelength;
        this.quantumEfficiency=quantumEfficiency;
    }

    public void calculateCoefficients(double nmedium,double lambda){
        //calculations
        double NumberOfAtoms=this.concentration*(this.initialMol/(this.initialDensity
            *this.initialVolume))*this.avagadro*1e3; //number of QD in 1m^3
```

```
    //scattering cross section
        double rx=2*Math.PI*this.rparticle*nmedium/lambda;
        double m=this.nQD/nmedium;
        this.scatteringCrossSection=8/3*Math.PI*Math.pow(this.rparticle, 2)*Math.pow(
            rx, 4)*Math.pow((Math.pow(m, 2)-1)/(Math.pow(m, 2)+2), 2);

    //absorption cross section
        double MolarExt408=this.MolarExt585*11/3.65;
        this.absorptionCrossSection=3.82e-21*MolarExt408*1e-4;

        //modifying sc and abs
        this.interactionCrossSection = this.absorptionCrossSection+this.
            scatteringCrossSection;
        this.meanFreePath=1/(interactionCrossSection*NumberOfAtoms);
        this.interactionCoefficient=1/this.meanFreePath;
    }
}
```

Medium class:

```
//author Basarbatu CAN

package qdemissionfiber3d;
import java.util.ArrayList;
import java.util.Random;

public class medium {

    //out of class variables
    double nmedium;
    double xmedium,ymedium,zmedium;

    //in class variables
    double s;
    double[] scCross;
    double scCrossTotal;
    double[] abCross;
    double abCrossTotal;
    double[] intCross;
    double intCrossTotal;
    double[] mut;
    double mutTotal;
    double[] emis;
    double[] qeff;
```

```
ArrayList<QD> QDlist;

//in class variable
double m=10; //photon roulette variable

public medium(double nmedium,double xmedium,double ymedium,double zmedium){
    this.nmedium=nmedium;
    this.mutTotal=0;
    this.xmedium=xmedium;
    this.ymedium=ymedium;
    this.zmedium=zmedium;
    this.QDlist= new ArrayList<>();
}

public void addParticle(QD newQD){
     newQD.calculateCoefficients(this.nmedium, 408e-9);
     this.QDlist.add(newQD);
     this.scCross = new double[this.QDlist.size()]; //scattering cross section
     this.abCross = new double[this.QDlist.size()]; //absorbtion cross section
     this.intCross = new double[this.QDlist.size()]; //interaction cross section
     this.mut = new double[this.QDlist.size()]; //total interaction coefficient
     this.emis = new double[this.QDlist.size()]; //emission wavelength
     this.qeff = new double[this.QDlist.size()]; //quantum efficiency
     this.scCrossTotal=0;
     this.abCrossTotal=0;
     this.intCrossTotal=0;
     this.mutTotal=0;
     for(int i=0;i<this.QDlist.size();i++){
         this.scCross[i]=this.QDlist.get(i).scatteringCrossSection;
         this.scCrossTotal+=this.scCross[i];
         this.abCross[i]=this.QDlist.get(i).absorptionCrossSection;
         this.abCrossTotal+=this.abCross[i];
         this.intCross[i]=this.QDlist.get(i).interactionCrossSection;
         this.intCrossTotal+=this.intCross[i];
         this.mut[i]=this.QDlist.get(i).interactionCoefficient;
         this.mutTotal+=this.mut[i];
         this.emis[i]=this.QDlist.get(i).emissionWavelength;
         this.qeff[i]=this.QDlist.get(i).quantumEfficiency;
     }
}

public void clearMedium(){
    if(this.QDlist.size()>0){ //if QD list has previous components in it, clear
        them all
```

```
            for(int i=0;i<=this.QDlist.size();i++){
                this.QDlist.remove(i);
            }
            this.abCrossTotal=0;
            this.scCrossTotal=0;
            this.mutTotal=0;
        }else{ //if QD has no previous components, just initialize coefficients
            this.abCrossTotal=0;
            this.scCrossTotal=0;
            this.mutTotal=0;
        }
    }

    public double propogationDistanceInMedium(double glueDistance){
        this.s=0;
        do{
            this.s=-Math.log(1-new Random().nextDouble())/this.mutTotal;
        }while(this.s<glueDistance);
        return this.s;
    }

    public int whichQD(photon photonIn){
        //selects that photon is hit by which QD
        int selection=-1;
        if(this.QDlist.size()>1){
            //there are more than 1 quantum dots in the medium
            //create a dummy array for determining the limits
            double[] plimits = new double[this.QDlist.size()];
            double initlim=0;
            for(int i=0;i<plimits.length;i++){
                initlim+=this.QDlist.get(i).interactionCoefficient;
                plimits[i]=initlim;
            }

            //example: if the interaction coef of individual QDs are 1,2 and 4, array
                will be 1 3 7. Unifrom RV between 0 and 7 will determine which QD is
                selected.
            double dummySelect = new Random().nextDouble()*this.mutTotal; //RV to
                select which particle is hit by the photon according to the algorithm
                as described above.
            for(int i=plimits.length-1;i>0;i--){
                if((dummySelect>plimits[i-1])&(dummySelect==-1)){
                    selection=i;
                }
```

```
            }
            if(selection==-1){
                selection=0;
            }
        }else{
            selection=0;
        }
        return selection; //QDs are in row in QDlist arraylist. Returns 0,1 or 2 for
            the corresponding QD.
    }

    public void scatterFromParticle(photon photonIn,double teta){
        // teta is the scatter angle, need to be chosen out of rayleigh scattering
            distribution
        double azi=new Random().nextDouble()*Math.PI*2;
        double[] dirs = new double[3];

        if(Math.abs(photonIn.uz)>0.99999){ //uz is very large, approxiamtion
            dirs[0]=Math.sin(teta)*Math.cos(azi);
            dirs[1]=Math.sin(teta)*Math.sin(azi);
            dirs[2]=Math.signum(photonIn.uz)*Math.cos(teta);
        }else{ //calculate the deflecton angles
            double mult1=Math.sin(teta)/(Math.sqrt(1-Math.pow(photonIn.uz, 2)));
            dirs[0]=mult1*(photonIn.ux*photonIn.uz*Math.cos(azi)-photonIn.uy*Math.sin
                (azi))+photonIn.ux*Math.cos(teta);
            dirs[1]=mult1*(photonIn.uy*photonIn.uz*Math.cos(azi)+photonIn.ux*Math.sin
                (azi))+photonIn.uy*Math.cos(teta);
            dirs[2]=-Math.sin(teta)*Math.cos(azi)*Math.sqrt(1-Math.pow(photonIn.uz,
                2))+photonIn.uz*Math.cos(teta);
        }

        //scatter the input photon and update its directional cosines
        photonIn.scatter();
        photonIn.setDirectionalCosines(dirs);
    }

    public void absorbByQD(photon photonIn,int selectedQD){
        photonIn.setLambda(this.QDlist.get(selectedQD).emissionWavelength); //
            updating the wavelength of the emitted photon
        photonIn.setWeight(photonIn.getWeight()*(this.QDlist.get(selectedQD).
            quantumEfficiency)); //updating the weight of the photon accordingly
        photonIn.scatter(); //creating a new photon is also scattering, increase
            scatter by 1
```

```
    //phisically new photon will be created, directions are determined such that they
         have uniform distribution
        double[] directions = new double[3];
        double teta=new Random().nextDouble()*Math.PI; //unifrom in 0-180
        double azi=new Random().nextDouble()*Math.PI*2; //unifrom in 0-360
        directions[0]=Math.sin(teta)*Math.cos(azi);
        directions[1]=Math.sin(teta)*Math.sin(azi);
        directions[2]=Math.cos(teta);
        photonIn.setDirectionalCosines(directions); //update the direction of the
            photon
    }

    public void photonRoulette(photon photonIn,double th){ //Parameter m is selected
        as 10, can be updated, selected randomly.
        //roulette for photon termination
        if(photonIn.getWeight()<th){
            if(new Random().nextDouble()<1/this.m){
                photonIn.setWeight(photonIn.getWeight()*this.m);
            }else{
                photonIn.kill();
            }
        }
    }

    //photon termination functions
    public void isPhotonOut(photon photonIn){
        if((Math.abs(photonIn.x)>=this.xmedium/2)||(Math.abs(photonIn.y)>=this.
            ymedium/2)||(photonIn.z>=this.zmedium)){
            photonIn.kill(); //photon is out of boundaries, kill the photon
        }
    }

    public void isPhotonScatteredEnough(photon photonIn, double scatterLimit){
        if(photonIn.scatters==scatterLimit){
            photonIn.kill();
        }
    }
}
```

Probability Density Fuction Reader class:

```
//author Basarbatu CAN

package qdemissionfiber3d;
import java.io.BufferedReader;
```

```
import java.io.FileReader;
import java.util.Random;

public class PdfReader {

    String xfile,yfile;
    double[] pdfx,pdfy;
    public PdfReader(String xfile,String yfile){
        this.xfile=xfile;
        this.yfile=yfile;
        this.pdfx=new double[181];
        this.pdfy=new double[181];
        try{
            FileReader inputFilex = new FileReader(xfile);
            FileReader inputFiley = new FileReader(yfile);
            BufferedReader bufferReaderx = new BufferedReader(inputFilex);
            BufferedReader bufferReadery = new BufferedReader(inputFiley);
            String line;
            int ind=0;
            while ((line = bufferReaderx.readLine()) != null)   {
                    this.pdfx[ind]=Double.valueOf(line);
                    ind++;
            }
            ind=0;
            while ((line = bufferReadery.readLine()) != null)   {
                    this.pdfy[ind]=Double.valueOf(line);
                    ind++;
            }
            bufferReaderx.close();
            bufferReadery.close();
        }catch (Exception e){
           System.out.println("Error while reading file line by line:"+e.getMessage()
               );
        }
    }

    public double custompdf(double[] x,double[] cdf){
        double dif;
        double threshold=1000000;
        double generatedNumber=0;
        Random generator = new Random();
        double u = generator.nextDouble();
        for (int i=0;i<cdf.length;i++){
            dif=Math.abs(cdf[i]-u);
```

```
            if(dif<threshold){
                threshold=dif;
                generatedNumber=x[i];
            }
        }
        return generatedNumber;
    }

    public double[] test(int times){
        double[] tester = new double[times];
        for (int i=0;i<tester.length;i++){
            tester[i]=custompdf(this.pdfx,this.pdfy)*180/Math.PI;
            //System.out.println(tester[i]*180/Math.PI);
        }
        return tester;
    }
}
```

main method:

```
//author Basarbatu CAN

public class QDemissionFiber3D {

    public static void main(String[] args) {

        //Simulation Parameters
        long numberOfPhotons=10000000000L; //how many photons are send from the fiber
        double glueDistance=0; //no scattering below this distance
        double totalScatters=100; //how much the photon is traced
        double photonTh=(1e-3/numberOfPhotons)/100; //below this threshold, photon
            roulette is played.
        //A type Fiber Parameters (Big)
        double cladA=15e-6;
        double diameterA=400e-6;
        double outPowerA=1e-3;
        double naA=0.48;
        double ncoreA=1.46927; //@408nm
        double r1=diameterA/2+2*cladA+diameterA/2;
        //B type Fiber Parameters (Small)
        double cladB=10e-6;
        double diameterB=50e-6;
        double outPowerB=1e-3/6;
        double naB=0.48;
        double ncoreB=1.46927; //@408nm
```

```
        double r2=diameterA/2+cladA+cladB+diameterB/2;
        //medium properties
        double nmedium=1.33;
        double wmedium=1e3;
        double tmedium=1e3;
        double hmedium=1e3;
        //Create the reference photon
        photon photon = new photon(0,0,0,0,0,0,0,0);
        //Fiber array which contains fiber objects
        fiber[] Fibers = new fiber[13];
        //Fiber In the Middle
        Fibers[0] = new fiber(photon,0,0,0,diameterA,cladA,ncoreA,nmedium,naA,
            outPowerA,numberOfPhotons,0,false,false);
    //Initial Locations
        double[] loc1= new double[2];
        loc1[0]=r1;
        loc1[1]=0;
        double[] loc2= new double[2];
        loc2[0]=r2*Math.cos(Math.PI/6);
        loc2[1]=r2*Math.sin(Math.PI/6);
        //Creating A type Fibers surrounding the middle fiber
        for(int i=0;i<6;i++){
            Fibers[i+1]=new fiber(photon,0,0,0,diameterA,cladA,ncoreA,nmedium,naA,
                outPowerA,numberOfPhotons,0,false,false);
            Fibers[i+1].setLocation(rotate2d(loc1,i*Math.PI/3));
        }
        //Creating B type Fibers surrounding the middle fiber
        for(int i=7;i<13;i++){
            Fibers[i]=new fiber(photon,0,0,0,diameterB,cladB,ncoreB,nmedium,naB,
                outPowerB,numberOfPhotons,0,false,false);
            Fibers[i].setLocation(rotate2d(loc2,(i-7)*Math.PI/3));
        }
        //filter CW
        double exc=408e-9;
        double em1=600e-9;
        //Assigning Illuminating Fibers
        Fibers[0].isEnabled=true;
        Fibers[0].isillum=true;
        Fibers[0].setWavelength(exc);
        //AssigningCollection Fibers
        Fibers[1].isEnabled=true;
        Fibers[1].setWavelength(em1);
        //Seperating illumination and collection fibers
        fiber[] illumFibers = new fiber[1];
```

```
        fiber[] collectFibers = new fiber[1];
        //Creating the Image Of the Fiber Bundle Tip
        //FiberTipPlotter fiberTipPlotter = new FiberTipPlotter(Fibers);
        //fiberTipPlotter.ArrayToImage(fiberTipPlotter.createImageArray(2048, 2e-3));
        //System.out.println("Image is created.");
        int il=0;
        int col=0;
        for(int i=0;i<Fibers.length;i++){
            if(Fibers[i].isEnabled){
                if(Fibers[i].isillum){
                    illumFibers[il]=Fibers[i];
                    il+=1;
                }else{
                    collectFibers[col]=Fibers[i];
                    col+=1;
                }
            }
        }
        //rayleigh scatter cdf
        String xfile="C:\\Users\\basarbatuca\\Documents\\NetBeansProjects\\
            QDemissionFiber3D\\src\\pdfRayleighx.txt";
        String yfile="C:\\Users\\basarbatuca\\Documents\\NetBeansProjects\\
            QDemissionFiber3D\\src\\pdfRayleighy.txt";
        PdfReader pdfreader = new PdfReader(xfile,yfile); //reading the distribution
            from rayleigh distribution
        //testing the rayleigh scatter, gives angles from -pi to pi
        //plotHistogram("sd",pdfreader.test((int)numberOfPhotons),300);
        int NumberOfPpmLevels=10;
        double[] ppmLevels = new double[NumberOfPpmLevels];
        double[] intensity = new double[NumberOfPpmLevels]; //creating two arrays for
             generating ouputs for different concentration levels
        double[] hitCount = new double[NumberOfPpmLevels];
    //modify the arrays here to test different concentration levels
        //define the medium
        medium water = new medium(nmedium,wmedium,hmedium,tmedium); //medium is
            created
    //start the monte carlo simulation
        double printIndex=0;
        for(int i=0;i<NumberOfPpmLevels;i++){ //for each ppm level
            ppmLevels[i]=(i+1)*(0.02);
            //initiating the problem
            for(fiber collectfiber : collectFibers){
                collectfiber.refresh(); //refresh the detectors at the end of the
                    fibers
```

```
}
water.clearMedium(); //clear the miedum
QD qd600 = new QD(ppmLevels[i],3.64,4e-9,0.5,6.5e-9,310342,3,600e-9,0.8);
    //(ppm,mg/mL,mol,mL,L/(mol*cm),refractive,m,QE) //define a QD
water.addParticle(qd600); //adding the particle into the medium
for(fiber illumfiber : illumFibers){ //for each illumination fiber
    for(int j=0;j<numberOfPhotons;j++){ //for each photon
        //Printing the progress
        if((double)j/numberOfPhotons*1e4>printIndex){
            System.out.println(printIndex/100+"%");
            printIndex++;
        }
        illumfiber.sendPhoton(); //send photon from illumination fiber
        while(!illumfiber.photon.isDead()){ //until the photon is dead (
            hit to boundary, absorbed by medium or accepted by fiber)
            double s=water.propogationDistanceInMedium(glueDistance);
            illumfiber.photon.move(s, illumfiber.z); //photon travels by
                s in the medium.
            water.isPhotonOut(illumfiber.photon); //if the photon is out
                of the boundary, kill the photon, omit this part if the
                problem is unbounded
            water.photonRoulette(illumfiber.photon, photonTh); //play
                roulette if the weight of the photon is below threshold
                limit.
            water.isPhotonScatteredEnough(illumfiber.photon,
                totalScatters); //if the photon reached to the desired
                scatter number, kill it.
            //after moving the photon check if the photon is accepted by
                any of the fibers
            if(illumfiber.photon.isDead()){ //Is photon dead? After
                checking for the boundaries of the problem, scatter range
                 and weight range
                continue; //Photon is killed. @ the boundaries or because
                     of its weight or because it scattered enough
            }
            if(illumfiber.photon.z==0){ //photon is at the fiber tip
                plane
                for(fiber collectfiber : collectFibers){ //check if the
                    photon is absorbed by each collection fibers
                   collectfiber.isPhotonIn(illumfiber.photon); //if the
                       photon is not accepted it is killed.
                }
                continue; //no need to recalculate the remaining part, go
                     back to check the condition and terminate the photon
```

```
                    lopp.
                }
                //photon is not dead, not in the fiber tip plane and in the
                    problem boundaries. Check the weight of the photon
                //PHOTON QD interaction
                int QDselection=water.whichQD(illumfiber.photon); //photon
                    traveled by s. It is hit by QD. Which QD is selected?
                    Returns QD index value
                //QD index is selected. Determine the absorption or
                    scattering.
                if(illumfiber.photon.getLambda()==exc){ //excitation photon,
                    it will be absorbed or scattered
                    double abselect = new Random().nextDouble()*water.QDlist.
                        get(QDselection).interactionCrossSection; //RV
                        between 0 and interaction coef
                    if(abselect<water.QDlist.get(QDselection).
                        absorptionCrossSection){ //RV in in the range of Abs
                        Coef, photon will be absorbed
                        water.absorbByQD(illumfiber.photon, QDselection);
                    }else{ //photon is not absorbed, scattered
                        water.scatterFromParticle(illumfiber.photon,pdfreader
                            .custompdf(pdfreader.pdfx, pdfreader.pdfy));
                    }
                }else{ //emission photon, only scatter
                    water.scatterFromParticle(illumfiber.photon,pdfreader.
                        custompdf(pdfreader.pdfx, pdfreader.pdfy));
                }
            }
        }
    }
    //photons from all illumination fibers are finished. Sum up photon
        weights at the detectors
    double powerSum=0;
    double hitSum=0;
    for(fiber collectfiber : collectFibers){
        powerSum+=collectfiber.totalPower;
        hitSum+=collectfiber.totalHit;
    }

    intensity[i]=powerSum;
    hitCount[i]=hitSum;
    System.out.println("Collected power: " + powerSum);
    System.out.println("Total hit: " + hitSum);
}
```

```
        //plotting
        if(intensity.length>1){
            plot2D(ppmLevels,intensity,"sd");
            plot2D(ppmLevels,hitCount,"ds");
        }
    }

    public static void plotHistogram(String title,double[] data,int n){
        Plot2DPanel figure = new Plot2DPanel();
        figure.addHistogramPlot("Histogram", data, n);
        JFrame frame = new JFrame(title);
        frame.setContentPane(figure);
        frame.setVisible(true);
        frame.setLocation(120, 160);
        frame.setSize(1200,600);
        frame.setDefaultCloseOperation(JFrame.EXIT_ON_CLOSE);
    }

    public static void plot2D(double[] x,double[] y,String title){
        Plot2DPanel figure = new Plot2DPanel();
        figure.addLinePlot(title, x, y);
        JFrame frame = new JFrame("Plot");
        frame.setContentPane(figure);
        frame.setVisible(true);
        frame.setLocation(120, 160);
        frame.setSize(1200,600);
        frame.setDefaultCloseOperation(JFrame.EXIT_ON_CLOSE);
    }

    public static double[] rotate2d(double[] input,double teta){
        double[] out={input[0]*Math.cos(teta)-input[1]*Math.sin(teta),input[0]*Math.
            sin(teta)+input[1]*Math.cos(teta)};
        return out;
    }

    public static double[] arraytodouble(ArrayList a){
        double[] dd=new double[a.size()];
        for(int i=1;i<a.size();i++){
            dd[i]=(double)a.get(i);
        }
        return dd;
    }
}
```

BIBLIOGRAPHY

[1] U. Resch-Genger, M. Grabolle, S. Cavaliere-Jaricot, R. Nitschke, and T. Nann, "Quantum dots versus organic dyes as fluorescent labels," *Nature methods*, vol. 5, no. 9, pp. 763–775, 2008.

[2] "Fluorescent probes," http://www.piercenet.com/method/fluorescent-probes, accessed: 2014-07-14.

[3] *BLUE-VIOLET LASER DIODE*, Thorlabs, 5 2008, ver.2.

[4] *Precision Switched Integrator Transimpedance Amplifier*, Texas Instruments, 6 1996.

[5] J. H. Seinfeld and S. N. Pandis, *Atmospheric chemistry and physics: from air pollution to climate change*. John Wiley & Sons, 2012.

[6] E. W. Weisstein. (2014) Disk point picking. [Online]. Available: http://mathworld.wolfram.com/DiskPointPicking.html

[7] *1/2" Unmounted N-BK7 Ground Glass Diffuser, 220 Grit*, Thorlabs.

[8] C. Fishman. The killer app - bar none. [Online]. Available: http://hub.aa.com/en/aw/so-woodland-bar-code-bernard-silver-drexel-university

[9] T. Seideman. Barcodes sweep the world by tony seideman. [Online]. Available: http://www.barcoding.com

[10] N. Woodland and S. Bernard, "Classifying apparatus and method," Oct. 7 1952, uS Patent 2,612,994. [Online]. Available: http://www.google.com/patents/US2612994

[11] R. Wilson, A. R. Cossins, and D. G. Spiller, "Encoded microcarriers for high-throughput multiplexed detection," *Angewandte Chemie International Edition*, vol. 45, no. 37, pp. 6104–6117, 2006. [Online]. Available: http://dx.doi.org/10.1002/anie.200600288

[12] S. M. Borisov and O. S. Wolfbeis, "Optical biosensors," *Chemical reviews*, vol. 108, no. 2, pp. 423–461, 2008.

[13] Z. Lukacs, A. Dietrich, R. Ganschow, A. Kohlschütter, and R. Kruithof, "Simultaneous determination of hiv antibodies, hepatitis c antibodies, and hepatitis b antigens in dried blood spots–a feasibility study using a multi-analyte immunoassay," *Clinical Chemical Laboratory Medicine*, vol. 43, no. 2, pp. 141–145, 2005.

[14] T. Chasteen, "Relaxation mechanism for excited state molecules," 2006.

[15] M. Han, X. Gao, J. Z. Su, and S. Nie, "Quantum-dot-tagged microbeads for multiplexed optical coding of biomolecules," *Nature biotechnology*, vol. 19, no. 7, pp. 631–635, 2001.

[16] J. Lee, A. Hung, S. Mardyani, A. Rhee, J. Klostranec, Y. Mu, D. Li, and W. Chan, "Toward the accurate read-out of quantum dot barcodes: Design of deconvolution algorithms and assessment of fluorescence signals in buffer," *Advanced Materials*, vol. 19, no. 20, pp. 3113–3118, 2007. [Online]. Available: http://dx.doi.org/10.1002/adma.200701955

[17] B.-K. Oh, J.-M. Nam, S. Lee, and C. Mirkin, "A fluorophore-based bio-barcode

amplification assay for proteins," *Small*, vol. 2, no. 1, pp. 103–108, 2006. [Online]. Available: http://dx.doi.org/10.1002/smll.200500260

[18] H. Lee, J. Kim, H. Kim, J. Kim, and S. Kwon, "Colour-barcoded magnetic microparticles for multiplexed bioassays," *Nature materials*, vol. 9, no. 9, pp. 745–749, 2010.

[19] E. J. Moran, S. Sarshar, J. F. Cargill, M. M. Shahbaz, A. Lio, A. M. Mjalli, and R. W. Armstrong, "Radio frequency tag encoded combinatorial library method for the discovery of tripeptide-substituted cinnamic acid inhibitors of the protein tyrosine phosphatase ptp1b," *Journal of the American Chemical Society*, vol. 117, no. 43, pp. 10 787–10 788, 1995.

[20] X.-Y. Xiao, Z. Parandoosh, and M. P. Nova, "Design and synthesis of a taxoid library using radiofrequency encoded combinatorial chemistry," *The Journal of Organic Chemistry*, vol. 62, no. 17, pp. 6029–6033, 1997.

[21] N. Pamme, "Magnetism and microfluidics," *Lab on a Chip*, vol. 6, no. 1, pp. 24–38, 2006.

[22] V. I. Klimov, *Semiconductor and metal nanocrystals: Synthesis and electronic and optical properties*. CRC Press, 2003.

[23] C. B. Murray, D. J. Norris, and M. G. Bawendi, "Synthesis and characterization of nearly monodisperse cde (e = sulfur, selenium, tellurium) semiconductor nanocrystallites," *Journal of the American Chemical Society*, vol. 115, no. 19, pp. 8706–8715, 1993. [Online]. Available: http://pubs.acs.org/doi/abs/10.1021/ja00072a025

[24] PlasmaChem. (2014) Zncdses alloyed quantum dots. [Online]. Available: http://www.plasmachem.com/shop/en/226-zncdses-alloyed-quantum-dots

[25] J. F. James, R. S. Sternberg, and S. A. Rice, "The design of optical spectrometers," *Physics Today*, vol. 23, p. 55, 1970.

[26] W. S. Boyle and G. E. Smith, "Buried channel charge coupled devices," Feb. 12 1974, uS Patent 3,792,322.

[27] L. Glasser and D. Troy, "A new high sensitivity differential colorimeter," *JOSA*, vol. 42, no. 9, pp. 652–657, 1952.

[28] J. T. Motz, M. Hunter, L. H. Galindo, J. A. Gardecki, J. R. Kramer, R. R. Dasari, and M. S. Feld, "Optical fiber probe for biomedical raman spectroscopy," *Applied optics*, vol. 43, no. 3, pp. 542–554, 2004.

[29] B. W. Pogue and G. Burke, "Fiber-optic bundle design for quantitative fluorescence measurement from tissue," *Applied optics*, vol. 37, no. 31, pp. 7429–7436, 1998.

[30] S. Smolka, M. Barth, and O. Benson, "Highly efficient fluorescence sensing with hollow core photonic crystal fibers," *Optics Express*, vol. 15, no. 20, pp. 12 783–12 791, 2007.

[31] H. Urey, A. YAGCI, C. ELBUKEN, B. CAN, O. AKGUN, and F. UYGURMEN, "A method and an apparatus for the detection of a tagging material in fluids," May 1 2014, wO Patent App. PCT/EP2012/070,947. [Online]. Available: https://www.google.com/patents/WO2014063725A1?cl=en

[32] Y. Gao, A. W. Lam, and W. C. Chan, "Automating quantum dot barcode assays using microfluidics and magnetism for the development of a point-of-care device," *ACS applied materials & interfaces*, vol. 5, no. 8, pp. 2853–2860, 2013.

[33] N. Pamme and A. Manz, "On-chip free-flow magnetophoresis: continuous flow separation of magnetic particles and agglomerates," *Analytical chemistry*, vol. 76, no. 24, pp. 7250–7256, 2004.

[34] S. D. Schwab and R. L. McCreery, "Versatile, efficient raman sampling with fiber optics," *Analytical Chemistry*, vol. 56, no. 12, pp. 2199–2204, 1984.

[35] *M-Type CW Laser Diode Driver*, ICHaus, 2006, rev. C1.

[36] J. B. Johnson, "Thermal agitation of electricity in conductors," *Physical review*, vol. 32, no. 1, p. 97, 1928.

[37] B. Wu and H.-Q. Gong, "Fluorescence-profile pre-definable quantum-dot barcodes in liquid-core microcapsules," *Microfluidics and nanofluidics*, vol. 13, no. 6, pp. 909–917, 2012.

[38] J. A. Lee, A. Hung, S. Mardyani, A. Rhee, J. Klostranec, Y. Mu, D. Li, and W. C. Chan, "Toward the accurate read-out of quantum dot barcodes: Design of deconvolution algorithms and assessment of fluorescence signals in buffer," *Advanced Materials*, vol. 19, no. 20, pp. 3113–3118, 2007.

[39] B. Wu and H.-Q. Gong, "Predefinable colorimetric quantum-dot barcodes with simple and express identification algorithm," *Applied optics*, vol. 52, no. 4, pp. 866–870, 2013.

[40] C. Zhu and Q. Liu, "Review of monte carlo modeling of light transport in tissues," *Journal of Biomedical Optics*, vol. 18, no. 5, pp. 050 902–050 902, 2013. [Online]. Available: http://dx.doi.org/10.1117/1.JBO.18.5.050902

[41] A. T. Young, "Rayleigh scattering," *Physics Today*, vol. 35, no. 1, pp. 42–48, 1982.

[42] L. Devroye, "Sample-based non-uniform random variate generation," in *Proceedings of the 18th conference on Winter simulation*. ACM, 1986, pp. 260–265.

[43] Wikipedia. (2014) Mean free path, wikipedia the free encyclopedia. [Online]. Available: http://en.wikipedia.org/wiki/Mean_free_path

[44] N. Ismail, F. Civitci, K. Wörhoff, R. M. de Ridder, M. Pollnau, and A. Driessen, "Efficiency of integrated waveguide probes for the detection of light backscattered

from weakly scattering media," *Appl. Opt.*, vol. 50, no. 6, pp. 935–942, Feb 2011. [Online]. Available: http://ao.osa.org/abstract.cfm?URI=ao-50-6-935

[45] G. Spencer and M. Murty, "General ray-tracing procedure," *JOSA*, vol. 52, no. 6, pp. 672–676, 1962.

[46] J. R. Lakowicz and B. R. Masters, "Principles of fluorescence spectroscopy," *Journal of Biomedical Optics*, vol. 13, no. 2, p. 9901, 2008.

[47] J. Hendricks and T. Booth, "Mcnp variance reduction overview," in *Monte-Carlo Methods and Applications in Neutronics, Photonics and Statistical Physics*. Springer, 1985, pp. 83–92.

[48] K. E. Sapsford, T. Pons, I. L. Medintz, and H. Mattoussi, "Biosensing with luminescent semiconductor quantum dots," *Sensors*, vol. 6, no. 8, pp. 925–953, 2006.

[49] Wikipedia. (2014) Planckeinstein relation, wikipedia the free encyclopedia. [Online]. Available: http://en.wikipedia.org/wiki/PlanckEinsteinrelation

[50] U. Frank, "Identification of petroleum oils by fluorescence spectroscopy," in *International Oil Spill Conference*, vol. 1975, no. 1. American Petroleum Institute, 1975, pp. 87–91.

[51] C. W. Brown, M. Ahmadjian, and P. F. Lynch, "Petroleum identification," Jul. 22 1975, uS Patent 3,896,312.